Tampere University

SUDHARSAN SRINIVASAN

Multiantenna Interference Mitigation Schemes and Resource Allocation for Cognitive Radio

Tampere University Dissertations 694

Tampere University Dissertations 694

SUDHARSAN SRINIVASAN

Multiantenna Interference Mitigation Schemes and Resource Allocation for Cognitive Radio

ACADEMIC DISSERTATION
To be presented, with the permission of
the Faculty of Information Technology and Communication Sciences
of Tampere University,
for public discussion in the auditorium TB109
of the Tietotalo Building, Korkeakoulunkatu 1, Tampere,
on 11th November 2022, at 12 o'clock.

ACADEMIC DISSERTATION
Tampere University
Faculty of Information Technology and Communication Sciences
Finland

Responsible supervisor and Custos	Prof. Emeritus Markku Renfors Tampere University Finland	
Supervisor	Dr. Sener Dikmese Ericsson Sweden	
Pre-examiners	Prof. Danijela Cabric University of California Los Angeles (UCLA) USA	Prof. Hanna Bogucka Poznan University of Technology Poland
Opponent	Dr. Kalle Ruttik Aalto University Finland	

Cover design: Roihu Inc.

ISBN 978-952-03-2620-3 (print)
ISBN 978-952-03-2621-0 (pdf)
ISSN 2489-9860 (print)
ISSN 2490-0028 (pdf)
http://urn.fi/URN:ISBN:978-952-03-2621-0

Carbon dioxide emissions from printing Tampere University dissertations have been compensated.

PunaMusta Oy – Yliopistopaino
Joensuu 2022

Dedication

To my Parents, Gopalan, Sindhu, Anirudh, and Atreya.

PREFACE

This study was carried out during the years 2012-2021 at the Faculty of Information Technology and Communication Sciences at Tampere University, Finland. First and foremost, I would like to express my sincere and deepest gratitude to Prof. Markku Renfors. For me, given all the distractions of life, his great effort, patience, vast knowledge, and continuous support has been the absolute guiding force in my research work. Without his patience and understanding I would have not completed this thesis. I cannot find enough words to express my gratitude, I am grateful for such a great opportunity. I would like to thank Dr. Sener Dikmese for his support and cooperation in our joint publications and this thesis. I would like to thank Dr. AlaaEddin Loulou for his collaboration and discussion during this thesis. I would also like to take this opportunity to thank Prof. Mikko Valkama for accommodating me in our department and providing me the needed support.

I thankfully acknowledge the generous financial support that I had received from Ulla Tuominen Foundation and the Tampere University for the work carried out for this thesis. I am also grateful to my employer Nokia for supporting my doctoral studies. I would like to thank all my colleagues, administrative staff, and professors at Tampere University for creating a wonderful and pleasant working environment.

I am very grateful to both Prof. Danijela Cabric and Prof. Hanna Bogucka for acting as the pre-examiners of this thesis and providing their valuable comments, corrections, and insights in improving this thesis. Furthermore, I thank Dr. Kalle Ruttik for agreeing to act as the opponent in the public examination of this thesis.

I would like to thank all my friend and their families for their support in my studies and other aspects of life in Finland.

Last but not the least, my deepest gratitude and sincere thanks to my parents, my wife and children for the endless support, care, and love.

ABSTRACT

Maximum and efficient utilization of available resources has been a central theme of research on various areas of science and engineering. Wireless communication is not an exception to this. With the rapid growth of wireless communication applications, radio frequency spectrum has become a valuable commodity. Supporting very high demands for data rate and throughput has become a challenging problem which requires innovative solutions. Dynamic spectrum sharing (DSS) based cognitive radio (CR) is envisioned as a promising technology for future wireless communication systems, such as fifth generation (5G) further development and sixth generation (6G). Extensive research has been done in the areas of CRs and it is considered to mitigate the spectral crowding problem by introducing the notion of opportunistic spectrum usage. Spectrum sensing, which enables CRs to identify spectral holes, is a critical component in CR technology. Furthermore, improving the efficiency of the radio spectrum use through spectrum sensing and dynamic spectrum access (DSA) is one of the emerging trends.

In the first part of this thesis, we focus on enhancing the spectrum usage of CR's using interference cancellation methods that provides considerable performance gains with realistic computational complexity, especially, in the context of the widely used multicarrier waveforms. The primary focus is on interference rejection combining (IRC) methods, applied to the black-space cognitive radio (BS-CR). Earlier studies on the BS-CR in the literature were focused on using CRs as repeaters for the primary transmitter to guarantee that the CR is not causing significant interference to nearby primary users' receivers. This kind of approaches are transmitter-centric in nature. In this thesis, receiver-centric approaches such as multi-antenna diversity combining, especially enhanced IRC methods, are considered and evaluated. IRC methods have been widely studied and adopted in several practical wireless communication systems. We focus on developing such BS-CR schemes under strong interference conditions, which has not been studied in the CR literature so far. Spatial covariance matrix estimation under mobility and high carrier frequencies is found to be the most critical part of such scheme. Algorithms and methods to mitigate these effects are developed in this thesis and they are

evaluated under realistic BS-CR receiver operating conditions. We use sample covariance estimation approach with silent gaps in the CR transmisison. Covariance interpolation between silent gaps improves greatly the robustness with time-varying channels. Good link performance can be reached with low mobility at carrier frequency considered for the TV white-spaced case. The proposed BS-CR scheme could be feasible at below 6 GHz frequencies with pedestrian mobilities.

The second part of this thesis investigates the effect of radio frequency (RF) impairments on the performance of the cognitive wireless communication. There are various unavoidable imperfections, mainly due to the limitations of analog high-frequency transmitter and receiver circuits. These imperfections include power amplifier (PA) non-linearities, receiver nonlinearities, and carrier frequency offset (CFO), which are considered in this study. These effects lead to significant signal distortion and, as a result of this, the wireless link quality may deteriorate. In multicarrier communications such signal distortions may lead to additional interference, and it is important to evaluate their effects on spectrum sensing quality and on the performance of the proposed BS-CR scheme. This part of the thesis provides critical analysis and insights into such issues caused by RF imperfections and demonstrates the need for designing proper compensation techniques required to avoid/reduce such degradations. It is found that the transmitter's PA nonlinearities affect in the same way as in basic OFDM systems and BS-CR receiver's linearity requirements are similar to those for advanced DSP-intensive software defined radios. The CR receiver's CFO with respect to the PU has the most critical effect. However, synchronizing the CR with the needed high accuracy is considered achievable due to the PU signal's high-power level.

The final part of the thesis briefly looks at alternate waveforms and techniques that can be used in CRs. The filter bank multicarrier (FBMC) waveforms are considered as an alternative to the widely used OFDM schemes. Here the core idea is interference avoidance, targeting to reduce the interference leakage between CRs and the primary systems, by means of using a waveform with good spectrum localization properties. FBMC system's performance is compared with OFDM based system in the context of CRs. The performance is compared from a combined spectrum sensing and resource allocation point of view through simulations. It is found that well-localized CR waveforms improve the CR link capacity, but with poorly localized primary signals, these possibilities are rather limited.

CONTENTS

ABBREVIATIONS

Abbreviation	Explanation
3GPP	Third Generation Partnership Project
4G	Fourth Generation
5G	Fifth Generation
6G	Sixth Generation
ACI	Adjacent Channel Interference
ADC	Analog to Digital Converter
AFB	Analysis Filter Bank
AWGN	Additive White Gaussian Noise
BC	Broadcast Channel
BER	Bit Error Rate
BS-CR	Black-Space Cognitive Radio
CCI	Co-Channel Interference
CP-OFDM	Cyclic Prefix OFDM
CR	Cognitive Radio
DAC	Digital to Analog Converter
dB	Decibel
DVB-T	Digital Video Broadcasting Terrestrial

F-OFDM	Filtered OFDM
FBMC	Filter Bank Multicarrier
FDMA	Frequency Division Multiple Access
FFT	Fast Fourier Transform
ITU	International Telecommunication Union
IFFT	Inverse Fast Fourier Transform
IRC	Interference Rejection Combining
LMMSE	Linear Minimum Mean-Squared Error
LTE	Long-Term Evolution
LTE-A	Long-Term Evolution Advanced
QAM	Quadrature Amplitude Modulation
QPSK	Quadrature Phase Shift Keying
MA	Multiple Access
ML	Maximum Likelihood
MMSE	Minimum Mean Square Error
MRC	Maximum Ratio Combining
MIMO	Multiple Input Multiple Output
OFDM	Orthogonal Frequency Division Multiplexing
OFDMA	Orthogonal Frequency Division Multiple Access
PA	Power Amplifier
PDF	Probability Density Function
PSD	Power Spectrum Density

PU	Primary User
RF	Radio Frequency
RMS	Root-Mean-Square
ROC	Receiver Operating Characteristics
RX	Receiver
SDR	Software Defined Radio
SFN	Single Frequency Network
SIR	Signal to Interference Ratio
SINR	Signal to Interference and Noise Ratio
SIMO	Single Input Multiple Output
SV	Steering Vector
SU	Secondary User
TDMA	Time Division Multiple Access
TV	Television
TVWS	TV White Space

LIST OF SYMBOLS

$*$	Convolution
$(x)^*$	Conjugate of x
x^T	Transpose of x
$(\mathbf{x})^H$	Hermitian transpose
X^{-1}	Inverse of matrix $\boldsymbol{X}$
$\lfloor x \rfloor$	Floor function
$\lceil x \rceil$	Ceiling function
$\lvert x \rvert$	Absolute value of x
$\lVert X \rVert$	Norm of $\mathbf{X}$
e^x	Exponential of x
$E[.]$	Expected value
$\mathbb{C}$	Set of complex numbers
$\mathbf{I}_a$	a x a Identity matrix
$Inf\{\quad\}$	Infimum of the set of numbers {}
$\ln(x)$	Natural logarithm of x
$\log_2(x)$	Logarithm of x to the base of 2

$\log_{10}(x)$	Logarithm of x to the base of 10
$\lim_{x \to x_0}\big(f(x)\big)$	Limiting value of function $f(x)$ when x approaches to x_0
max( )	Maximum value of set
min( )	Minimum value of set
$P(x)$	Probability of x
$Q(.)$	Q function
$Q^{-1}(.)$	Inverse Q function
$\mathbb{R}^+$	Set of positive real numbers
$\sin(x)$	Sine of x
sup{ }	Supremum of the set of numbers {}
Var[.]	Variance

ORIGINAL PUBLICATIONS

[P1] S. Srinivasan, S. Dikmese and M. Renfors, "Spectrum Sensing and Spectrum Utilization Model for OFDM and FBMC based Cognitive Radios, " in Proc. IEEE 13th International Workshop on Signal Processing Advances in Wireless Communications (SPAWC), 2012, pp. 139-143.

[P2] S. Dikmese, S. Srinivasan, M. Shaat, F. Bader and M. Renfors, "Spectrum Sensing and Resource Allocation for Multicarrier Cognitive Radio Systems under Interference and Power Constraints," EURASIP Journal on. Advanced. Signal Process. 2014, 68 (2014).

[P3] S. Srinivasan and M. Renfors, "Interference Rejection Combining for Black-Space Cognitive Radio Communications". In: Moerman I., Marquez-Barja J., Shahid A., Liu W., Giannoulis S., Jiao X. (eds) Cognitive Radio Oriented Wireless Networks. CROWNCOM 2018. Lecture Notes of the Institute for Computer Sciences, Social Informatics and Telecommunications Engineering, vol 261. Springer, Cham (2019)

[P4] S. Srinivasan, S. Dikmese and M. Renfors, "Enhanced Interpolation-based Interference Rejection Combining for Black-space Cognitive Radio in Time-varying Channels, " EURASIP Journal on. Wireless Communication Network 2020, 238 (2020).

[P5] S. Srinivasan, S. Dikmese and M. Renfors, "Effects of RF Imperfections on Interference Rejection Combining Based Black-Space Cognitive Radio, " in Proc. IEEE 93rd Vehicular Technology Conference (VTC2021-Spring), 2021, pp. 1-6.

1 INTRODUCTION

1.1 Background and Motivation

The electromagnetic spectrum is a scarce and precious resource. Like any other natural resource, efficient utilization of the electromagnetic spectrum is not only an essential condition for sustainable development, but also for competitiveness in telecommunication industry. Traditionally, the entire available spectrum is divided into smaller bands and each band is licensed for the exclusive use of one or few wireless applications. Some of the available spectrum is left as unlicensed spectrum or bands for free usage to encourage innovation. For example, the bands of frequencies between both 2.4 - 2.5 GHz and 5.725 - 5.875 GHz are used for industrial scientific and medical (ISM) applications without the need to obtain a license to use the spectrum from the local regulator. Unlicensed spectrum is almost completely occupied by a host of devices from Wi-Fi and Bluetooth devices to cordless devices.

A US Federal Communications Commission (FCC) report [1] published in November 2002 (for which measurements and studies had already started in 1995) shows that once the time and space variations of spectrum occupation are considered and fixed, a rigid utilization plan emerges. Such a rigid spectrum licensing policy results in inefficient spectrum allocation and low spectrum utilization. This imbalance between the spectrum scarcity and low utilization motivates the concept of cognitive radio (CR) networks. The inefficient allocation of spectrum leads to unused or under used spectrum. At any particular time in a particular geographical location, the unused parts of radio spectrum are called spectrum holes or white space. Shared usage of such spectrum through secondary (unlicensed) users can help to increase the spectrum utilization. This process of using the spectrum owned by a licensed spectrum user by one or many unlicensed secondary users is called spectrum sharing [7], [24], [69], [107], [108]. Thus, spectrum sharing can help to increase the spectrum efficiency [147]. Encouraged by these findings, FCC introduced the

secondary markets initiative [2]. This initiative aims to remove unnecessary regulations which act as a barrier to new, secondary market-oriented policies like spectrum leasing, dynamic spectrum access (DSA) or sub-leases of spectrum and spectrum pooling [147]. As continuation of these policy efforts, and getting these policies implemented, there emerged, three major standardization activities. These standards targets were to work on the algorithms and architectures related to the CRs.

1. The IEEE 802.22 [40], [80] standards committee, aiming at developing CR algorithms and architectures for wireless regional area networks (WRANs) for local and regional coverage.

2. The IEEE Dynamic Spectrum Access Networks Standards Committee (DySPAN-SC) develops basic CR system and DSA technology standards [27] with the focus on the improved use of spectrum in any spectrum band.

3. The third major standardization body is the ETSI's Reconfigurable Radio Systems Technical Committee (RRC) on CRs and software defined radio (SDR)[3], [4], [111]. The ETSI's RRC is a European initiative which is complimentary to the IEEE 802.22 standard and the DySPAN activities, aimed on SDR standards beyond the IEEE scope, CR/SDR standards addressing the specific needs of the European Regulatory Framework, and CR/SDR TV white space (TVWS) standards adapted to the digital TV signal characteristics in Europe and elsewhere.

One of the key aspects of the SDR/CR standards activities were aimed at getting both the wide area wireless network and the short-range wireless networks to co-exist in a particular geographical location.

Spectrum sharing techniques are broadly classified [67], [69], [78], [151] as real-time secondary spectrum access and non-real-time secondary spectrum access, based on the way in which they access the spectrum in the time dimension. From the perspective of coexistence, the spectrum sharing can be classified as underlay, overlay, and interweave [67], [78], [151]. In interweave systems, the CRs opportunistically exploit spectral holes to communicate without disrupting other transmissions. The interweave systems can also be thought of as an interference

avoidance type of a communication system. For this type of system, the secondary users need to know the time-frequency gaps in the spectrum of primary user (PU). The constraints that need to be satisfied here are that there must be no interference between the primary and secondary transmissions and the primary and secondary transmissions are orthogonal either in time or frequency. The most common and well-known examples are the time division multiple access (TDMA) and frequency division multiple access (FDMA) approaches.

In the underlay paradigm, cognitive users could operate if the interference caused to noncognitive users is below a given threshold. Here the secondary and primary users are allowed to transmit over the same spectrum, in such a way that the interference seen by the PUs from the cognitive users is controlled to an acceptable level as seen by the primary with respect to some quality of service (QoS) constraints. The cognition required here is the knowledge of the "acceptable levels" of interference at PUs within a cognitive user's transmission range. This type of system can be thought of as an interference control type of spectrum sharing method. After identifying such transmission opportunities, they are aggregated and grouped to form a wideband transmission channel.

In overlay systems, the CRs use the same spectrum as PUs by means of sophisticated signal processing and coding to maintain or improve the communication of noncognitive radios while also obtaining some additional bandwidth for their own communication. This method of spectrum sharing mainly aims at interference mitigation. This method needs information about the primary's waveform and codebook in details, in addition to channel information of primary and secondary.

The CR can be thought of as a flexible SDR which is envisioned to be a solution that improves the spectrum utilization [4], [107], [111]. Generally, the CR is a generic term used to describe a radio that is aware of the radio environment around it and can adapt its transmissions according to the interference it sees. Some of the defining characteristics of CR are agility and cognition for coexistence, through cooperation. One of the definitions for CR according to [69] and publications [67], [78], [140], [151] is: "Cognitive radio is an intelligent wireless communication system" where "intelligence" can be thought of as the capability to analyze and understand the radio environment, namely the radio channel conditions, radio spectrum of operation, waveforms and codebooks and the messages of other radio systems that co-exists in the same spectrum in which it operates.

Cognition is not a new concept in wireless communications. In a wireless communication system, essential information describing the radio environment, like the wireless channel condition, modulation types, transmit and received power, usage of available radio resources, etc., can be usually obtained by sensing the surrounding wireless environment from received signals or it can be explicitly signaled to the receiving end. Techniques like channel estimation and sensing the presence of other users, can be seen as elementary forms of applying cognition in wireless networks. CRs further this idea of cognition to enable dynamic spectrum access, so that the temporal and spatial variation in the spectrum utilization can be exploited for enhancing its usage. While DSA is the goal, the spectrum usage etiquettes need to still be observed by the CR [32].

1.2 Objectives and Scope of the Thesis

In this thesis, the focus is mainly directed towards overlay cognitive approach, with high power primary transmission present in the frequency channel used by the CR. This is also known as black space cognitive radio (BS-CR) [69]. Traditionally, one of the efficiency metrics of any wireless communication system is spectral efficiency. Spectral efficiency can be seen as the number of bits that can be communicated per channel use. It is well known that the efficiency of spectrum utilization is a function of channel attenuation, noise in that channel and the interference from the other transmissions using the same channel. Huge amounts of time and effort have been spent in research to improve the spectral efficiency, especially, by designing innovative waveforms and signal processing. Multi-antenna systems and large antenna arrays are important recent additions to the traditional selection of such tools. They aim at improving spectral efficiency by increasing the signal to interference and noise ratio (SINR) or by cancelling the interference between various simultaneous channel uses or transmissions.

In this thesis, especially, we work on multi-antenna interference cancellation-based BS-CR using various signal processing methods. Even though the CR methods are applicable for many different primary systems like WLAN and cellular systems, we focus on the terrestrial television spectral bands and TVWS as an application area to test and explore the algorithms considered in this thesis.

One of the best ways to aggregate the available transmission opportunities for CR is by using multicarrier communication methods. Of the various multicarrier

techniques that are available, in this thesis, orthogonal frequency-division multiplexing (OFDM) based multicarrier methods [38], [118], [149] are primarily studied and used. Additionally, enhanced multicarrier techniques such as filter bank multicarrier (FBMC) methods [15], [16], [23] [124], [137] are explored as an alternative to OFDM. Actually, the second topic of the thesis is investigating the benefits of FBMC versus OFDM in case of interference avoidance, i.e., the interweave CR paradigm. In this part we consider resource allocation in the presence of adjacent channel interference (ACI) leakage between primary and secondary systems due to imperfect spectrum localization and transmitter power amplifier (PA) nonlinearity. Other important enhanced multicarrier waveforms, especially in the 5G and beyond context, include windowed OFDM (known as WOLA) [14], [105], [148], [154] and filtered OFDM [57], [88], [101], [124], [156]. We find that many of our results and conclusions on the proposed interference avoidance and interference cancellation techniques are applicable also with these waveforms, as shown in [P1], [48] for the interweave scenario.

The main objective of this thesis is to study and analyze existing CR techniques and newly develop CR algorithms for interference cancelation and interference avoidance in order to answer the following questions:

1. Interference cancellation in BS-CR systems: How well can the secondary receiver adapt to the very strong primary interference and which algorithms are the most effective for the secondary receiver? In the process of answering this question, we have developed enhanced interference cancellation algorithms using multiple antenna techniques that can enable the design and practical implementation of enhanced interference cancellation-based receivers.

2. Concerning both interweave and BS-CR schemes, how do the transmitter and receiver impairments, especially the RF and front-end impairments, impact the performance of such algorithms? The role of carrier frequency offset (CFO), power amplifier nonlinearities, as well as receiver nonlinearities and quantization effects in ADC are considered.

3. Interference avoidance in interweave CR systems: Can spectrum localization of secondary transmission improve cognitive wireless communication performance under ACI? Can proper resource allocation strategies help to improve the wireless transmission under ACI?

1.3 Thesis Contribution and Structure

In achieving the above objectives, we develop models, methods, and enhanced algorithms. These proposed methods are simulated and evaluated to ensure their performance, reliability, and suitability in practice.

- In Chapter 2, we discuss CR technology, specifically overlay CRs in the context of BS-CR, particularly explaining the use of black spaces, which are occupied by PUs as high-power interferers. We explain the principle and use of multi-antenna-based interference cancellation, analyze the signal-to-interference ratio (SIR) in the basic BS-CR scenario based on the PU and CR transmission powers and path losses. This chapter's contents are partially based on the publication [139] where the basic multi-antenna-based BS-CR scheme is proposed and developed.
- In Chapter 3, an enhanced interference cancellation method with spatial covariance matrix interpolation-based, interference rejection combining (IRC) for BS-CR is developed and the resulting performance is evaluated with mobility. The contents of this chapter are based on the publication [P3], [P4], and [139]. [P3] presents an initial study with sub-optimal resource allocation process, also ignoring the interference leakage from CR to PUs, while [P4] presents a comprehensive study on the topic. Here we develop the enhanced interference cancellation model and elaborate the utilization of silent gaps and spatial covariance interpolation in the IRC process.
- In Chapter 4, the effects of RF impairments, such as PA nonlinearities, CFO issues, receiver nonlinearities, and ADC quantization effects on the interference cancellation algorithms are studied. This chapter's work is based on the publication [P5]. The studies of Section 4.4 on the effects of receiver nonlinearities and quantization in ADC have not been published elsewhere.
- In Chapter 5, the waveforms that could be used in the CRs are explored, especially in the context of joint resource allocation and spectrum sensing as applied to the interweave type CR systems. Detailed performance analysis is completed on OFDM and FBMC based multicarrier methods for CR systems. This chapter's contents are due to [P1], [P2], and [52]. [P1] presents

an initial study with sub-optimal resource allocation process, also ignoring the interference leakage from CR to PUs, while [P2] presents a comprehensive study on the topic.

- Chapter 6 summarizes the thesis and lists the directions for further studies.

This thesis work summarizes the methods, algorithms and techniques investigated primarily in [P1]-[P5]. For detailed analysis, elaborate treatment of the topics and thorough discussion of the results kindly refer to the publications listed above. The publications [P1]-[P5] were partly based on the learnings and work done by the author in publications [48], [52] [138], and [139], even though they are not included in this thesis.

1.4 Authors Contribution to the Publications

Altogether, most parts of this thesis are based on the works reported in publications which were all carried out at the Electrical Engineering unit of the Faculty of Information Technology and Communication Sciences, Tampere University, Finland. From the technical contributions, the contents of Section 4.4 on receiver nonlinearity effects have not yet been published elsewhere. The author of the thesis is the first author and main contributor in publications [P1], [P3], [P4] and [P5]. In the [P1] the initial idea was proposed by Prof. Markku Renfors and further developed by the author of the thesis along with Dr. Sener Dikmese. In [P2] the resource allocation idea was suggested, formulated, and simulated by the author of the thesis, partly based on earlier studies by Dr. Musbah Shaat and Prof. Faouzi Bader in [134]. Dr. Sener Dikmese along with Prof. Markku Renfors suggested and helped to combine the spectrum sensing and the resource allocation parts. In [P3] & [P4] the author of the thesis performed the mathematical analysis, system simulations and results formulation based on the ideas and inputs given by Prof. Markku Renfors. Dr Sener Dikmese greatly helped with refining covariance estimation and provided extensive feedback on the writing of the publication. In [P5] the author carried out the formulation of the issue and ran extensive system simulations based on the inputs from Prof. Markku Renfors. Dr. Sener Dikmese helped in the proper modeling of the power amplifier and with the writing of the publication. In [P2], on resource allocation and spectrum sensing, the technical contents and presentation were equally contributed by the Author and Dr. Sener Dikmese, and this publication is

included also in Dr. Dikmese's thesis. Dr. Sener Dikmese is a co-author of [P1], [P2], [P4] and [P5] and has collaborated in the research on spectrum sensing, interference cancellation and filter bank-based methods. The thesis supervisor Prof. Markku Renfors is a co-author of all publications and made valuable contributions regarding the technical contents and presentation.

2 COGNITIVE RADIO SYSTEMS

The CR systems rely on the idea of spectrum reuse as discussed in the previous chapter. The idea of spectrum reuse is not new and has been a well-established concept in the areas of cellular network planning [106]. Static spectrum reuse is a well-known and well understood concept in wireless cellular systems. One of the biggest limitations that previously prevented the dynamic reuse of cellular spectrum is the inflexibility in configuring the radio hardware dynamically so that it can adapt to its radio environment. With the emergence of SDRs and circuit design technology and architectures [29], [56], [116], [120], [122], [126], [160] that allow practical implementation, real-time frequency, transmission parameter, and waveform changes can be made on the fly by higher layers in a wireless communication system. Apart from this, there has been several advances in the areas of analog and digital RF hardware required for the CR, such as effective algorithms which are needed at the baseband and digital front-end, high sampling rate capability, high resolution analog to digital converters (ADCs) with large dynamic range, and high-speed signal processors. With the evolution of technology and the advent of better processors and other systems such as the 5G/6G wireless systems, such capabilities are prevalent in both the baseband processing and the RF electronics these days.

According to [69], the primary functions performed by CRs can be broadly classified as the functions done at the transmitter and receiver:

- The radio-scene analysis and channel identification are usually done in the receiver of the CR system.

- The dynamic spectrum management and power control are done in the transmitter side of the CR system.

During the radio-scene analysis, the CR estimates the interference temperature and detects the spectral holes. Both these tasks are dynamic and adaptive in nature. Even though they are performed by the receiver, these activities are essential for the transmitter to adapt its signal transmission. The receiver, through the process of

feedback, provides this information to the transmitter. This feedback information about the spectrum and the channel is very useful in many transmitters related actions, like understanding the time-frequency characteristics of the primary signal & spectrum, transmit power control, adaptive beamforming for interference cancelation, and resource allocation.

The RF environments in the present day are heavily transmitter centric [77]. The transmission power and its spectral characteristics are designed in such a way that the transmitted power attains a predefined noise floor for a given distance. This is generally known as the "radio signal coverage". The coverage situation changes if there is interference, in addition to the common channel degradation processes like path loss, fading, and thermal noise [68], [118]. The most important metric defined in the CR research community, to quantify and measure interference is the interference temperature [67], [108]. This metric can be used to characterize and manage the sources of interference. The term interference temperature limit [1] can be used to define the worst-case RF environment in a frequency band and in a geographical location in which a transmitter can function without causing additional performance degradation. It can also be viewed as the additional margin available for cognitive or secondary systems in terms of the RF energy that can be introduced by the secondary system without introducing any performance degradation to the primary receivers. In CRs and more generally radio signals are non-stationary. Due to the non-stationarity of the radio signals generated by the transmitters [69], the time component is included in the analysis of such signals. The time-frequency analysis of signals and extensive results on this topic can be found in [39], [141] and references therein. Given the nature of CR as a receiver centric system, efficient spectrum and interference estimation is very crucial for the reliable functioning of CR. Passive sensing of the RF-scene based on the spectra is classified into three broad categories as follows [69]:

- White spaces in spectrum are generally free of any interfering transmission such as primary or other CR transmissions and contain only the thermal noise and possible other natural sources of radio noise.
- Black spaces in spectrum which are occupied by high-power local interferers, at least some part of the time over the expected channel access period.
- Grey spaces are partially occupied by low-power interferers.

Generally, in the CR literature [19], [66], [67], [75], [76], [78] the whitespaces and grey spaces are recommended to be used, but the black spaces are generally not as interesting as the white and grey spaces due to the high-powered nature of the primary signals. Given that the CRs' resources are functions of the triplet time, frequency, and location and when the geographical locations of the primary and secondary are considered, black spaces become very interesting especially in the terrestrial TV bands [17], [26], [133], [128], [129]. In this thesis, the primary concern is about overlaying a CR system on a digital TV frequency channel.

2.1 Cognitive Radios in Television Spectrum

TV transmitters are high-powered broadcast transmitters, transmitting TV signals to a large geographical area. Given the high-powered nature and the large areas that these transmitters cover, they are usually far apart from each other. This is done deliberately to ensure that there is limited or no cochannel interference. By design, the TV network and receiver are designed to withstand certain amount of cochannel inference. There is also a frequency separation between geographically close transmitters, to further reduce any possibility of the cochannel interference. This encourages us to use secondary systems that share the TV bands in such a way that they are not adding to the interference and affecting the TV reception. The SINR for any wireless receiver and in particular TV receivers [127], [128] can be given by the formula

$$SINR = \frac{P_{rx}}{\sum_k I_k + P_n} \tag{2.1}$$

where P_{rx}, P_n and I_k are the received power, thermal noise power and interference power from other cochannel interferers, respectively. A detailed discussion on the digital TV's performance and characteristics can be found from [5].

We are particularly focused on the case where the CR is operating in the same frequency channel as the digital TV transmission. We refer to this type of simultaneous usage of the same frequency channel as the primary TV signal as "TV black space". This contrasts with the TVWS where secondary or cognitive transmission is allowed only when there is no primary transmission. An extensive

study of CR in TVWS is done in [128]. TVWSs have a disadvantage that they are mainly available in the rural areas where the population density is lower and hence have lower demand for wireless communications. Therefore, black-space transmission becomes attractive option in areas with higher population density, where also the terrestrial TV signal levels are usually high. Feasibility of such BS-CR in the TV band with cellular mobile network as the secondary service is studied in [17], [26], [129] and [133].

2.2 Capacity of Cognitive Networks

A generic communication channel is usually characterized by its probabilistic nature and modeled by the conditional probabilities of inputs and outputs. Such a characterization leads to the notion of fundamental limits of communication that is possible through the channel. There are many metrics that can be used for expressing these fundamental limits. One of the well-known and useful metrics is the capacity of the channel. Capacity is defined as the supremum over all rates for which reliable communication may take place [135], [136].

$$\mathrm{C} = \sup_{\mathrm{p(x)}} \mathrm{I(X;Y)} \tag{2.2}$$

where supremum is taken over all possible probabilities of the input X, $p(x)$.

Any simple communication system can be modeled by the affine equation as follows:

$$r(n) = \sqrt{P} g \cdot x(n) + \eta(n) \tag{2.3}$$

in which the received signal is a scaled version of transmitted signal with additive white Gaussian noise (AWGN), where $x(n) \in \mathbb{C}$, is the complex baseband equivalent of the transmitted signal $P, g \in \mathbb{R}^+$ where P and g are the transmitted power and the channel gains respectively, and $\eta(n) \epsilon\, \mathbb{C}$ is the complex AWGN sequence. For the AWGN channel, the capacity achieving distribution is shown to be circular Gaussian distributed signal [135], [136].

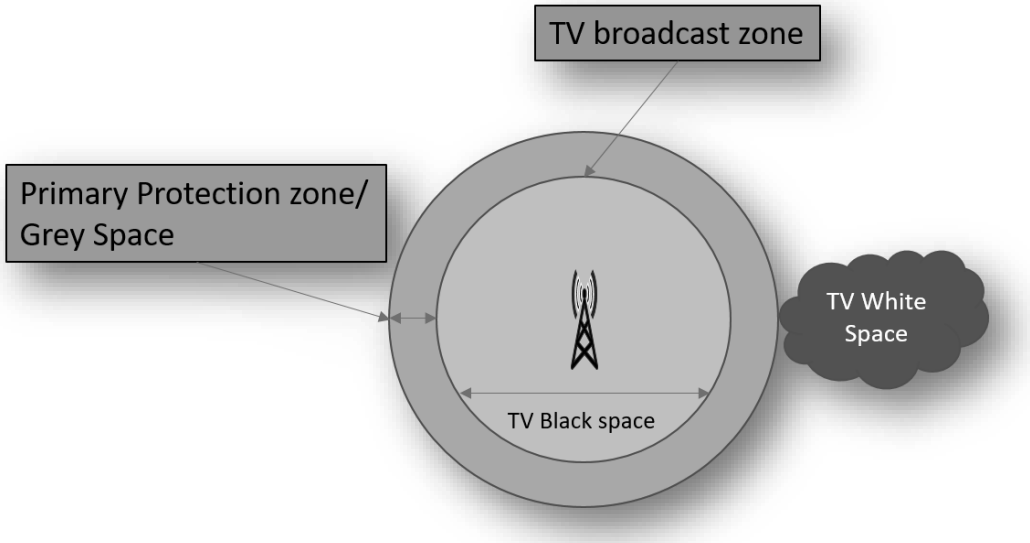

Figure 1. TV broadcast and secondary access regions.

The maximum capacity in bits per transmitted symbol for the AWGN channel with channel bandwidth B is given by

$$C = B\log_2(1 + \frac{P_\mathrm{s}}{BP_\mathrm{n}}), \tag{2.4}$$

where P_s and P_n are the signal and noise power, respectively. In OFDM-based multicarrier communication systems, each subcarrier is flat-fading and follows the AWGN channel capacity expression. With practical multipath channel models, linear convolution of the transmitted signal with the channel impulse responses is used instead of the gain factor in Eq. (2.3). In OFDM, the capacities of different subcarriers are different, and the overall capacity is obtained as the sum of capacities of active subcarriers. The same model applies approximatively for FBMC systems.

While channel capacity is fundamental in nature to the study of information theory, finding the capacity of practical mobile channels is challenging. Usually as an alternative, achievable rates and outer bounds are readily available for various channels in [55], [93], [94] and the references therein. In CR context, the cognition of primary can be used as side information and the achievable capacity regions can then be plotted [43]-[46].

Generally, in wireless communication networks, and specifically in CR networks, there are multiple transmitters and receivers. At any given point in time, it is very likely that there are multiple communication links active simultaneously. This leads to some additional terms in the Eq. (2.3) and it changes into

$$r(n) = h_T(n)x_T(n) + \sum_{l=1}^{L} h_l(n)x_l(n) + \eta(n). \quad (2.5)$$

Here $r(n)$ is the received signal, $h_T(n) = P_T g_T(n)$ is related to target transmission and $h_l(n) = P_l g_l(n)$ is related to the interference from the primary and other cochannel interferers. In this thesis publications, we start with an assumption that the there is only one interfere, namely the primary transmission, and later generalize the discussion to multiple interferes, mainly considering also possible other co-channel CR systems.

2.2.1 Interference Channels in Cognitive Radios

As discussed in the previous chapter of this thesis, we have three CR paradigms that are well known, the overlay, the underlay, and the interweave approaches [67], [78], [151]. This thesis largely focuses on the overlay approach which is interesting scenario because the primary system is transmitting all the time and the CR is within the same region of coverage as the primary. The foundation for analyzing two user channels originate from the seminal works of [130], [131] later expanded to multiple users in the celebrated paper [31]. In the basic interference channel, as shown in Figure 2 , we have two transmitters and two receivers, and more generally, there are multiple transmit-receive pairs communicating in the presence of mutual interference. This means that transmission of each user's message is affected by the channel perturbations which are random in nature and affect the interference power received from the other users.

Although the information theoretic view of CRs and their analysis are foundational, the research topics of this thesis are more towards the signal processing aspects of CRs. A concise summary of the information theoretical topics

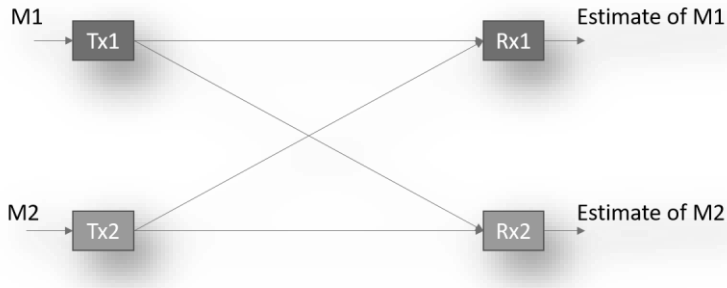

Figure 2. Basic interference channel.

can be found in [19], [31], [43]-[46], [83], [130]. Detailed discussion and survey of cognitive information theoretic topics can be found in [43]-[46], [65], [84], [86], [112].

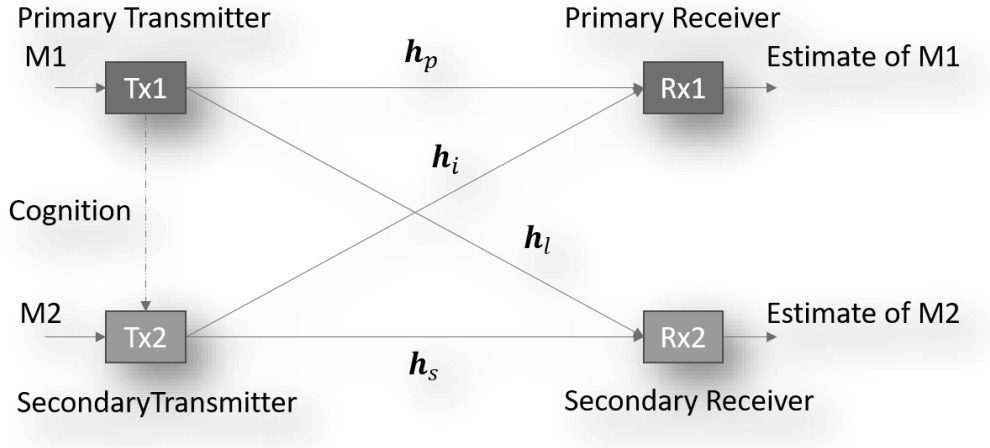

Figure 3.Cognitive interference channel.

The basic interference channel, when applied in the CR context, changes to the form shown in Figure 3. As can be seen in [43], the cognitive channel is the same as the two-user interference channel with the additional knowledge of the waveform and the power that the primary is transmitting. This knowledge or cognition can be translated into knowledge about interference that the secondary or the cognitive transmission will encounter. The achievable rate region for such CRs is derived in [43]. Network aspects of cognitive radios can be found in publications [26], [33], [76], [84], [96].

Practical CR setups mainly must handle the interference in two directions: the interference that emanates from the CR to the primary and, on the other hand, we have to combat the interference that comes from PU to the CR. Of course, when multiple CR systems are operating in the same region, we have the CR-to-CR interference which can be treated as multiuser interference and handled in the receiver with sophisticated signal processing. The interference that comes to the primary due to CR is measured using the interference temperature metric [108]. As a digression from traditional transmitter centric approaches that seek to regulate interference indirectly by controlling the emission power, geographical locations of interfering transmitters, or time, the interference temperature model takes a receiver-centric approach and aims to directly manage interference at primary receivers through interference temperature limits. These limits characterize the worst-case interference scenario that is permissible towards a PU in each geographical location and in its frequency band of operation. Several practical models of such interference are presented in [26], [33], [34], [74] and [97]. The interference to the PU can be avoided by ensuring that the secondary system transmission does not influence the primary connections at all, for example, by making the primary and the cognitive transmissions orthogonal to each other. Or by making sure that the link degradation due to the introduction of the cognitive transmission is small enough that the primary link does not suffer in quality. This way of working is widely known as the "underlay approach" [67], [69], [151]. This is also the simplest approach as the knowledge of the primary transmission parameters are not essential.

The last way is to ensure the primary link quality that is to make CR system cooperate with the primary system and amplify the primary connection quality using a fraction of the CR's transmission power to retransmit the primary signal [19], [69], [128], [129], [151]. Then, the interference from cognitive signal transmission brings up the quality at least to the minimum required level, ensuring the primary connection target quality.

For the interference from the primary towards the CR network, as already discussed, the CR receivers use passive sensing techniques to measure the impact of primary signals on the CR reception. The power spectral density (PSD) of the interfering primary signal determines if spectrum is black space, whitespace, or a gray space. Such classifications of the spectrum are very crucial and essential for the cognitive receiver to assess its interference. Theoretical models for such

classifications are developed and discussed in [75]. Figure 1 illustrates the regions of black, grey, and white spaces in a TV transmission scenario.

2.2.2 Managing & Mitigating Interference in Cognitive Networks

In cognitive networks, effective interference management is essential for its coexistence with the primary networks. CR networks are not supposed to cause any significant interference to the primary system [76]. To this end, interference management becomes an important consideration in CR networks. Interference management can be handled in CR networks using various ways like signal processing at the physical layers, radio resource management in the medium access control (MAC) layer, and through the radio network planning and other system design aspects [117]. In Chapter 3 of this thesis, we focus on the interference cancellation aspects at the physical layer, while ACI management in interweave CR systems is considered in Chapter 5.

Interference in wireless communication can be handled at the transmitter and/or at the receiver. Most of the interference avoidance and interference alignment schemes are transmitter oriented, while the interference cancellation schemes are receiver oriented. The idea of interference avoidance is to be proactive and avoid interfering with other users using techniques such as the transmitter precoding or beamforming to steer the transmission in such a way that the interference victim is in the null space [12]. Under the interference cancelation (IC) schemes, there are many well-known techniques, such as [13], [97]:

- Using an adaptive scheme, like Wiener filtering, to filter out the interfering primary signal in the CR receiver.
- Using some transform domain characteristics of the interfering signal to eliminate it in the receiver; or using statistical properties of interference signal, that vary periodically over time, for filtering them out from the received signal; or use higher order statistical difference (usually, statistics of order greater than two) between the target signal and the interference to eliminate the interference.
- In certain scenarios, a receiver may manage the interference by detecting first the dominant interferer signal and cancelling it from the received signal, before detecting the target signal. Such schemes are considered in

the BS-CR approach of [17], [129], and [133] and for device-to-device (D2D) communication underlaying a cellular network in [158] and [159].

- There is also the idea of receiver beamforming, where the receiver uses multiple antenna signals, which are weighted differently, so that the received signal from a particular direction is emphasized in comparison to other directions [92]. As an application and extension of this case, we introduce the multiantenna IRC method in the next section.

2.3 Multiantenna Based Interference Rejection Combining

Generally, interference rejection through receiver antenna arrays has been well studied in [13], [35], [42], [54], [70], [90], [91], [97], [114], [115], [150], [159] and the references therein. In multiuser scenarios like the BS-CR, for a detector to be optimum under interference, it must be a multi-user detector [146]. The overriding constraint to this fact is that such optimum detectors require sufficient information about other users, such as modulation order and radio channel propagation characteristics, and are therefore highly complex. An implicit interference cancellation technique, like IRC, which eliminates some of the above requirements, becomes attractive in these situations.

The use of multiple antennas in CRs has been considered in earlier studies, for example in [12], [13] and [150]. These systems reduce the effects of the channel by forming a linear combination of multiple copies of the received signal, obtained through different antennas, and thereby improve the detection of the transmitted signal. The use of multiple antennas allows for spatio-temporal signal processing, which improves the detection capability of the receiver under fading multipath channel and interference. Various other methods of interference cancellation are found in [13], [91] and [97].

Motivated by this, in [P3], we study the interference rejection capabilities of multi-antenna CR receivers, focusing on the performance of the well-known linear minimum mean square error (LMMSE) [103] based IRC [11], [13], [42], [70], [90], [91], [115], [123] and [143]. Recently, IRC has been considered widely especially in the context of LTE and 5G new radio (NR) networks [35], [42], [115], [123] and [143]. However, to the best of our knowledge, it has not been applied to the BS-CR scenario before [138] and [P3]. IRC can be used in cases of both CCI and ACI. ACI

rejection helps in utilizing whitespace more effectively, while CCI rejection forms the foundation for black-space CR.

2.4 SIR Analysis

SIR analysis is fundamental for CRs. The critical parameters in BS-CR operation are the SIRs at the CR and PU receivers. In the basic scenario with PU interference only, the SIRs can be expressed in dB units as follows:

$$SIR_{\mathrm{CR}} = (P_{\mathrm{CR}} - L_{\mathrm{CR-CR}}) - (P_{\mathrm{PU}} - L_{\mathrm{PU-CR}}) \quad (2.6)$$

$$SIR_{\mathrm{PU}} = (P_{\mathrm{PU}} - L_{\mathrm{PU-PU}}) - (P_{\mathrm{CR}} - L_{\mathrm{CR-PU}}), \quad (2.7)$$

where P_{CR} and P_{PU} are the transmission powers of CR and PU, respectively, in dBm units, while the other parameters, such as $L_{\mathrm{PU\text{-}CR}}$, are transmission losses in dB units of relevant transmission links. The first part of the subscript indicates the transmitter and second part the receiver of the corresponding link. From these equations, it is straightforward to derive the maximum SIR of the CR receiver in terms of the minimum SIR of a PU receiver, $SIR_{\mathrm{PU,min}}$:

$$SIR_{\mathrm{CR,max}} = (L_{\mathrm{CR-PU}} - L_{\mathrm{CR-CR}}) + (L_{\mathrm{PU-CR}} - L_{\mathrm{PU-PU}}) - SIR_{\mathrm{PU,min}}. \quad (2.8)$$

The maximum SIR of the CR link depends on the differences of the channel losses from CR TX to both receivers and from PU TX to both receivers. For example, if the losses of the main links (CR-CR and PU-PU) are equal to the losses of the corresponding interfering links (CR-PU and PU-CR), then the CR RX would be able to operate with the SIR of $-SIR_{\mathrm{PU,min}}$. If the main link losses are lower than those of the interference links, the $SIR_{\mathrm{CR,max}}$ would be higher. The critical cases are:

1. If the losses of the main links (CR-CR and PU-PU) are much higher than the losses of the corresponding interfering links (CR-PU and PU-CR), then SIR of the CR receiver may be limited by the minimum acceptable PU SIR to a highly negative value.
2. If the PU transmitter is very close to the (short-range) CR system, then

$$SIR_{\mathrm{CR,max}} = P_{\mathrm{CR,max}} - L_{\mathrm{CR-CR}} - (P_{\mathrm{PU}} - L_{\mathrm{PU-CR}}). \quad (2.9)$$

Then the SIR of the CR receiver may be limited to a highly negative value by the maximum transmit power of the CR device, which could be much lower than that of the PU transmitter.

In both cases, the performance of the IRC scheme would be limited by the RF imperfections (e.g., receiver nonlinearity effects) in practice. The latter limitation appears especially in the TVWS application, but in rather limited geographical regions. Considering the first kind of limitation in the worst-case scenario, one should consider the hidden node margin (typically around 25-30 dB in the TVWS case [8] for the loss difference from PU ($L_{\mathrm{PU-PU}} - L_{\mathrm{PU-CR}}$), which would lead to very low SIR for the CR TX, unless the loss from the CR to the PU RX can be guaranteed to be much higher than that of the CR link. On the other hand, in short-range CR communication, especially if PU receivers would use directive (possibly roof-top) antennas, the mentioned case where the SIR of CR RX is no less than $-SIR_{\mathrm{PU,min}}$ should be possible. Then, if the CR system is able to operate with SIR_{CR}=-30 dB (which can be considered feasible for IRC based BS-CR based on the results of Chapter 4), then the SIR of the PU link would be no less than 30 dB. Generally, the CR TX should have knowledge of the link losses in order to maximize its transmission power while not causing excessive interference to the PU link. The physical layer capabilities of IRC based BS-CR, and detailed procedures for controlling the CR operation remain as a topic for future studies. One possible way to enhance BS-CR operation would be cooperative spectrum sensing of CR devices to reliably estimate the PU power level in the CR operation region. Since the BS-CR is assumed to utilize multicarrier waveform, it can choose to operate on a partial frequency band of the PU signal, on strong subcarriers where the safely achievable SIR of the CR link is maximized.

3 ENHANCED INTERFERENCE CANCELLATION FOR BS-CR

There are various scenarios and radio conditions in which CRs could be implemented. Advanced signal processing algorithms have been used at the transmitter and/or at the receiver end of the CR link to enhance the communication performance. In this chapter, we consider the CR receiver-based signal processing methods that enable it to successfully operate under higher levels of interference from primary networks. Considering a CR receiver operating in a given frequency band, it first performs primary signal sensing and identifies the band as a white, grey, or black space. Based on the sensing results, the CR receiver can then choose to apply corresponding advanced signal processing techniques to obtain optimized performance. Even though various alternatives are possible for any given situation, the BS-CR operation is the topic of interest in this chapter.

BS-CR is a CR that deliberately transmits simultaneously along the primary signal at the same time-frequency resources without causing objectionable interference. An underlay CR is ignorant about the existence of PUs in its frequency band. Commonly, it uses very low PSD and wide bandwidth, such that it does not cause interference to the PU transmission under any conditions [67], [69], [144], [151]. BS-CR adapts its waveform and signal parameters depending on the on-going PU transmissions and uses advanced signal processing techniques on the receiver side to facilitate low SIR at the receiver. BS-CR systems effectively reuse the spectrum for communication over short distances as illustrated in Figure 4.

It can operate with limited spectrum resources and can be used without any additional spectrum sensing. One of the major requirements for CR operation is to minimize the interference to the primary transmission system. In BS-CR, this is reached by setting the CR transmission power at a small-enough level. Theoretically, the most important factor that enables such a radio system is that stronger interference is easier to deal with as compared to weaker interference [31], [43] if proper interference cancellation techniques are utilized. Previous studies on this from information theory provide theoretically achievable bounds for such CRs [43],

[44], [46]. To improve the sensitivity of the CR receivers and to enhance signal reception under interference multi-antenna systems could be used. Multi-antenna systems allow for spatio-temporal signal processing, which not only improve the detection capability of the receiver, but also improve performance in fading multipath channels with interference [19], [68], [114], [150].

3.1 BS-CR in Terrestrial TV Bands

In the scenario considered here, the CR operates within the frequency band of the PU, the terrestrial TV frequency band. The PSD of the PU is very high in comparison to the CR. The PU is assumed to be always present and transmitting when the secondary user is operating. The primary transmitter is usually the dominant interfere to the cognitive transmission. The CR in this case operates closer to the noise floor of the primary receiver, and due to this the primary communication link is protected. If the TV channel becomes inactive, this can be easily detected by each of the CR stations in the reception mode. Then, the CR system may, for example, continue operation as a spectrum sensing based CR system. We focus on a scenario with multi-antenna CR receiver having IRC capability to mitigate CCI generated by a single PU transmitter and multiple independent (uncoordinated) CR systems. Generally, interference covariance matrix estimation is a key element of IRC schemes. For this purpose, we propose to use sample covariance calculated from the received signal during silent periods (gaps) in the target CR transmission.

Figure 4, we especially consider frequency reuse over small distances, such as an indoor CR system. The multi-antenna configuration studied here is that of single-input multiple-output (SIMO). Here the PU is an OFDM-based DVB-T system. The CR system is also an OFDM based multicarrier system similar to 802.11af [58] but with different OFDM numerology. Both the primary and the CR systems use M-QAM subcarrier modulation. The cognitive transmitter is assumed to have a single transmit antenna while the CR receiver terminal is assumed to have multiple receiver antennas.

In the basic scenario, the received CR signal consists of contributions from both the desired CR communication signal and the primary transmission signal (constituting the interference), which are received through different block-fading multipath channels.

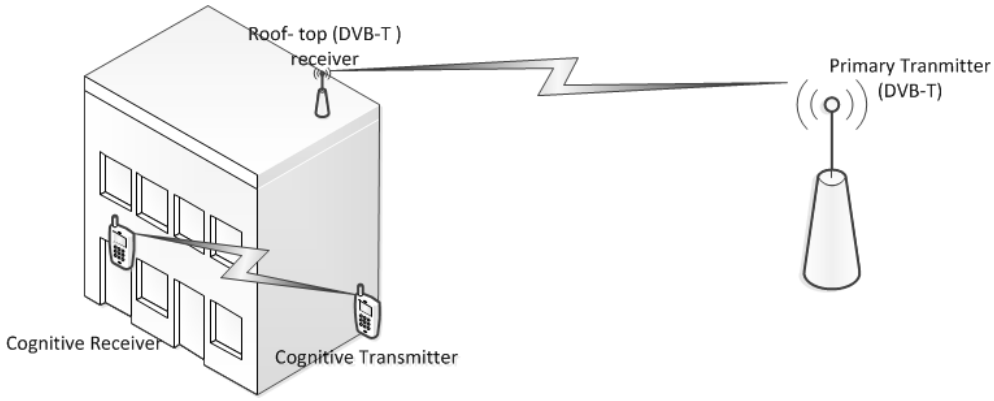

Figure 4. Set up of black-space CR in TV spectrum.

A block-fading channel model assumes that the fading is constant for a pre-defined number of symbols called "a block". The fading process is also assumed to change independently from one block to another. We also consider scenarios where there are other CR systems introducing additional interference to the target CR transmission.

3.2 IRC for Black-Space Cognitive Radio

The IRC receivers have the significant advantage in comparison to the other receivers. Especially, in multi-user scenarios that they do not need detailed information about the interfering signals, such as modulation order and radio channel propagation characteristics. For CR scenarios, IRC receivers in general are simple and desirable compared to optimum detectors. IRC techniques and algorithms are widely applied for mitigating CCI, e.g., in cellular mobile radio systems like 5G and LTE-A [42], [115]. The IRC algorithm makes a linear combination of the CR receiver antenna signals in such a way that the PU interference is cancelled [54], [90], [91], [150] and the SIR of the target CR signal is maximized. This process also implements subcarrier-wise channel equalization for the CR link. Generally, IRC can cancel interference from multiple sources. This is useful in situation where other nearby CR systems are introducing interference to the target CR link, in addition to the PU. $L + 1$ antennas are needed at the CR receiver to cancel interference from L sources with different spatial channels. If N is the number of CR receiver antennas, then $N - L$ is the diversity order of the CR transmission. It is assumed that the target

CR transmission is silent while observing the (noisy) interference signal(s) for IRC weight calculation.

The following developments are presented at the subcarrier level of the target CR system. For the CR transmission link, block-fading channel model is assumed, and frequency-flat subcarrier model is valid as CP-OFDM based CR system is assumed. CR systems use the same OFDM numerology as PU and operate quasi-synchronously, meaning that the CP length is sufficient to cover the channel delay spread in the presence of timing offsets. Ideally, there are no frequency offsets between the target CR and interfering transmissions. The effects of CFO analysed in Chapter 4. The CR receiver is synchronized to the PU transmission, but the subcarrier spacing is assumed to be small enough such that the flat-fading model applies also to link from the PU transmitter to the CR receiver. The CR transmitter is assumed to cause some negligible interference to the primary transmission system [97]. However, the secondary transmission system experiences huge interference due to the strong PU. The challenge from the CR perspective is to effectively communicate under severe interference due to the primary transmission. The transmitter is assumed to transmit in a subcarrier an M-QAM symbol x_T through the channel $\boldsymbol{h}_T$ to the receiver antennas. The receiver is assumed to use N receive antennas and therefore the received signal $\boldsymbol{r}$ is an $N \times 1$ vector

$$\mathbf{r} = \mathbf{h}_{\mathrm{T}} x_{\mathrm{T}} + \sum_{l=1}^{L} \mathbf{h}_{\mathrm{I},l} x_{\mathrm{I},l} + \boldsymbol{\eta}. \tag{3.1}$$

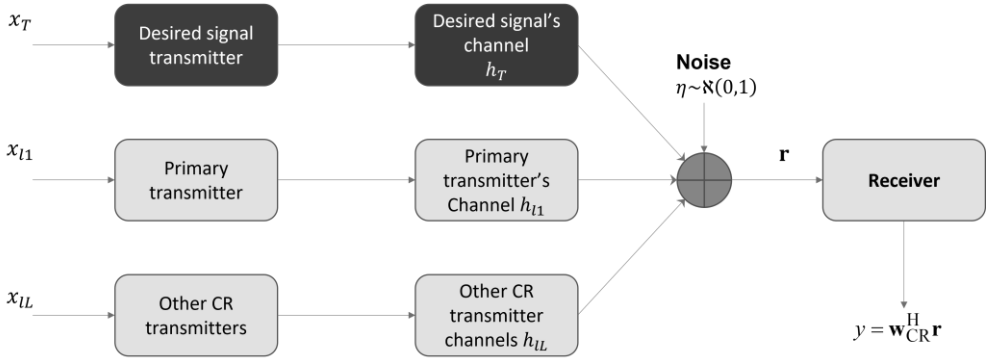

Figure 5. System model for the BS-CR link at subcarrier level.

Here $\mathbf{h}_{\mathrm{T}} = \left[h_{\mathrm{T},1}, h_{\mathrm{T},2}, \ldots, h_{\mathrm{T},N}\right]^{\mathrm{T}}$, $x_{I,l}$ is the lth interfering signal, and $\mathbf{h}_{\mathrm{I},l} = \left[h_{\mathrm{I},l,1}, h_{\mathrm{I},l,2}, \ldots, h_{\mathrm{I},l,N}\right]^{\mathrm{T}}$is the channel vector for the lth interferer. The channel vectors consist of the complex channel gains from the corresponding transmit antenna to nth antenna of the CR receiver. Finally, $\boldsymbol{\eta}$ is the AWGN vector. In this generic system model, it is assumed that the PU is the dominant interferer, and the other interference sources are other CR systems introducing CCI at relatively low power level. The overall interference to the CR is still very high and under such circumstances the channel estimation process for the target CR is not possible. So, the interference covariance matrix is estimated during silent gaps in the target CR transmission. The proposed algorithm [P4] extracts from the received signal a set of signals which span the interference-free subspace in spatial domain. The weight vector for the target CR signal is based on pilot-based target channel estimation in this subspace. The target CR link performance is very sensitive to the quality of the interference covariance estimate. Therefore, linear interpolation is used for the interference covariance matrix to track the channel variations between consecutive interference covariance estimates, obtained during the consecutive silent gaps. The use of multiantenna interference cancellation techniques in the CR receiver helps to mitigate CCI generated by a single PU transmitter and multiple independent (uncoordinated) CR systems. The algorithm is portrayed in Figure 6 and explained in detail in [P4].

3.2.1 Covariance Matrix Estimation

As it is illustrated in Figure 6, the interference minimizing IRC weights are obtained during a silent period in the target CR transmission, while the CCI sources are active. Due to that, Eq. (3.1) can be modified during silent gaps of CR operation as

$$\hat{\mathbf{r}} = \sum_{l=1}^{L} \mathbf{h}_{\mathrm{I},l} x_{I,l} + \boldsymbol{\eta} \,. \tag{3.2}$$

Here it is assumed that only interferences and noise are present during the silent period in the signal $\hat{\mathbf{r}}$ observed by the CR. Linear combiner is used for the signals from different antennas with a weight process in detection as follows:

$$y = \mathbf{w}^{\mathrm{H}}\mathbf{r} \,, \tag{3.3}$$

where y is the detected signal, $\mathbf{w}$ is the weight vector with N elements, and superscript H denotes the Hermitian (complex-conjugate transpose).

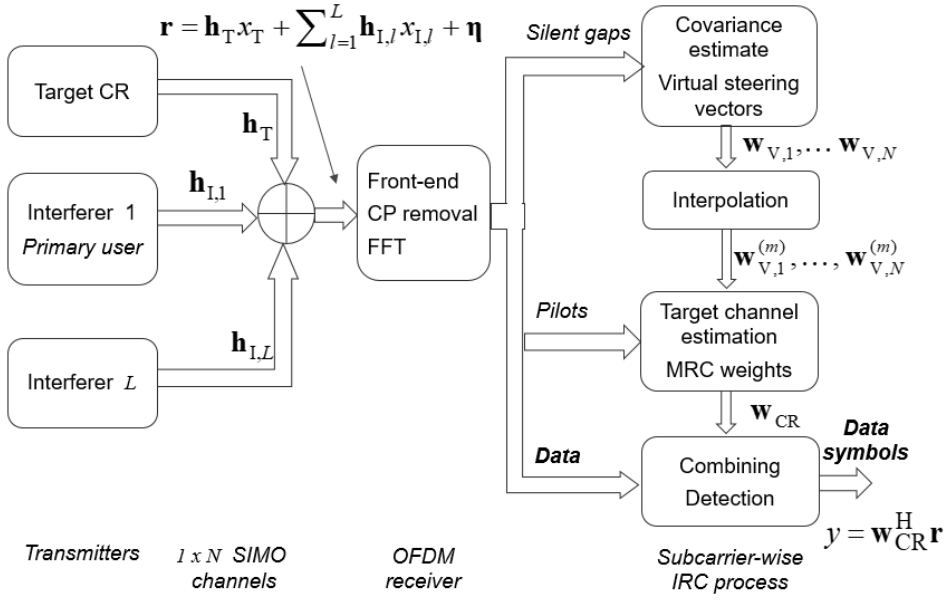

Figure 6. IRC combining in BS-CR with silent gap interpolation.

Determining the optimum weight values is an optimization problem which can be solved with the linear minimum mean-squared error (LMMSE) criterion [35], [123] that aims to minimize the mean-squared error with respect to the target signal x_T,

$$J = E[|x_{\mathrm{T}} - \mathbf{w}^{\mathrm{H}}\mathbf{r}|^2]. \tag{3.4}$$

When knowledge of the covariance matrix is available, IRC can be applied. Two cases are considered below: (i) calculating interference covariance from known PU channel coefficients and (ii) sample covariance-based approaches.

To solve the LMSSE problem, the famed Wiener-Hopf Eqs. [70], [113] are used. The solution of the minimization problem can be written as

$$E[\mathbf{r}\mathbf{r}^{\mathrm{H}}]\mathbf{w} = E[\mathbf{r}x_T^*] \tag{3.5}$$

and

$$(\mathbf{h}_T P_T \mathbf{h}_T^* + \mathbf{\Sigma}_{\mathrm{NI}})\mathbf{w} = P_T \mathbf{h}_T. \tag{3.6}$$

Here the interference covariance matrix can be expressed as

$$\mathbf{\Sigma}_{\mathrm{NI}} = \sum_{l=1}^{L} P_l \mathbf{h}_{\mathrm{I},l} \mathbf{h}_{\mathrm{I},l}^{\mathrm{H}} + P_{\mathrm{N}} \mathbf{I}, \tag{3.7}$$

where P_{N} and $P_{\mathrm{I},l}$ are the noise variance and variance of interferer at the transmitter l , respectively, I is the identity matrix of size $N \times N$. Here the first term is due to interfering PU and CR transmissions and the last term is due to AWGN. Interference covariance matrix can be considered as a matrix representing the correlation of the different antenna signals, i.e., the spatial correlation of the received signal including noise and interference from other users of the channel. Assuming that the matrix $\mathbf{h}_T P_T \mathbf{h}_T{}^H + \mathbf{\Sigma}_{\mathrm{NI}}$ is invertible, the solution for the optimum weights becomes

$$\mathbf{w} = (\mathbf{h}_T P_T \mathbf{h}_T{}^* + \mathbf{\Sigma}_{\mathrm{NI}})^{-1} P_T \mathbf{h}_T. \tag{3.8}$$

Using the matrix inversion lemma [70], the general solution for the optimization using LMMSE criteria is

$$\mathbf{w} = \mathbf{\Sigma}_{\mathrm{NI}}^{-1} \mathbf{h}_{\mathrm{T}} \left(\mathbf{h}_{\mathrm{T}}^{\mathrm{H}} \mathbf{\Sigma}_{\mathrm{NI}}^{-1} \mathbf{h}_{\mathrm{T}} + \frac{1}{P_{\mathrm{T}}} \right)^{-1}. \tag{3.9}$$

where P_T is the target CR transmitters signal power and unit noise variance is assumed. This is known as the IRC solution [P3]. In the special case of AWGN or spatially uncorrelated noise only, $\mathbf{\Sigma}_{NI} = E[\boldsymbol{\eta}\boldsymbol{\eta}^*] = P_N \mathbf{I}$, and the solution becomes the maximum ratio combiner (MRC):

$$\mathbf{w} = \mathbf{h}_T (\|\mathbf{h}_T\|^2 + P_N / P_T)^{-1} \ . \tag{3.10}$$

3.2.2 Sample Covariance-Based Case without PU Channel Information

The IRC process starts from interference covariance matrix estimation during silent gaps in the receiver. It is difficult to have the perfect channel state information of the PU at the CR receiver side. Alternatively, the joint interference and noise covariance matrix can be estimated for each subcarrier by the sample covariance

matrix of the corresponding received subcarrier signal (after CP removal and FFT) in the absence of the target transmission, i.e., during the silent gaps as

$$\bar{\mathbf{\Sigma}}_{\mathrm{NI}} = \frac{1}{M} \sum_{m=1}^{M} \hat{\mathbf{r}}(m)\hat{\mathbf{r}}(m)^{H}. \tag{3.11}$$

Here m is the OFDM symbol index and M is the observation length in subcarrier samples, which is chosen equal to the length of the silent gap.

In the IRC process, the linear interference minimizing weights are calculated directly using Eq. (3.11), without explicit estimation of the spatial channels of the interference. The spatial channels from the interferers are implicitly estimated through the interference covariance matrix. This covariance estimate, as well as the weights must be recomputed within a small enough interval, depending on the coherence time of the channel [P4].

3.3 Covariance Tracking Under Mobility

The mobility of PU transmitter, CR transmitter and the CR receiver have different effects. If the PU transmitter and CR receiver are stationary, the mobility of CR transmitter is easier to handle, because the dominating PU interference is stationary, and the variations in the noise and interference covariance matrix are only due to the co-channel CR interferes. However, even in this case, radio environment of the CR receiver may vary due to the movement of people or vehicles nearby. Therefore, some tolerance to mobility is required also in such scenarios, at least with pedestrian mobilities. The mobility of PU transmitter or CR receiver makes the dominant interference time-varying, and in the BS-CR scenario, the CR link performance is very sensitive to the quality of the PU interference covariance matrix estimate. Therefore, it is important to investigate these mobility effects and consider enhanced schemes for tracking the interference covariance with mobility.

The optimal length of the silent gap (i.e., observation length) is an important and depends on the delay spread. While considering the sample covariance-based approach, increased observation (silent gap) length gives better PU interference covariance estimate in the stationary case or with low mobility. However, the channel variations during the silent gap affect critically the quality of the PU interference covariance matrix. We apply linear interpolation for the covariance matrix elements

when calculating the weight vectors for the data symbols between two consecutive silent gaps.

There are two key parameters in this process, the silent gap length and the data block length between two consecutive gaps. Increasing the gap length improves the performance with low mobility but degrades the performance with higher mobility and increases the overhead in throughput. Increasing the data block length increases the throughput but degrades the performance with mobility. These trade-offs are investigated through simulations in Section 3.5 and in [P3] and [P4].

3.4 IRC Process

As indicated in the model shown in Figure 6, the CR channel cannot be estimated before the step of the interference cancellation, and the optimal steering vector for IRC cannot be directly calculated. Here we develop an IRC scheme which utilizes N orthogonal virtual steering vectors in the receiver's internal channel estimation process, which is based on pilot symbol structures typically used in OFDM systems [38], [71], [73], [109], [110], [125], [152]. The $N - L$ vectors would be enough since IRC consumes only L degrees of freedom. But this way the model is more straightforward, and the IRC process is generic and robust since there is no need to estimate the number of interferers. Without loss of generality and for simplified computations, the following unit vectors are applied as the virtual steering vectors,

$$\mathbf{h}_{\mathrm{V},1} = [1,0,0,0,\cdots,0]^T, \quad \mathbf{h}_{\mathrm{V},2} = [0,1,0,0,\cdots,0]^T$$
$$\cdots$$
$$\mathbf{h}_{\mathrm{V},N} = [0,0,0,0,\cdots,1]^T . \tag{3.12}$$

Basically, the weight vectors obtained when applying the virtual steering vectors for $\mathbf{w}$ in Eq. (3.3) span the interference-free subspace in spatial domain. Steering vectors are in principle a set of beamforming weights applied in such a way the received SINR is maximized. Assuming that the interference covariance is correctly estimated, using any linear combination $\mathbf{h}$ of these vectors instead of $\mathbf{h}_{\mathrm{T}}$ in Eq. (3.9) provides interference cancellation. Then, we have to find the linear combination of these interference-free weight vectors $\mathbf{w}_{\mathrm{V},n}$, that maximizes the signal power for the spatial CR channel $\mathbf{h}_{\mathrm{T}}$. The following process finds the combination of the virtual steering vectors for the actual target signal by first estimating the spatial channel vectors

corresponding to the different virtual steering vectors. The weight vectors used in channel estimation are as follows:

$$\mathbf{w}_{\mathrm{V},n} = \bar{\mathbf{\Sigma}}_{\mathrm{NI}}^{-1}\mathbf{h}_{\mathrm{V},n}. \tag{3.13}$$

It should be noted that the denominator (inverse term in the end) of Eq. (3.9) is a complex scaling coefficient, which will be included in the MRC weights in later developments.

3.4.1 Target Channel Estimation with Linear Interpolation and MRC Combining

In the second stage, data symbols of the CR link are transmitted together with the training/pilot symbols. While receiving pilot symbols, the weighted output signals corresponding to each virtual steering vector are calculated as

$$y_n = \mathbf{w}_{\mathrm{V},n}^{\mathrm{H}}\mathbf{r},\ n = 1,2,\dots,N. \tag{3.14}$$

The IRC process cancels the interference from all of the weighted output signals, y_n corresponding to different virtual steering vectors. For each subcarrier, the N channel coefficients for each of the weighted output signals can be estimated using the pilot symbols as follows:

$$\hat{g}_{\mathrm{V},n} = \frac{y_n}{p} = \frac{\mathbf{w}_{\mathrm{V},n}^{\mathrm{H}}\cdot\mathbf{r}}{p},\ n = 1,2,\cdots,N, \tag{3.15}$$

where p is the transmitted pilot symbol value.

3.4.2 Linear Interpolation for Channel Estimation

In the traditional pilot-based channel estimation process, it is required to use efficient interpolation techniques, such as Wiener interpolation, based on the channel information at pilot sub-carrier symbols. For simplicity and to avoid excessive received signal buffering over high number of OFDM symbols, we apply linear interpolation. The performance of linear interpolation technique is better than the piecewise-constant interpolation methods [38], [71], [109], [110], [152]. In the

simulation studies of Section 3.5, a basic training symbol scheme is assumed where training symbols contain pilots in all active subcarriers, and the interpolation is done in time domain only, between two consecutive pilots in each subcarrier.

The MRC weights for a data symbol are then calculated as

$$\mathbf{w}_{\mathrm{MRC}} = \frac{[\bar{g}_{\mathrm{V},1}, \bar{g}_{\mathrm{V},2}, \cdots, \bar{g}_{\mathrm{V},N}]^{\mathrm{T}}}{\sqrt{\sum_{n=1}^{N} |\bar{g}_{\mathrm{V},n}|^2}}, \tag{3.16}$$

where $\bar{g}_{\mathrm{V},n},\ n = 1, \ldots, N$, denote the corresponding interpolated channel estimates. Generally, the interpolated channel estimates are different for each subcarrier in each OFDM symbol. For simplicity, the subcarrier and OFDM symbol indexes are not included in the notation above. Then, the interpolated channel estimates are given as

$$\bar{g}_{\mathrm{V},n}^{(k,m)} = \left(m - S_{\mathrm{p}}\right) \cdot \hat{g}_{\mathrm{V},n}^{(k,S_{\mathrm{p}})} + \left(S_{\mathrm{f}} - m\right) \cdot \hat{g}_{\mathrm{V},n}^{(k,S_{\mathrm{f}})} \tag{3.17}$$

where m is the OFDM symbol index, k is the subcarrier index, S is the pilot spacing, $S_{\mathrm{p}} = \left\lfloor \frac{m}{S} \right\rfloor \cdot S$ is the preceding training symbol index, $S_{\mathrm{f}} = \left\lceil \frac{m}{S} \right\rceil \cdot S$ is the following training symbol index and $\lfloor . \rfloor$ and $\lceil . \rceil$ stand for the floor and ceiling operations, respectively.

3.4.3 Combining for Detection

In the final stage, while receiving data symbols, the equalized data symbols are calculated by maximum ratio combining the N samples obtained by applying the virtual steering vectors. The effective weight vectors for CR can be obtained as,

$$\mathbf{w}_{\mathrm{CR}} = \left[\mathbf{w}_{\mathrm{V},1}, \mathbf{w}_{\mathrm{V},2}, \cdots, \mathbf{w}_{\mathrm{V},N}\right] \mathbf{w}_{\mathrm{MCR}}$$

$$= \sum_{n=1}^{N} \frac{\left(\mathbf{w}_{\mathrm{V},n}\, \bar{g}_{\mathrm{V},n}\right)}{\sqrt{\sum_{n=1}^{N} |\bar{g}_{\mathrm{V},n}|^2}}$$

$$= \sum_{n=1}^{N} \frac{\left(\tilde{\mathbf{\Sigma}}_{\mathrm{NI}}^{-1} \mathbf{h}_{\mathrm{V},n}\, \bar{g}_{\mathrm{V},n}\right)}{\sqrt{\sum_{n=1}^{N} |\bar{g}_{\mathrm{V},n}|^2}}$$

$$= \frac{\boldsymbol{\Sigma}_{\mathrm{NI}}^{-1}\bar{\mathbf{g}}}{\|\bar{\mathbf{g}}\|} \tag{3.18}$$

where $\bar{\mathbf{g}} = \left[\bar{g}_{\mathrm{V},1}, \bar{g}_{\mathrm{V},2}, \cdots, \bar{g}_{\mathrm{V},N,}\right]^{\mathrm{T}}$ appears as the spatial channel estimate for the target CR transmitter. It is enough to calculate and use this weight vector $\mathbf{w}_{\mathrm{CR}}$, instead of separately applying the MRC weights on the samples obtained by the weight vectors $\left[\mathbf{w}_{\mathrm{V},n}\right]$. The equalized data symbols are then calculated as follows:

$$\hat{d} = \mathbf{w}_{\mathrm{CR}}^{\mathrm{H}}\mathbf{r}. \tag{3.19}$$

Overall, this is the zero-forcing IRC solution which maximizes the received signal power over normalized steering vectors.

3.4.4 Computational Complexity of Proposed IRC Scheme

IRC has been widely deployed, e.g., in 4th and 5th generation OFDM-based wireless cellular systems. Here we briefly discuss the computational complexity of the proposed IRC scheme in relation to the existing IRC solutions, which are commonly based on estimating the spatial covariance matrix utilizing transmitted pilots or reference signals. Here the main difference is due to the use of sample covariance of the interference signals during silent gaps in the target transmission. The computational complexity is evaluated in terms of real multiplications needed in the IRC process per transmitted data symbol. In this way, the complexity metric is independent of the number of active subcarriers, depending mainly on the number of antennas (N), silent gap length (M), number of data symbols per transmission block, and the number of pilot symbols per transmission block. Continuous stream of transmission blocks is assumed, such that the spatial covariance is estimated once per transmission block. The IRC signal processing is based on complex signals, and it is assumed that one complex multiplication takes 4 real multiplications.

The complexities of the processing steps (in terms of real multiplications) are as follows:

1. Covariance matrix calculation while making use of the conjugate symmetry the covariance matrix.

a. Channel estimation based, Eq. (3.7) without noise term: $2N^2$

b. Sample covariance based, Eq. (3.11): $2MN^2$

2. Covariance matrix inversion, based on [123]: $4(N^3 + \frac{7N^2}{2} + \frac{5N}{2} - 4)$

3. Weight coefficient calculation, making use of the real-valued diagonal elements of the covariance matrix.

   a. Channel estimation based, Eq. (3.9): $4N^2 - 2$

   b. Proposed IRC scheme: $8N^2 - 4$. This includes calculation of the N initial weight vectors, Eq. (3.13), and the final weight vector, Eq. (3.18).

   Here also N divisions are needed to normalize the final weight coefficients, along with the norm calculation.

4. Symbol detection, Eq. (3.19): $4N$

Steps 1 and 2 are done once per processing block, step 3 once for each pilot symbol, and step 4 for each data symbol. The weight normalization in step 3, and the interpolation of weight coefficients for each data symbol can be done with minor additional complexity, which is common to both schemes, and these are not included in the following numerical results.

Generally, the covariance matrix inversion dominates the computational complexity, but in the proposed scheme, calculation of the sample covariance matrix has a high additional complexity. As an example, we consider the case with N=4 antennas, silent gap length of M=16 and OFDM block length of 17, consisting of 14 data symbols and 3 pilots, and assuming covariance interpolation. Then the channel estimation-based scheme needs 67.6 real multiplications per data symbol, while the sample covariance-based scheme needs 115.1 real multiplications, i.e., the complexity is increased by about 70 percent. Naturally, the other elements of the OFDM receiver, which are not included in these calculations, contribute significantly to the overall complexity. Most importantly, FFT computations have a significant

effect on the overall complexity of OFDM systems. As an example, with the FFT-size of 2048, 1200 active subcarriers, and L=4 antennas, the FFT's take about 75 real multiplications when assuming the basic FFT complexity of $N \cdot \log_2(N)$. Then the overall complexity is increased by about 33 percent due to the use of sample covariance, while ignoring various other signal processing stages which are common to both schemes.

3.5 Results and Discussion

The simulations were carried out for the system setup explained in Section 3.1. The carrier frequencies of CR and PU are the same and it is here set to 700 MHz, which is close to the upper edge of the terrestrial TV frequency band. The modulation order used by CR varies between 4-QAM, 16-QAM, and 64-QAM. The pilot symbols are binary and have the same power level as the data symbols. The primary transmitter signal follows the DVB-T model with 16-QAM modulation, 8 MHz bandwidth, and CP length of 1/8 times the useful symbol duration, i.e., 28 μs. The IFFT/FFT length is 2048 for both systems. The DVB-T and CR systems use 1705 and 1200 active subcarriers, respectively. PUs frame structure and pilots follow the DVB-T standard. Data in all signals are generated randomly. ITU-R Vehicular A channel model (about 2.5 μs delay spread) [85] is used for the CR system. For short-range/indoor CR communication, Rician-fading channel model would be more relevant, but the Rayleigh-fading Vehicular A model is used as worst-case model. We have also tested basic scenarios with the Rician-fading SUI-1 model (0.9 μs delay spread) [85] for the CR, showing slight improvements in performance. Hilly Terrain channel model (about 18 μs delay spread) [85] is used for PU transmission. In simulations without mobility ("block-fading channel"), the channel is assumed to be constant over each transmission block consisting of single silent gap, pilot symbols, and data symbols, while the channels for different transmission blocks are independent. In simulations with mobility, the channel is continuously fading depending on the specified speed of mobility, channel power delay profile, and carrier frequency. The CR receiver is assumed to have four antennas, and uncorrelated 1x4 SIMO configurations are used for both the primary signal and the CR signals.

The number of spatial channel realizations simulated in these experiments is 300-1000. The ratio of CR and PU signal power levels at the CR receiver (referred to as the SIR) is varied. In case of co-channel CR interference, the average power levels of interfering and target CRs are the same at the target receiver and the channels are independent instances of the Vehicular A model with random timing offsets, while all multipath delays remain with the CP. The lengths of the OFDM symbol frame and silent gap for interference covariance matrix estimation are also varied (expressed in terms of CP-OFDM symbol durations). A very basic training symbol scheme is assumed for the CR: training symbols contain pilots in all active subcarriers and the spacing of training symbols is 8 OFDM symbols. Frame length is selected in such a way that training symbols appear as the first and last symbol of each frame, along with other positions. Channel estimation uses linear interpolation between the training symbols. We have tested the BS-CR link performance with SIR values of {-10, -20, -30} dB using silent gap durations of {8, 16, 32, 128} OFDM symbols, and data block lengths of {17, 25, 33, 41} OFDM symbols.

3.5.1 The Effect of Silent Gap Length

This sub-section analyses the BER performance of the proposed sample covariance-based IRC process using Eqs. (3.11) – (3.15) and (3.17) – (3.19), considering the known channel-based process as an ideal reference. As it was explained in Section 3.2, the known channel case assumes perfect knowledge of the interference channel and it provides a theoretical performance bound for practical IRC schemes. It uses the LMMSE solution Eq. (3.9) with known channel-based covariance estimate Eq. (3.7). Otherwise, the receiver process is the same as in the sample covariance-based scheme, thus providing a theoretically achievable bound for the practical sample covariance-based approach. First, the known channel model is applied with PU interference only, while results with cochannel CR interferers are presented in Section 3.5.2. Some initial results for the sample covariance-based scheme without covariance interpolation and with different gap and OFDM block durations can be found in [P3].

Figure 7 shows the BER performance considering both the known channel and sample covariance-based approaches in stationary case (no mobility). Here the silent gap durations are 8, 16, 32, and 128 OFDM symbols and the data block length is 17.

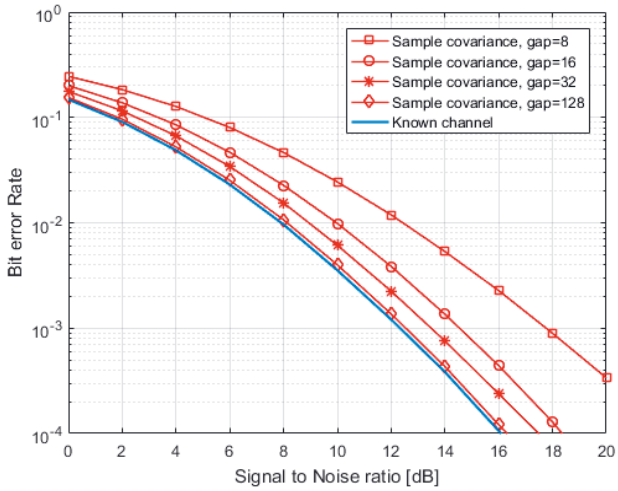

Figure 7. Performance of QPSK BS-CR systems with known channel based and sample covariance-based approaches for SIR = -30 dB considering block-fading channel (no-mobility) with silent gap lengths of 8, 16, 32 and 128 symbols, and OFDM frame length of 17 symbols.

With zero-mobility, link performance is independent of the data block length and short block is used here mainly to reduce simulation time.

It can be observed that the sample covariance-based simulation results converge to the corresponding known channel results with increasing gap length, since the covariance estimate is improved with increasing sequence length. This demonstrates that the known channel based bound is theoretically achievable.

A detailed comparison between the required SNR values of the known channel and sample covariance-based approaches for BER=0.01 is provided in Table I. As seen in the table, the required SNR values of known channel and sample covariance-based algorithms match adequately under the gap length of 128 OFDM symbols. Additionally, the numerical results clearly show that the differences in required SNR values are almost independent of the SIR while considering the SIR values of {-10, -20, -30} dB. The SNR loss due to limited gap length is about 0.3 dB, 1 dB, 1.9 dB, and 4.4 dB for gap lengths of 128, 32, 16, and 8, respectively.

Table 1. Required SNR values of known channel and sample covariance based approaches for the BER=0.01 in QPSK BS-CR systems for SIR values of {-10, -20, -30} dB considering block-fading channel (no-mobility) with silent gap lengths of 8, 16, 32 and 128 symbols, and OFDM frame length of 17 symbols.

Req. SNR for BER=0.01	SIR= -30 dB		SIR= -20 dB		SIR= -10 dB	
	Known Channel	Sample Cov.	Known Channel.	Sample Cov	Known Channel	Sample Cov.
Gap =8	7.9 dB	12.3 dB	7.9 dB	12.3 dB	7.9 dB	12.2 dB
Gap =16	7.9 dB	9.8 dB	7.9 dB	9.8 dB	7.9 dB	9.7 dB
Gap =32	7.9 dB	8.9 dB	7. 9 dB	8.9 dB	7.9 dB	8.8 dB
Gap =128	8.0 dB	8.3 dB	8.0 dB	8.3 dB	8.0. dB	8.2 dB

3.5.2 Performance Analysis of Proposed Scheme with Mobility

This sub-section reports the performance analysis of the proposed algorithms also considering the effects of mobility and different system parameters. It is noted that only sample covariance-based approach is considered in the following results. The results presented above still serve as ideal reference when evaluating the effects of mobility in different configurations. First, we evaluate the performance with slow mobilities with and without covariance interpolation, still assuming that the interference is due to the PU only.

Figure 8 shows the impact of covariance matrix interpolation on the BS-CR link performance. Here the data block length and gap duration are fixed to 17 and 16 OFDM symbols, respectively. This choice provides performance that is no more than 1 dB from the configuration reaching 1% or 10% BER with lowest SNR, among the tested configurations with even higher overhead. We can see that covariance interpolation provides significant improvement of robustness in time-varying

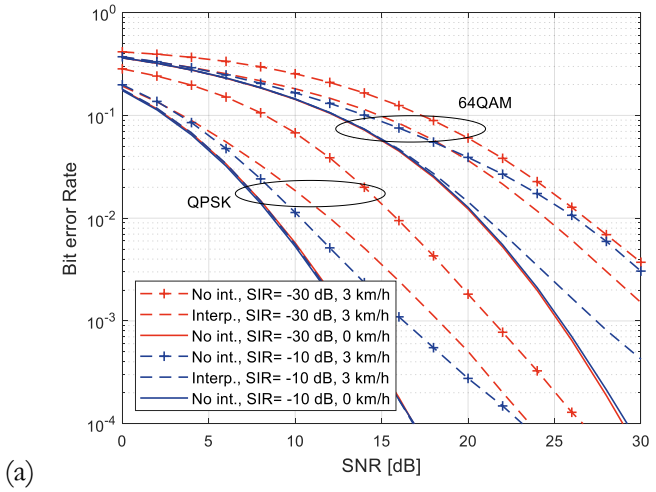

(a)

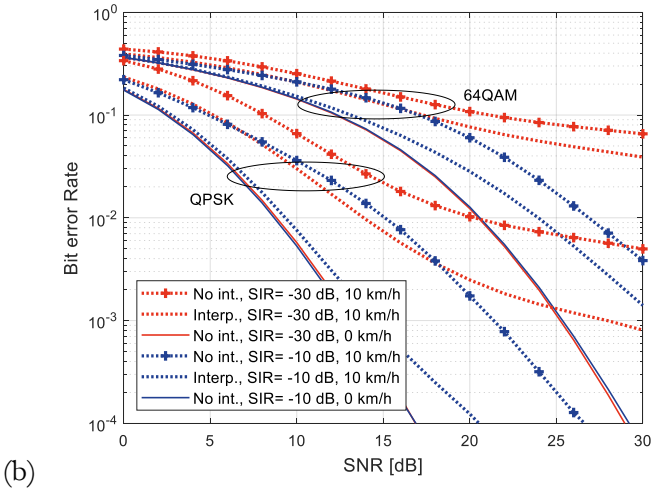

(b)

Figure 8. Performance of QPSK and 64-QAM BS-CR systems for SIR = {-10, -30} dB with or without covariance matrix interpolation. (a) 0 and 3 km/h CR receiver mobilities. (b) 0 and 10 km/h CR receiver mobilities. Silent gap length of 16 symbols, and OFDM frame length of 17 symbols.

channels. Focusing on the 1 – 10 % BER region, the performance with interpolation at 10 km/h mobility clearly exceed the performance at 3 km/h without interpolation.

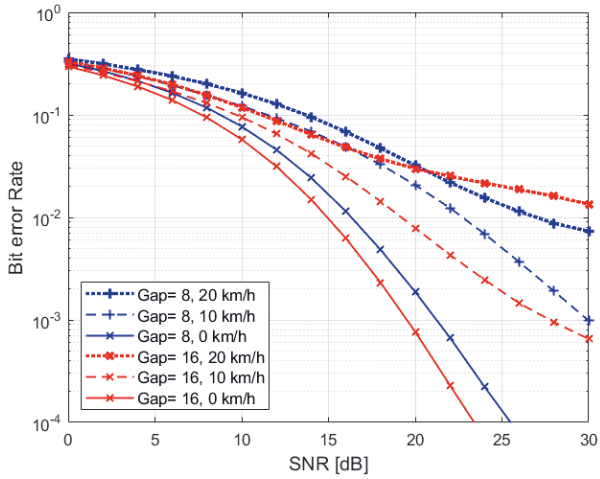

Figure 9. Performance of 16-QAM BS-CR systems for SIR = -20 dB with covariance matrix interpolation for CR receiver mobilities of 0, 10 km/h, and 20 km/h. Silent gap length of 8 or 16 symbols and OFDM frame length of 17 symbols.

However, for the 64-QAM case with -30 dB SIR, this is true only for BER of 10 % or higher, due to the high error floor at very low SIR and high mobility. In Figure 9, the effect of silent gap duration is tested with 16-QAM modulation, SIR of -20 dB, and data block length of 17. The overhead in data rate is about 58 % and 44 % for gap lengths of 16 and 8, respectively. The shorter gap length results in about 1.5 dB performance loss in the 1 – 10 % range in stationary case and about 1.8 – 3.5 dB loss with 10 km/h mobility, compared to the gap length of 16. With 20 km/h mobility, the corresponding loss is about 2.2 dB at 10 % BER, but longer gap leads to higher error floor, and the performance with shorter gap becomes better for BER below 3 %.

Finally, we evaluate the link performance in the presence of co-channel CR interference, in addition to PU interference in Figure 10. While still assuming four antennas in the target CR receiver and -20 dB SIR for the PU signal, also two interfering CR signals are included in the model. All CR signals are at the same average power level and their channels are independent instances of the Vehicular A

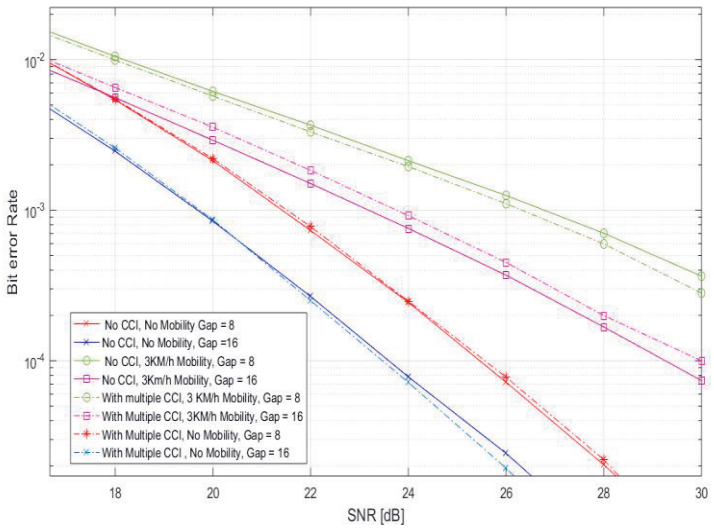

Figure 10. Link performance in the presence of PU and two CR co-channel interferers using gap lengths of 8 and 16, OFDM frame length of 17 symbols, mobilities of 0 and 3 km/h, 16QAM modulation in target CR link, SIR of -20 dB for PU, and equal power levels of all CR signals.

channel model. The results are shown in Figure10, indicating that the impact of co-channel CRs on the target link performance is very minor.

3.6 Chapter Summary

The performance of BS-CR transmission links in the presence of strong interferences and mobility was investigated using spatial covariance interpolation between silent gaps. The interference rejection capability of IRC using multiple receive antennas for various modulation orders under varying mobility and channel setups was studied. It was found that the IRC performs very well in the basic SIMO-type BS-CR scenario when stationary channel model is applicable, e.g., in fixed wireless broadband scenarios. However, the scheme is rather sensitive to the fading of the PU channel, e.g., due to people moving close to the CR receiver. Due to the strong interference level, the interference cancellation process is affected by relatively small errors in the covariance matrix estimate. For covariance estimation, the silent gap length in the order of 16 - 32 OFDM symbols provides best

performance with stationary channels, but even with 3 km/h mobility, the performance degrades significantly when considering SIR levels below -10 dB. The data block length should be of the same order or less, which leads to high overhead due to the silent gaps. Covariance interpolation was shown to greatly improve the robustness with time-varying channels, such that good link performance can be obtained with up to 20 km/h mobility at 700 MHz carrier frequency. This indicates that the proposed BS-CR scheme could be feasible at below 6 GHz frequencies with pedestrian mobilities. However, there is a significant tradeoff between link performance and overhead in data rate due to the silent gaps.

In the basic TV black-space scenario, there is only one strong TV signal present in the channel, in agreement with our assumption about the primary interference sources. DVB-T system allows also single-frequency network (SFN) operation and the use of repeaters to improve local coverage [5], [81], [129], [133]. In both cases, the primary transmissions can be seen as a single transmission, with a spatial channel that depends on the specific transmission scenario, and the proposed scheme is still applicable. One important issue in the proposed scheme is its sensitivity to the nonlinearities of the CR receiver's analog front-end. Wide linear range is required in order to prevent nonlinear distortion from the high-power PU signal from degrading the CR link performance. This is a common issue with opportunistic CR operating in white spaces close to high-power PU channels, and also with digital signal processing (DSP) intensive receiver architectures. An interesting technology in this context is advanced DSP algorithms for compensating the nonlinear effects of the receiver's analog front end [145]. On the other hand, sample covariance-based IRC may exhibit some capability to also reject the nonlinear distortion due to the strong PU signal. This topic is further studied in the next chapter in this thesis.

4 EFFECTS OF RF IMPARIMENTS IN COGNITIVE RADIOS

This chapter investigates the effects of RF transceiver's imperfections on the IRC based BS-CR operation. In particular, the effects of PA nonlinearities, carrier frequency offset (CFO), and receiver nonlinearities on the blind IRC technique are evaluated. An analytical framework for modeling CFO effects, together with experimental study of CFO and nonlinearity effects is considered. The performance of the IRC scheme is evaluated considering terrestrial digital TV broadcasting (DVB-T) as the primary service.

CRs are expected to operate in radio environments with a high level of interference and, simultaneously, produce negligible interference to the PUs. For this condition to be satisfied, CR transmitters (TXs) must have good PAs that have reasonably good efficiency and high linearity [104]. Two conflicting requirements of the PAs, which further complicate the situation, are the efficiency and linearity requirements. In addition, there is also the need to use the spectrum as efficiently as possible, which mandates the use of spectrally efficient modulation techniques such as OFDM, in which both the phase and the amplitude of the signal carry information. OFDM systems are very sensitive to the nonlinear distortions introduced by the analogue parts, especially at the TX side. To avoid significant degradation of the signal quality, the requirements of the analogue RF components such as PA are becoming stricter [104].

Given these constraints, it is vital to study the effects of RF imperfections also in the design of transceivers for CRs [6], [9], [28], [29], [41], [59], [56], [63], [64], [72], [89], [102], [104], [121], [122], [126], [132], [145]. This is particularly important for interference cancellation-based BS-CR operation as some of the RF imperfections may become critical due to the wide signal dynamic range in the receiver [72], [102], [122]. In BS-CR, the RF nonidealities may affect in two different ways: (i) directly degrading the CR link performance and/or (ii) harming the IRC process leading to reduced PU interference suppression capability, e.g., by distorting the spatial covariance estimate.

4.1 Signal Model and Experimental Setup

The IRC based BS-CR scenario, shown in Figure 6, is considered with covariance interpolation. In this scenario, we consider a CR receiver using multiple antennas to receive data from a single-antenna cognitive transmitter. The CR operates within the frequency band of the PU, and the PSD of PU is very high in comparison to that of the CR. The PU transmitter generates a lot of interference to the CR transmission, which operates closer to the noise floor of the primary receiver, and due to this, the PU communication link is protected. We consider frequency reuse over relatively small distances, such as an indoor CR system. Further, the details of IRC based BS-CR were described in Chapter 3. In here, we use that model to study the effects of PA nonlinearity and how CFO affects the performance of the IRC based BS-CR receiver.

4.2 Effects of Non-Linear PA on BS-CR

The nonlinearity of transmitter PAs causes significant effects on the performance with respect to spectrum characteristics, multiuser interference on the desired signal, and transmit power, depending on the used modulation scheme [41], [59], [89], [104], [157], [160]. Especially, the non-linearity brings about spectral regrowth causing ACI and in-band performance degradation. The latter one is in the focus of our study. Generally, the SIR metric quantifies the in-band distortion causing performance loss in bit error rate (BER).

4.2.1 Effects of PA nonlinearity

The effects of PU and CR transmitter nonlinearities are studied through simulations. For simplicity, it is assumed that there are no other interference sources. Firstly, the spectral regrowth due to nonlinearities is demonstrated considering both linear PA and the 5G uplink PA model [6] for PU TX and CR TX. The details of this model can be found in publication [P5].

Here and in all later simulations, we use the same main parameters as in Chapter 3. It is assumed OFDM IFFT/FFT size of 2048 and the subcarrier spacing of

4.4643 kHz, corresponding to the 2k mode of DVB-T. The CP length is $\frac{1}{8}$ times the main OFDM symbol duration, and the PU signal has all the elements of DVB-T transmission. For the CR signal, we use the same main parameters and 1200 active subcarriers in the center of the DVB-T spectrum. Here we use the silent gap length of 24 OFDM symbols, and data block length of 65 OFDM symbols between silent gaps. Training symbols (with pilots in all active subcarriers) are used for CR channel estimation, with the spacing of 8 OFDM symbols. These parameters, which are based on the studies of Chapter 3 and [P3], [P4], reach realistic tradeoff between overhead and performance under slowly fading channels. In this case, about $38\,\%$ of OFDM symbols are used for silent gaps and pilots.

Both the sample covariance and known channel-based IRC schemes are considered in the simulations. In the sample covariance-based case, the covariance matrix is estimated from the received signal during silent gaps of length 24 in the target CR transmission. Covariance matrix interpolation is not applied since we are not considering mobility effects in this context. The reference case is based on perfect knowledge of the PU-CR channel. The CR channel is estimated using training symbols and 1x4 SIMO antenna configuration is used in all simulations.

Next, the BER performance of the CR link with PA nonlinearity is discussed. The CR TX nonlinearity should not affect the interference covariance estimation, so we expect that it affects the BS-CR link performance in the same way as in basic OFDM transmission with the same numerology. Regarding the PU TX nonlinearity, we notice that basic PA nonlinearity models do not harm the cyclic convolution model of CP-OFDM, i.e., the end part of the main OFDM symbol is affected in the same way as its copy, the CP. Then the interference covariance should not be affected by PU TX nonlinearity, and we don't expect significant effects in the link performance. However, if the PA exhibits strong memory effects, the cyclic convolution model might be distorted, and this effect is worth investigating in future studies.

Monte Carlo simulation results are provided for the CR link performance with PA nonlinearity, assuming the CR/PU power ratio of $SIR_{\mathrm{PU}} = -30$ dB and 64QAM subcarrier modulation. We use a back-off value of 9 dB as the modest case for the CR TX, and a back-off value of 5 dB as the worst case for the PU TX. The latter choice, as well the use of 5G-UL PA model for the PU TX is for demonstrating the robustness of BS-CR operation towards the PU TX nonlinearity. For these results, we use the Hilly terrain (HT) channel model having about 18 μs maximum

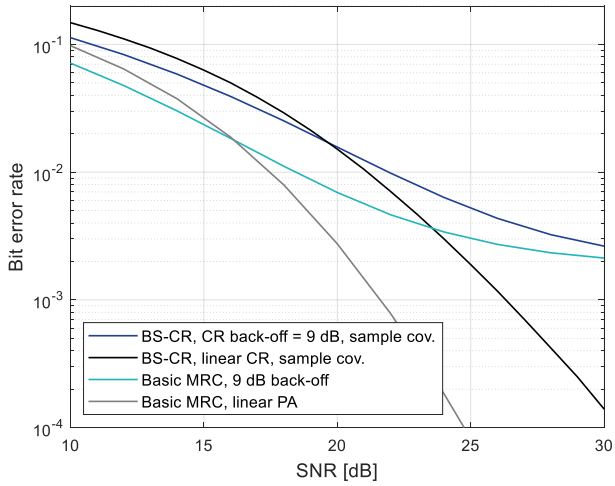

Figure 11. BER performance of sample covariance based BS-CR with 64QAM modulation vs. basic transmission link with MRC based receiver diversity. 5G-UL PA model with 9 dB backoff is used for the target link, linear PA in PU TX.

delay spread for the PU signal and the ITU-R Vehicular A (VehA) model with about 2.5 μs maximum delay spread for the CR signal [85].

Figure 11 shows the sample covariance-based BS-CR link's BER performance with linear and nonlinear PA models in comparison to a basic interference-free link using MRC based receiver diversity. We can see that the used modest nonlinearity affects in a similar way in BS-CR and basic OFDM systems with the same numerology and same antenna configuration. With used parameters, the sample covariance-based BS-CR has about 3.5 dB SNR loss due to PU interference at 1 % BER level.

In Figure 12, the BER performances with linear/nonlinear PA in PU or CR TX are depicted for both sample covariance and known channel-based schemes. We can see that even very hard nonlinearity tested for PU TX has very minor effect on the CR link performance. It is also interesting to notice that, at 1 % BER level, the proposed sample covariance-based method has about 1.2 dB SNR loss in comparison to the known channel-based reference method.

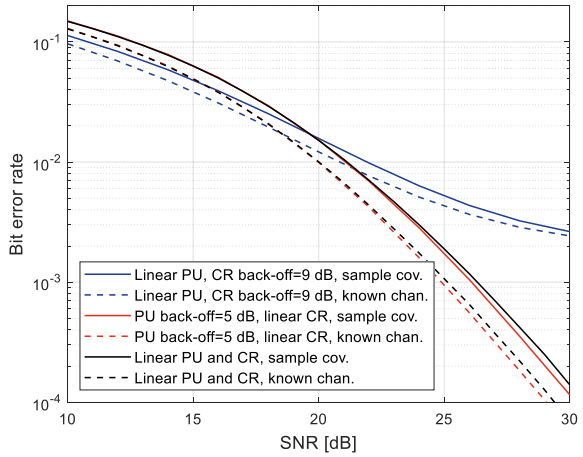

Figure 12.BER performance of BS-CR with 64QAM subcarrier modulation and linear or nonlinear 5G-UL PA model for PU or CR transmitter.

4.3 Analysis of CFO Effects in BS-CR

The effect of non-synchronized interferers on OFDM systems using MMSE-based IRC has been investigated in [161] in terms of outage probability for a given channel power delay profile. Here we develop an analytical expression for the SIR at a CR receiver in IRC-based BS-CR scenario, based on knowledge of the root-mean-square (RMS) channel delay spread of the PU-to-CR channel.

In the following analysis, we assume that the CR receiver is synchronized to the target CR signal while there is a frequency offset between the PU and CR carrier frequencies. We ignore the possible inconsequential initial phase offset in the receiver. For convenience of notation, without loss of generality, we also assume that the active subcarriers are indexed from 0 to N_A-1. Then the PU interference part of the received digital baseband multi-antenna signal can be expressed in the presence of CFO as:

$$\mathbf{r}_{PU}(n) = \tilde{\mathbf{h}}_{PU}(n) * x_{PU}(n) e^{\frac{j2\pi\delta_{CFO} n}{N}} \tag{4.1}$$

where n is the time index, δ_{CFO} is the CFO normalized to the subcarrier spacing, $\widetilde{\boldsymbol{h}}_{\mathrm{PU}}(n)$ is the vector of channel impulse responses from PU to the CR receiver antennas, $x_{\mathrm{PU}}(n)$ is the PU signal, and $*$ denotes cyclic convolution. Then, after the receiver's FFT process, the corresponding PU interference contributions to the kth subcarrier samples of different antenna branches can be expressed as [9].

$$\begin{aligned}\mathbf{Y}_{\mathrm{PU,k}} &= \sum_{\mathrm{n=0}}^{\mathrm{N-1}}\left(\sum_{\mathrm{l=0}}^{\mathrm{N_A-1}}\mathbf{h}_{\mathrm{PU,l}}\mathrm{d}_{\mathrm{PU,l}}\mathrm{e}^{\mathrm{j2\pi ln/N}}\,\mathrm{e}^{\frac{\mathrm{j2\pi\delta_{CFO}n}}{\mathrm{N}}}\right)\mathrm{e}^{-\frac{\mathrm{j2\pi kn}}{\mathrm{N}}}\\ &= \textstyle\sum_{\mathrm{l=0}}^{\mathrm{N_A-1}}\mathbf{h}_{\mathrm{PU,l}}\mathrm{d}_{\mathrm{PU,l}}\sum_{\mathrm{n=0}}^{\mathrm{N-1}}\mathrm{e}^{\frac{\mathrm{j2\pi(l-k+\delta_{CFO})n}}{\mathrm{N}}}\\ &= \textstyle\sum_{\mathrm{l=0}}^{\mathrm{N_A-1}}\phi(\mathrm{l}-\mathrm{k}+\delta_{\mathrm{CFO}})\beta(\mathrm{l}-\mathrm{k}+\delta_{\mathrm{CFO}})\mathbf{h}_{\mathrm{PU,l}}\mathrm{d}_{\mathrm{PU,l}}\end{aligned} \tag{4.2}$$

where $\boldsymbol{h}_{\mathrm{PU},l}$ is the PU channel vector for subcarrier l, $d_{\mathrm{PU},l}$ is the PU data symbol in subcarrier l, and

$$\begin{aligned}\phi(\mathrm{z}) &= \mathrm{e}^{\frac{\mathrm{j\pi z(N-1)}}{\mathrm{N}}}\\ \beta(\mathrm{z}) &= \frac{\sin(\pi\mathrm{z})}{\mathrm{N}\sin\left(\frac{\pi\mathrm{z}}{\mathrm{N}}\right)}\end{aligned} \tag{4.3}$$

with $z = l - k + \delta_{\mathrm{CFO}}$. The orthogonality of subcarriers is maintained only if the CFO is zero or integer, i.e., if the frequency offset is an integer multiple of subcarrier spacing. Otherwise, the samples observed at the kth subcarrier contains intercarrier interference (ICI) from all other active subcarriers.

Now, the known PU channel based spatial covariance matrix for subcarrier k can be evaluated as

$$\begin{aligned}\widetilde{\boldsymbol{\Sigma}}_{\mathrm{PU,k}} &= \left(\sum_{\mathrm{l=0}}^{\mathrm{N_A-1}}\phi(\mathrm{z})\beta(\mathrm{z})\mathbf{h}_{\mathrm{PU,l}}\right)\left(\sum_{\mathrm{l=0}}^{\mathrm{N_A-1}}\phi(\mathrm{z})\beta(\mathrm{z})\mathbf{h}_{\mathrm{PU,l}}\right)^{\mathrm{H}}\\ &= \sum_{\mathrm{l=0}}^{\mathrm{N_A-1}}\phi(\mathrm{z})\beta(\mathrm{z})\mathbf{h}_{\mathrm{PU,l}}\left(\phi(\mathrm{z})\beta(\mathrm{z})\mathbf{h}_{\mathrm{PU,l}}\right)^{\mathrm{H}}\end{aligned}$$

$$= \sum_{l=0}^{N_A-1} \beta^2(l-k+\delta_{CFO})\boldsymbol{\Sigma}_{PU,l}, \tag{4.4}$$

where $\boldsymbol{\Sigma}_{PU,l}$ is the spatial covariance matrix of subcarrier l in the absence of CFO. The cross-terms between different subcarriers are not included here, based on the common assumption that the subcarrier symbol sequences are uncorrelated.

In the following, we aim to model the effect of CFO on the interference covariance matrix in the IRC context using basic parameters of the channel model. For this purpose, we first introduce a model for the correlation of the spatial channels of different subcarriers. We use the model commonly applied in Wiener filtering-based channel estimation [73] for the correlation between the channel coefficients of different subcarriers. It is based on assuming uniform power delay profile with maximum delay spread of τ_{max}. We also assume that the spatial channel of each subcarrier is uncorrelated. Then, the correlation between subcarriers k and l can be expressed as [73],

$$R(k,l) = \mathrm{sinc}\left((k-l)\tau_{max} f_s/N\right) e^{-\frac{j(k-l)\tau_{max} f_s}{N}}. \tag{4.5}$$

It should be noted that in the case of flat-fading channel, different subcarriers have equal channel matrices and, consequently, equal spatial covariance matrices. In this case, CFO affects the channel covariance matrices only by an inconsequential real scaling factor. On the contrary, with highly frequency selective channels, the spatial covariance matrix of each subcarrier is distorted by the uncorrelated parts of the channel vectors of other subcarriers. Noting that $R(k,k) = 1$, we can express the spatial covariance matrix of subcarrier k as

$$\widetilde{\boldsymbol{\Sigma}}_{PU,k} = \beta^2(\delta_{CFO})\boldsymbol{\Sigma}_{PU,k} + \sum_{\substack{l=0 \\ l\neq k}}^{N_A-1} \left(1-R(k,l)\right)^2 \beta^2(l-k+\delta_{CFO})\boldsymbol{\Sigma}_{PU,l}\,. \tag{4.6}$$

The actual spatial covariance matrix of each subcarrier is scaled by $\beta^2(\delta_{CFO})$, while the distorting uncorrelated part of the covariance of subcarrier k is given by the latter term. We assume that the IRC process suppresses completely the PU interference power corresponding to the first term, but the uncorrelated part remains as interference to the target CR signal. Let $SIR_{PU} = \frac{P_T}{P_{PU}}$ denote the ratio of the target CR power at the CR receiver, P_T, to the PU interference power before interference cancellation, P_{PU}.

Assuming that the subcarriers have equal power levels, the target signal's SIR due to the CFO of the PU signal can be evaluated as:

$$\mathrm{SIR}_{\mathrm{CFO}}(\delta_{\mathrm{CFO}}) = \frac{\mathrm{SIR}_{\mathrm{PU}}}{\sum_{\substack{l=0 \\ l\neq`k}}^{N_A-1}(1-R(k,l))^2\beta^2(l-k+\delta_{\mathrm{CFO}})}. \quad (4.7)$$

In the numerical results, we show the average of this expression overactive subcarriers. This calculation can be simplified by noting that subcarriers $k+\kappa$ and $k-\kappa$ contribute equally to the interference and that considering all active subcarriers, there are $2(N_A-\kappa)$ subcarriers at the distance of $|l-k|=\kappa$.

Figure 13 compares the theoretical SIR values based on Eq. (4.7) with simulated SIR values considering both sample covariance based and known channel -based IRC schemes with different values of CFO. Here the known channel reference case is based on perfect knowledge of the PU channel in the absence of CFO. The subcarrier modulation is 16QAM, and the other parameters are as mentioned in [P5]. Here both HT and VehA channels are considered for the PU signal. No channel noise is included in these simulations, so the interference is due to imperfect spatial covariance matrix estimation, CFO, and the limitations of sample covariance-based estimation in the corresponding case. The CFO-based SIR is shown also for the basic OFDM scheme. We can see that the CFO requirements are 3-10 times higher than in basic OFDM schemes, depending on the channel delay spread and covariance estimation scheme. We can see that with the VehA-type PU channel, there is a very good match between the theoretical model and the known channel-based simulation results. With HT-type PU channel, the theoretical model is somewhat pessimistic. We can also see that the sample covariance-based estimation gives clearly better SIR than the theoretical model or the case of CFO-free channel knowledge-based covariance estimation. This is because the sample covariance-based estimation can take into account the CFO-induced contribution to the covariance estimates of different subcarriers.

Figure 14 shows the BER performance with 64QAM modulation and VehA channel for the CR link and CFO values of $\delta_{\mathrm{CFO}} \in \{0,\ 0.01,\ 0.005\}$, while the other parameters are the same as in the other numerical results. We can see that with CFO=0, the PU channel's delay spread has a very minor effect on the performance. When relating these results with SIR performance of Figure 13, it should be noted that the interference covariance is estimated in the absence of channel noise, but in low SNR region of Figure 14, the covariance estimate is degraded due to noise. However, we can see that in the high SNR region, the performance of sample covariance -based scheme may exceed the performance of the known channel -based

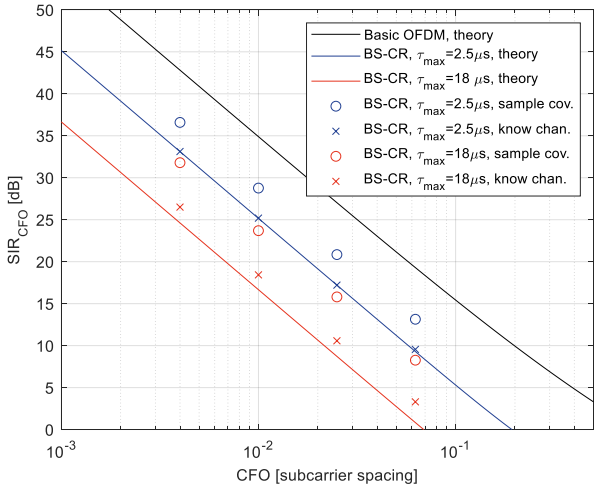

Figure 13. CFO-based SIR in BS-CR with Vehicular-A and Hilly terrain channel models and SIR_{PU} = -30 dB.

covariance estimate. Generally, the hard requirements for CFO can be seen also in these results. However, reducing the CFO from 1 % to 0.5 % of subcarrier spacing improves the performance greatly.

4.4 Effects of Receiver Nonlinearity and ADC Resolution

It is also important to consider the effects of CR receiver's nonidealities on the interference suppression capability of IRC. In [145], the effects of signal quantization and clipping in the analog-to-digital converter (ADC), as well as nonideality of automatic gain control (AGC) were evaluated by simulations. Here we focus on ADC quantization and the inevitable nonlinearities of the analog front-end. These can be expected to distort the spatial covariance estimate. Furthermore, in the IRC-based BS-CR scenario, wide dynamic range is needed for the ADC because the PU interference is at much higher level than the target CR information signal. In this section, we study these effects experimentally.

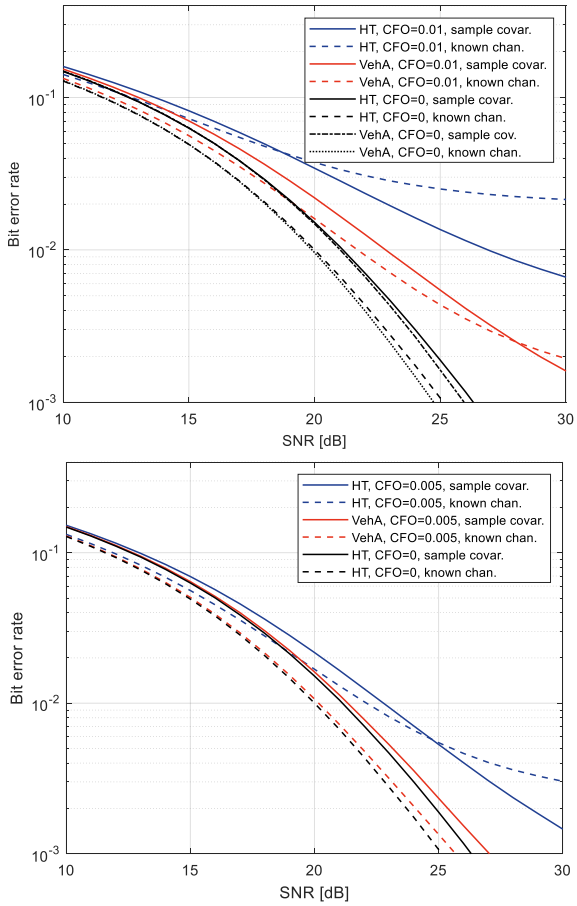

Figure 14. BER performance with different CFO values for 64QAM subcarrier modulation, SIR_{PU} = -30 dB, VehA channel for CR link, and VehA or HT channel for PU.

4.4.1 Receiver Nonlinearity Effects

For the CR receiver, we use a simple polynomial model including the third-order amplitude nonlinearity only. This is the most significant part of practical RX front-end nonlinearities and widely used in receiver front-end system design. Then the amplitude of observed signal can be expressed as

$$|\bar{r}| = |r| + c_3 \cdot |r|^3 \quad (4.8)$$

while the phase is not affected. Here *r* is the ideal received signal. The nonlinearity has a significant effect on the high-powered PU interference, while its effect on the low-level target signal is minor. The main issue is then the distortion of the sample covariance estimates, or the channel knowledge based spatial covariance estimate. Concerning the sample covariance-based scheme, one may expect that the effect is reduced if the different antenna branches experience similar nonlinearity effects. Then the covariance estimates can be expected to match better with the actual spatial channel of the PU. Therefore, we consider two alternative schemes for the automatic gain control (AGC) of different receiver antenna branches:

1. Per-antenna AGC: The gain of each antenna branch is adjusted in such a way that the average powers are equal to 1.
2. Joint AGC: The gains of antenna branches are equal, and the maximum power is 1.

We use a baseband nonlinearity model corresponding to direct-conversion receiver architecture [102], which is widely used in current receivers. It should be noted that in superheterodyne receivers, i.e., when the nonlinearities appear at the RF carrier frequency or at intermediate frequency (IF), the third-order intermodulation products are filtered away from the signal, and better performance would be expected.

Figure 15, shows the resulting BER performance for per-antenna AGC and joint AGC. The results are shown for 16QAM and 64QAM modulations with -30 dB PU SIR, while the other parameters are the same as earlier in this section. The results are shown for linear receiver and for 3rd-order nonlinearity coefficients of c_3= {0.0023, 0.00127}. The values correspond to signal to interference ratios of SIR_{NL}= {45, 50 dB}, correspondingly. We can see that with per-antenna AGC, the sample covariance -based scheme is somewhat worse than the known channel cases, while the effect of CR RX nonlinearity is rather similar in the two cases. Joint AGC has minor effect in the known channel case, while the performance of sample covariance approach is greatly improved, especially with stronger nonlinearity in the high SNR region. We can conclude that 50 dB SIR due to RX nonlinearity is acceptable even with 64QAM nodulation, causing about 0.8 dB performance loss at 1 % BER level

compared to linear receiver, when joint AGC is used. With 16QAM modulation, SIR_{NL}= 45 dB gives about 0.5 dB loss compared to linear RX. These nonlinearity requirements are significantly tighter then in relaxed communication receiver design using superheterodyne architecture but should be doable in practice.

It should be noted that reaching equal nonlinear behavior for different antenna branches is not easy in analog electronics. The used nonlinearity model is very simple, and further studies are needed with more practical modes, corresponding to the used architecture for the receiver front-end.

4.4.2 ADC Effects

We consider only the ideal model of signal quantization in the ADC with given number of bits, ignoring various other imperfections practical ADCs. It is important to take into consideration the effect of high PAPR of the ADC. While the average signal powers are scaled to 1 (or lower in most branches of the joint AGC case), we assume the signal range [-4, 4) for both real and imaginary parts, i.e., two of the bits are used for the integer part. This corresponds to PAPR of 12 dB for purely real (or purely imaginary) signal. Saturating nonlinearity is used to limit possible peaks of the signal exceeding this range. Figure 16 shows the results with 12-bit quantization of I and Q signals, joint AGC with 16QAM and 64QAM modulations for linear RX and nonlinear RX with SIR_{NL}= 50 dB.

The quantization error is an uncorrelated random process, so we don't expect differences due to quantization in the spatial covariance estimate due to different AGC models, and this was also verified by simulations. In the 64QAM case, the performance loss at 1 % BER level due to quantization is about 0.6 dB for linear receiver and 0.8 dB for nonlinear RX with SIR_{NL}= 50 dB. In 16QAM case with the same nonlinearity and quantization, the loss is about 0.2 dB compared to linear receiver without quantization.

In conclusion, the required ADC resolution is significantly higher than in traditional receivers where the channel filtering is done in analog domain. However, it should be noted that in advanced software-defined radio architectures, channel filtering in DSP domain is desired, which leads to great differences in power levels. between the wanted signal and adjacent channels and other spectral components entering the ADC. Then similar and even much harder requirements for the RX linearity and ADC resolution are encountered

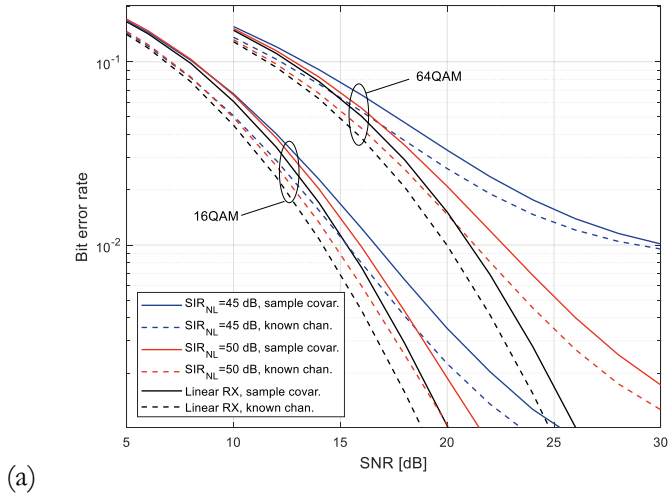

(a)

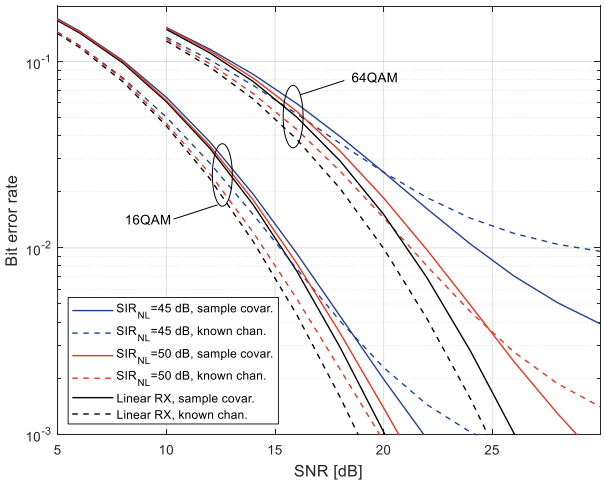

(b)

Figure 15. IRC performance with SIR_{PU}= -30 dB for 16QAM and 64 QAM with different levels of RX nonlinearity: linear RX and SIR_{NL}= {45, 50 dB} corresponding to c_3={0.0023, 0.00127}, respectively. (a) Per-antenna AGC. (b) Joint AGC.

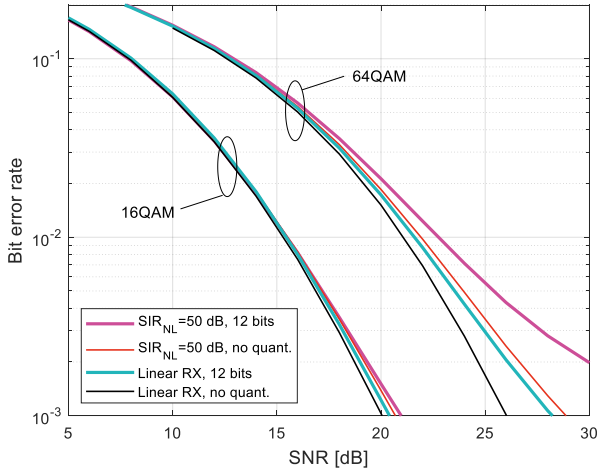

Figure 16. IRC performance with joint AGC, and SIR_{PU}= -30 dB for 16QAM and 64 QAM with 12-bit quantization for linear RX and nonlinear RX with SIR_{NL}= 50 dB.

4.5 Summary and Discussion

The most critical one among the considered RF imperfections is the CFO between the PU signal and CR receiver. However, since the PU signal is received at a high-power level, synchronizing the CR stations to the PU signal with the needed high accuracy should be achievable. Considering other cases, e.g., when both the PU and target CR signal have CFOs, the effect of the high-powered PU signal dominates and remains the most critical issue. The effects of PA nonlinearity in PU and CR transmitters were also tested, and found to less critical, as expected. The developed analytical model for the PU CFO effect could be a basis for analytical modeling BS-CR scenarios with mobility, which was tested experimentally in our earlier work in publication IV. This is an important topic for future studies. Also, the nonlinearity of the CR receiver electronics may be critical due to the wide signal power range to be dealt with. Anyway, the receiver linearity requirements for BS-CR are similar or milder than those for advanced DSP-intensive software defined radio architectures.

5 MULTICARRIER MODULATION AND RESOURCE ALLOCATION IN COGNITIVE RADIOS

In the previous chapters, CR receiver centric signal processing methods were studied targeting at efficient reuse of the black-space frequency spectrum. In this chapter, the focus is on transmitter centric signal processing techniques directed at the so-called whitespaces in the spectrum. First alternative multicarrier schemes are discussed as CR waveform candidates, with focus on spectrum localization aspects.

In the subsequent parts of this chapter, the joint spectrum sensing and resource allocation algorithms under adjacent channel interference are studied. A recent study on this topic is [36], [37] where optimal ways to find the joint spectrum and transmission schedule are studied. The joint spectrum sensing function is briefly discussed, with focus on FFT or filter bank-based sensing, and later the spectrum utilization function implementing optimized resource allocation under power and interference constraints is studied and evaluated in a multicarrier WLAN scenario.

5.1 Multicarrier Modulation Schemes for Cognitive Radio

The core tasks of a CR include spectrum sensing and efficiently utilizing the spectrum with negligible impact to PUs. Choosing the most efficient data transmission technique for CRs from this perspective is a challenging task. The favorite scheme for such a system is OFDM and its variants, mainly due to simplicity and robustness. OFDM also works straightforwardly in multiuser scenarios. CP-OFDM is the most prevalent and popular waveform among various OFDM variants. Its main limitation is that it does not provide proper spectrum localization, which limits its efficiency in dynamic use of the radio spectrum. The limitation is due to the high out of band (OOB) emission around the active frequency channels. This means that wide guard bands are needed, which reduces the efficiency of the spectrum use.

Several alternatives and enhancements have been suggested in the literature [22] [61], [151] to CP-OFDM, ranging from time domain filtering [57], [88], [100], [101], [156] to time domain windowing which is referred to as weighted overlap add OFDM (WOLA-OFDM) [14], [105], [148], [154]. These methods are not without disadvantages of their own. Filtered OFDM (F-OFDM) suffers from inter symbol interference (ISI) and inter carrier interference (ICI) due to the filtering operation. The filtering operation reduces the orthogonality of subcarriers, leading to such issues. For effective windowing-based solution, there is a need for relatively long CP, leading to spectrum efficiency loss. Given these limitations, FBMC shows some promise and is widely considered for the CR applications, especially in the TVWS context [16], [15], [22].

FBMC waveforms are generated using very sharp filters applied at the subcarrier level to suppress the OOB emission that are relatively significant in the CP-OFDM waveforms. FBMC has traditionally been implemented using polyphase networks along with discrete Fourier transform (DFT) or with inverse discrete Fourier transform (IDFT) [23], [124], [137], FBMC also requires the use of offset quadrature amplitude modulation (OQAM) methods to ensure orthogonality between the subcarriers. The higher complexity and other overheads can be reduced by using fast convolution filter banks (FC-FB)[15], [16], [25], [101], [124]. Given these advantages of FBMC, especially the OOB suppression capability, closer inspection of the FBMC performance in the CR context is essential and considered in this chapter.

5.2 Spectrum Sensing in Cognitive Radios

To enable non-interfering transmission between the CR and the PU, proper spectrum sensing is essential. Spectrum sensing provides the CR with appropriate knowledge of the radio spectrum, indicating a white space for transmission that is interference free. Several spectrum sensing techniques have been used in the CR community. For example, [99] and [153] review many of the well-known spectrum sensing techniques. Of the myriad of sensing methods available, energy detector-based spectrum sensing algorithms have been widely considered due to their low computational complexity and reasonable performance. The energy detector-based spectrum sensing performance is sensitive to noise uncertainty, since small error in the noise variance estimate is reflected as significant change in the sensing threshold,

which is critical at low PU power levels [142]. To overcome such disadvantages, advanced sensing techniques have been proposed in [20], [21], [48]- [51], [79], [99], [153], [155]. In the eigenvalue-based sensing method [51], [155], the noise variance is not needed for eigenvalue computations. The main limitation of this method is its relatively high complexity and its performance sensitivity to ACI [21], [50]. To overcome the effects of ACI, the cyclostationary based methods have been suggested [79], [122]. In these methods, the cyclostationary features of the PU signal are used to detect them. The modulated signal from the PU has specific spectral correlation compared to the noise which is wide sense stationary. The primary disadvantage of this method is that its computational complexity is high. Detailed treatment of the spectrum sensing methods can be found in [21], [36], [48]-[51], [77], [79], [98], [142], [153], [155] and the references therein.

5.3 Signal Model and Setup

In our study on the performance of the sensing and resource allocation process during CR transmission, the PU is primarily assumed to be 802.11g standard compliant CP-OFDM based system and the CR system is assumed to use 802.11g like FBMC signal model. Comparisons are extended to include also configurations with FBMC based PU [P1], [P2], [48]. Furthermore, both AFB and FFT based spectrum analysis are considered for spectrum sensing at subband level. The PU and CR systems operate in the same radio band, as illustrated in Figure 11. The transmitters of the PU and CR are denoted by PU-TX and CR-TX, and PU-RX and CR-RX denote the PU and CR receivers, respectively. The radio channels H_0, H_1, H_2 and H_3 are considered as frequency-selective channels between the PU and CR stations. The CR system is assumed to operate in a spectrum gap which has on-going primary transmission on either or both sides of the spectrum gap. Due to this, ACI is unavoidable between different PUs and CRs. The CR and the PU are assumed to use time division duplexing (TDD), in which case reciprocity of uplink and downlink channels can be assumed. Further, it is assumed that there is no cognitive control channel, so that the CRs have no means to exchange control information with each other before establishing the CR communication link. As shown in the Figure 17, there are two PU radio systems that operate in the ISM band and there is

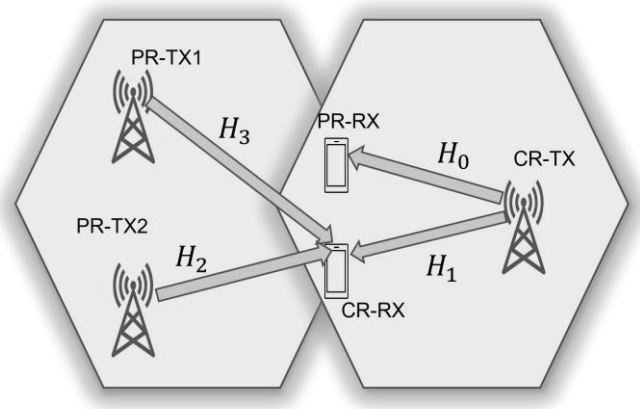

Figure 17. CR spectrum sharing model.

a CR radio system trying to utilize the spectrum gap between the PU channels[P2]. However, the CR needs to consider possible additional weak PU signals in the spectrum gap. Therefore, it must apply spectrum sensing.

The two PU signals are considered to use 3rd and 8th WLAN channels. There is an 8 MHz nominal bandwidth or spectral gap between the two active PU channels. The signal models also include the spectral regrowth effects of a practical nonlinear PAs, which is modelled by the widely used Rapp PA model [119]. The PU spectra are illustrated in [P2] for different backoff levels. Using the complex, I/Q baseband model, the amplitude function at the output of the Rapp PA model is given as

$$g_A = \frac{\kappa A}{(1+\left[\frac{\kappa A}{A_0}\right]^{2p})^{\frac{1}{2p}}}, \tag{5.1}$$

where A is the input amplitude, κ is small signal gain, A_0 is the saturated amplitude, and p is the amplitude smoothness factor of the transition from linear to saturated amplitude range. The AM-PM conversion part, i.e., the amplitude dependant phase distortion of the Rapp model is not included here. Three cases with respect to the PA non-linearity are considered in this study. No regrowth is the ideal reference case, while considering effects of the Rapp PA non-linearity with two different back-off values of 15 dB (modest case) and 5 dB (worst case), are illustrated in Figure 18. Parameters of the Rapp model have been chosen according to the practical model

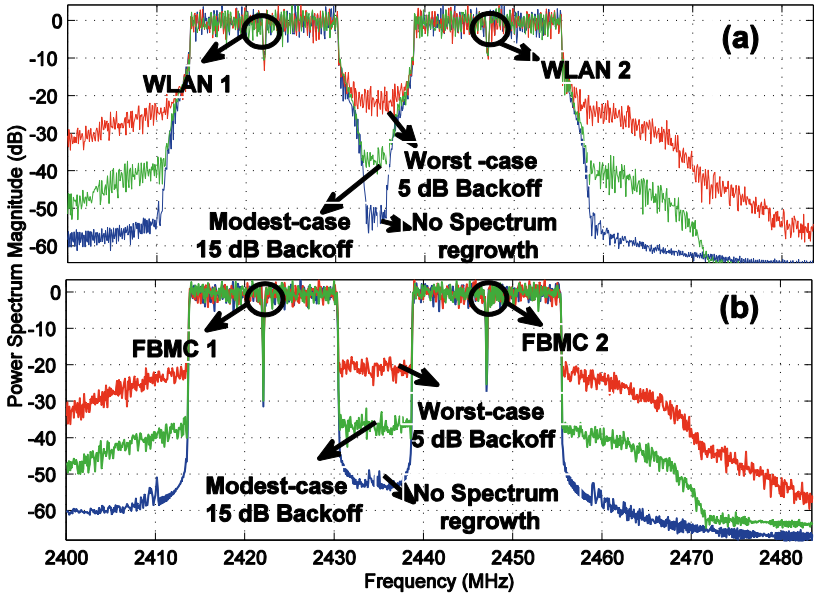

Figure 18. Rapp power amplifier effects on the (a) OFDM (b) FBMC PU spectra.

for PU signals based on [134]. In our study, we use $\kappa = 1, p = 3$ and $A_0 = 1$ as the Rapp model parameters.

The 802.11g based WLAN signal specifications allow the spectral regrowth in this scenario to be at the level of about -20 dB with respect to the passband, i.e., close to the worst-case model. We investigate how the CR system performance is affected by the improved spectral containment of the PU signal through enhanced multicarrier waveform and/or improved PA linearity. These effects for both sensing and utilization functions are addressed in the study.

5.3.1 Signal Model for Cognitive Radio

The enhanced CR waveform chosen here is FBMC along with OQAM as subcarrier modulation. OQAM is used for FBMC based CRs to achieve orthogonality of subcarriers. For FBMC/OQAM, a signal model with real valued symbol sequence at twice the QAM symbol rate is applied, instead of complex QAM symbols. The synthesis filter bank (SFB) for transmitter and the analysis filter bank (AFB) for receiver are designed with this idea in mind; details of this signal model are explained

in [P2]. In the system model shown in Figure 17, H_0 is the channel from CR transmitter to a possible PU receiver within the CR transmission channel, while H_1 is the channel from the CR transmitter to the CR receiver. H_2 and H_3 are channels from the two adjacent-channel PU transmitters to the CR receiver. H_1 is estimated using the usual channel estimation procedure of the CR system whereas the knowledge of H_2 and H_3 could be obtained through the channel reciprocity in TDD operation, which is assumed here for the PU system.

5.3.2 Definition of the Interference Problem

The CR system is assumed to coexist with the primary transmission system in the same geographical region. The CR transmitter causes some interference (ACI) to the primary transmission system and, similarly, the secondary transmission between the two active PU spectra experiences some ACI due to the PUs. There are N_{gap} active subcarriers in the spectrum hole and the subcarrier spacing is Δf. Since the transmitter and receiver are assumed to be static or slowly moving, the effect of ICI between subcarriers can be ignored. The primary and secondary transmission systems occupy contiguous frequency slots. The interference that the CR produces to each of the primaries is required to be less than the maximum interference that can be tolerated by the primary, I_{th}. The spectral distance d_{PU} of a PU is defined as the frequency separation from the DC subcarrier of the CR to the center frequency of the PU (positive for a PU above the upper edge of the gap, negative for a PU below the gap). The interference to the primary transmission due to the k^{th} CR subcarrier depends on the CR subcarrier powers P_k and d_{PU}. Fixing the origin of the frequency axis at the DC subcarrier of the CR, the interference is given by

$$I_k(P_k) = \int_{k\Delta f-\frac{B}{2}}^{k\Delta f+\frac{B}{2}} |H_0(f)|^2 P_k \Phi\ (f - k\Delta f)\Psi(f - d_{PU})df = P_k \Omega_k. \tag{5.2}$$

Here $H_0(f)$ is the channel frequency response between the CR transmitter and a primary receiver. $\Phi(f)$ represents the subcarrier power spectral density of the underlying multicarrier technique employed by the CR. $\Psi(f)$ denotes the PU sensitivity mask characterizing the effects of the PU receiver filtering. B denotes the CR subcarrier bandwidth which is considered significant for the interference estimation. Finally, Ω_k represents the combined interference factor for the k^{th} CR

subcarrier. The SINR due to interference introduced by an adjacent channel primary signal to the k^{th} subcarrier at the receiving CR is given by the equation

$$\mathrm{SINR_k} = \frac{\mathrm{P_k}|\mathrm{H_{1,k}}|^2}{\sigma_w^2 + \int_{k\Delta f - \frac{B}{2}}^{k\Delta f + \frac{B}{2}} |\mathrm{H_2(f)}|^2 \Phi_{CR}(\mathrm{f}-k\Delta f)\psi_{PA}(\mathrm{f}-\mathrm{d_{PU}})\mathrm{df}} = \frac{\mathrm{P_k}}{\sigma_w^2 + \mathrm{J_k}} \quad (5.3)$$

where $H_2(f)$ is the channel frequency response between the primary transmitter and CR receiver. $H_{1,k}$ is the channel gain between the CR transmitter and the CR receiver at the frequency of k^{th} subcarrier. This channel can be assumed to be flat fading at the subcarrier level. $\Psi_{PA}(f)$ is the power spectral density as seen at the output of the PU's transmitter antenna. $\Phi_{CR}(f)$ is the CR receiver's sensitivity mask characterizing the CR receiver subband filtering effects and σ_w^2 is the variance of AWGN. As explained in [P2], we can assume that $\Phi_{CR}(f) = \Phi(f)$.

5.3.3 Filter Bank Energy Detector Based Spectrum Sensing Algorithms

The focus of this study is on subband-based energy detection using either FFT or AFB for spectrum analysis. The energy of the received signal is compared with a pre-computed threshold value. The threshold is calculated according to both noise variance and desired false alarm probability while detecting spectral holes.

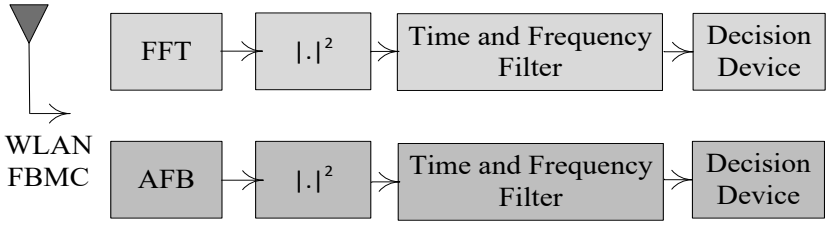

Figure 19.Block diagram of energy detector with AFB and FFT based spectrum analysis.

A block diagram of alternative FFT and AFB based spectrum sensing algorithms is shown in Figure 19. The subband sampling rate is equal to the ADC sampling rate divided by the number of FFT/AFB frequency bins. With a subband-wise spectrum sensing method [P2], the subband signals can be expressed as

$$Y(m,k) = \begin{cases} W(m,k) & H_0 \\ S(m,k) + W(m,k) & H_1 \end{cases} \quad (5.4)$$

where $S(m,k)$ is the transmitted WLAN or FBMC based PU signal as seen in sub-band k during the m^{th} symbol interval. When there are no PU signals (hypothesis $\mathcal{H}_0$), the noise samples $W(m,k)$ are modeled as AWGN with zero-mean and variance σ_w^2. When a PU signal is present (hypothesis $\mathcal{H}_1$), the observed noisy WLAN or FBMC based PU signals can also be modeled as zero-mean Gaussian distribution with variance $\sigma_{PR,k}^2 + \sigma_w^2$.

The time frequency averaging of the signals yields the test statistics

$$\tilde{T}(m,k) = \frac{1}{L_t L_f} \sum_{l=k-\left\lfloor \frac{L_f}{2} \right\rfloor}^{k+\left\lceil \frac{L_f}{2} \right\rceil - 1} \sum_{u=m-L_t+1}^{m} |Y(u,l)|^2. \quad (5.5)$$

Here, L_t and L_f are the window lengths in time and frequency domain averaging, respectively. The value of $\tilde{T}(m,k)$ is used in the decision device to determine the possible occupancy of the corresponding frequency band at the corresponding time interval. The window length in frequency direction is selected based on the expected minimum bandwidth of the PU signal and then the required time domain window length can be calculated from the target false alarm and missed detection probabilities. As $Y(m,k)$ has Gaussian distribution, the probability density function of $\tilde{T}(m,k)$ can be approximated as Gaussian distribution under both $\mathcal{H}_0$ and $\mathcal{H}_1$.

Next, we consider using this spectrum sensing approach in the spectrum slot between two PU channels. With Gaussian approximation, the effects of the spectral leakage from the adjacent PU transmitters on the actual false alarm probability $\tilde{P}_{FA}(k)$ can be estimated as

$$\tilde{P}_{FA}(k) = Q\left(\frac{\lambda - (\sigma_w^2 + I_{adj}(k))}{\sqrt{\frac{1}{L_t L_f}\left(\sigma_w^2 + I_{adj}(k)\right)}} \right) \quad (5.6)$$

where the leakage power from the adjacent PU transmitter to the sensing frequency band between frequencies f_1 and f_2 is given by

$$I_{adj}(k) = \int_{f_1}^{f_2} |H_2(f)|^2 \psi_{PA}(f) df. \quad (5.7)$$

$I_{adj}(k)$ is assumed to be of zero mean circular Gaussian model and $H_2(f)$ is the channel frequency response between the PU transmitter and the CR receiver. If strong PU signals are present on both sides, the sum of their ACI contributions should be used for $I_{adj}(k)$ in (5.7).
The sensing threshold λ can be obtained as follows:

$$\lambda = Q^{-1}\left(\tilde{P}_{FA}(k)\right)\sqrt{\frac{1}{L_t L_f}}\left(\sigma_w^2 + I_{adj}(k)\right) + \left(\sigma_w^2 + I_{adj}(k)\right). \tag{5.8}$$

Given this threshold, the detection probability P_D, is given by

$$P_D(k) = Q\left(\frac{\lambda - ((\sigma_w^2 + I_{adj}(k) + \sigma_{PU,k}^2)}{\sqrt{\frac{1}{L_t L_f}}\left(\left(\sigma_w^2 + I_{adj}(k)\right) + \sigma_{PU,k}^2\right)}\right). \tag{5.9}$$

Due to the statistical nature of the spectrum sensing process and spectral leakage effects of PU, different number of empty subbands, N_{gap}, are detected under different SNR conditions, which is taken into consideration in the resource allocation process.

5.4 Spectrum Utilization and Resource Allocation

Once the main problem of identifying a spectrum gap is solved by using the algorithms stated in the previous section, utilization of this spectrum efficiently becomes the area of focus. The sensing algorithm gives a number of available subbands along with the information about the non-active (white space) band edges. The Shannon capacity dictates that in case of multicarrier schemes, the maximum rate [18], [47], [60], [62], [87], [112] is given by

$$R_{CR} = \sum_{k=1}^{N_{gap}} \Delta f \cdot log_2(1 + \frac{P_k}{\sigma_k^2}) \tag{5.10}$$

where the $\sigma_k^2 = \sigma_w^2 + \sum_{i=1}^{N_{PU}} J_{k,i}$. $J_{k,i}$ is the effective interference power contributed by i^{th} primary at the k^{th} CR subcarrier. N_{PU} is the number of PU's contributing to the interference at the receiving CR station. In our case study, $N_{PU} = 2$, i.e., there are PUs' adjacent to the lower and upper edges of the white space. The model could

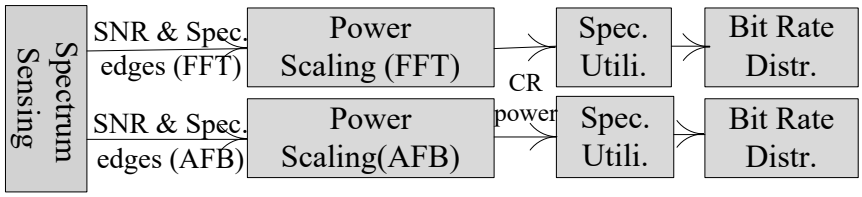

Figure 20. Spectrum utilization block diagram with AFB and FFT based spectrum sensing.

be simplified by assuming that these PUs affect only the lower and upper half of the subcarriers, respectively. P_k is the transmit power used by the CR for subcarrier k. It is assumed that the channel changes slowly so that the channel gains, and consequently $J_{k,i}$, will be approximately constant during each transmission frame. Further, there is no ICI in the CR reception, due to low mobility. Figure 20 shows the main functions of the spectrum utilization part.

As derived in [P2], the maximization of the capacity given in Eq. (5.10) can be formulated as an optimization problem:

$$R_{CR} = \max_{\{P_k\}} \sum_{k=1}^{N_{gap}} \Delta f \cdot log_2(1 + \frac{P_k}{\sigma_k^2}) \tag{5.11}$$

subject to $\sum_{k=1}^{N_{gap}} P_k \leq P_T$, $\sum_{k=1}^{N_{gap}} P_k \Omega_k \leq I_{th}$ and $P_k \geq 0, \forall k \in \{1,2,\dots,N_{gap}\}$, where I_{th} is the PU interference threshold. This is a convex optimization problem and the Lagrangian can be written as

$$G_{snr} = \sum_{k=1}^{N_{gap}} \Delta f . log_2(1 + \frac{P_k}{\sigma_k^2}) - \lambda_0 \sum_{k=1}^{N_{gap}} (P_k - P_T) - \lambda_1 (P_k \Omega_k - I_{th}) + \lambda_2 (\sum_{k=1}^{N_{gap}} (P_k) . \tag{5.12}$$

Using the Karush-Kuhn-Tucker (KKT) conditions, which are derived in detail in [87], [134], the optimum solution can be written as

$$P_k = \left[\frac{1}{\lambda_0 \Omega_k + \lambda_1} - \frac{\sigma_k^2}{|h_k|}\right]^+ \tag{5.13}$$

where $[y]^+ = max(0, y)$. The optimal solution has high computationally complexity, hence a lower complexity algorithm called the power interference (PI) algorithm which divides the problem into stages has been developed in [87]. First

the interference constraint is ignored, keeping only the total power constraint and this leads to the classical water filling solution

$$P_k = \left[\gamma - \frac{\sigma_k^2}{|h_k|}\right]^+ \tag{5.14}$$

where γ is the water filling level. When the total power is ignored, the solution [P2] becomes

$$P_k = \left[\frac{1}{\lambda_0 \Omega_k} - \frac{\sigma_k^2}{|h_k|}\right]^+. \tag{5.15}$$

The value of λ'_0 can be obtained by substituting Eq (5.15) into the constraint $\sum_{k=1}^{N_{gap}} P_k{}'\Omega_k = I_{th}$ to get

$$\lambda_0 = \frac{|N_{gap,l}|}{I_{th}^{N_{gap}} + \left(\sum_i \frac{\Omega_k \sigma_k^2}{|h_k|^2}\right)}. \tag{5.16}$$

The above solution is optimal only when the total power is greater than or equal to the power under the interference constraint, in which case P_k takes nonnegative value for each *k*. Mostly, in practice this condition is not true after completing these steps. This is the motivation for the PI algorithm, which iteratively discards subcarriers with lowest SINR until nonnegative values are obtained for each *k*. Detailed discussion and its comparison to various other algorithms for spectrum utilization are available in [P2], [P3], [48], [52] and the references therein.

5.5 Results and Discussion

In the considered scenario, the CR's spectrum sensing function has identified a potential spectral gap between two relatively strong PUs, as illustrated in Figure 12. We consider the worst-case scenario, where the two adjacent PUs are at the same power level. Also, there is the possibility that there is another, relatively weak PU signal, using one of the WLAN channels 4…7, and fully or partly occupying the gap between channels 3 and 8. Thus, the CR needs to ensure the principal purpose of spectrum sensing which is to make sure that there is no other PUs active in the considered gap. It is assumed that there are no additional signals within the spectral gap, but the spectrum sensing makes anyway false alarms. Especially close to the

edges of the gap, the spectrum leakage from the adjacent PU's raises the false alarm probability. This effect depends on the power level of the PUs, which is indicated below by the SNR of the PUs.

In this case study, the spectrum sensing, and CR transmissions use a smaller subband spacing of 78.125 kHz, instead of the 312.5 kHz subcarrier spacing of WLANs, in order to reduce the effects of frequency selective channels. Targeting at -5 dB SNR in spectrum sensing, the false alarm probability of 10 % and detection probability of 90 %, the required sample complexity is around 250 complex samples. The time and frequency averaging lengths are chosen as 50 and 5, respectively. The spectral hole starts from the upper sidelobes of WLAN 1 signal (channel 3) and ends at the lower sidelobes of WLAN 2 (channel 8) spectrum. The available number of subbands, i.e., bandwidth of the spectrum hole, is obtained after subband based energy detection, using FFT or AFB for spectrum analysis. The initial SINR estimation and spectrum allocation are done based on the sensing results. Then, the SINR estimates are updated during CR system operation to track the changing radio environment under frequency selective fading channel conditions. It is assumed that the spectrum sensing is done in regular intervals during gaps in the CR transmission and this helps in detecting reappearing PU signals in the spectral gap. Different independent instances of the frequency selective channel models with 90 ns delay spread and 16 taps [85] are used for the channels H0 – H3.

The bandwidth of the detected spectral hole is shown in Figure 21 as a function of the average adjacent PU SNR at the CR RX. The spectral leakage due to PU's PA nonlinearity is affecting significantly on the width of the detected hole. In this respect, three different cases, as explained in Section 5.3.1, ideal PA, modest PA nonlinearity with 15 dB back-off, and worst-case nonlinearity with 5 dB back-off are considered and plotted. The actual false alarm probabilities in the spectral gap as a function of the PU SNR can be found in [P2] for different levels of spectral regrowth. A number of subbands, which are determined to be occupied with FFT or AFB based spectrum sensing, are empty in the spectrum utilization phase. The power of these occupied subchannels is reallocated to the other subbands that can be used by the CR.

The power allocation is done by utilizing the PI algorithm, and the resulting capacity, in terms of bits/s/Hz, is shown in Figure22. It shows the capacity of a CR in a spectral gap between two Pus versus PUSNR when using PI algorithm for power allocation with ideal PA model and with RappPA model with 15dB backoff a the

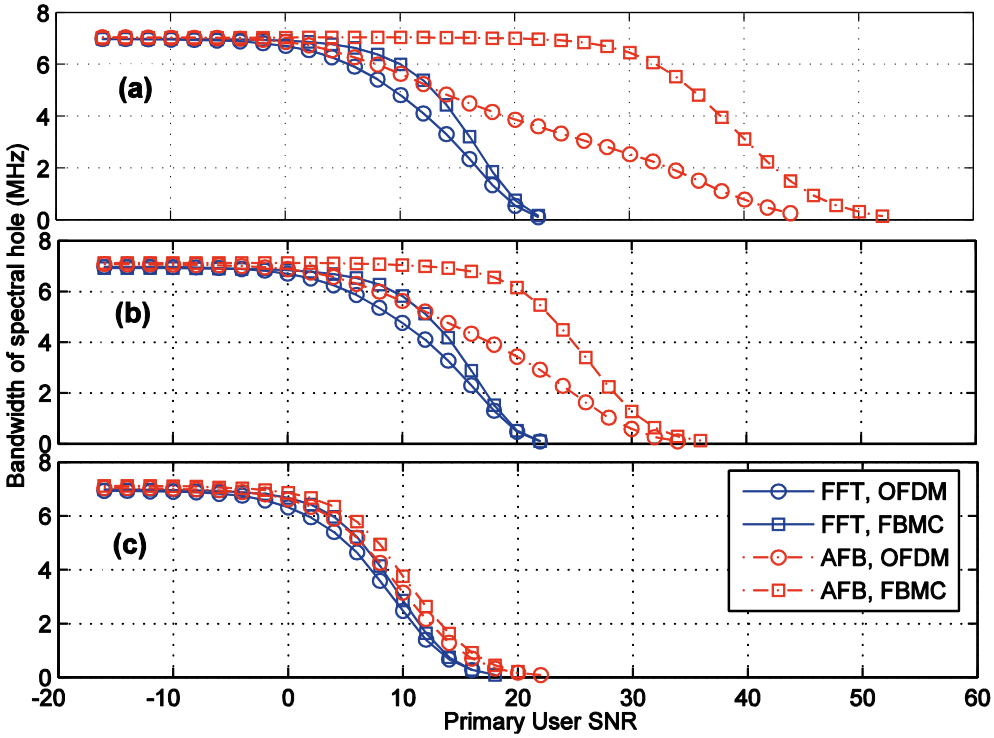

Figure 21. Average bandwidth of the detected spectral hole using sample complexity of 250 under frequency selective channel model with (a) ideal PA model, (b) Rapp PA with 15 dB backoff as the modest case, (c) Rapp PA with 5 dB backoff as the worst case.

modest case and with 5dB backoff as the worst case. Both FFT and AFB based sensing are included for OFDM and FBMC primaries.The PU interference threshold I_{th} is selected to be 6 dB below the thermal noise level to get rid of significant performance loss in case the primary receiver is operating close to the sensitivity level. In these results, we can see that the capacity is greatly affected by the spectrum localization of the PU waveform and the nonlinearity of the PAs of the primaries. Regarding spectrum sensing, we can see significant benefit from AFB based spectrum analysis.

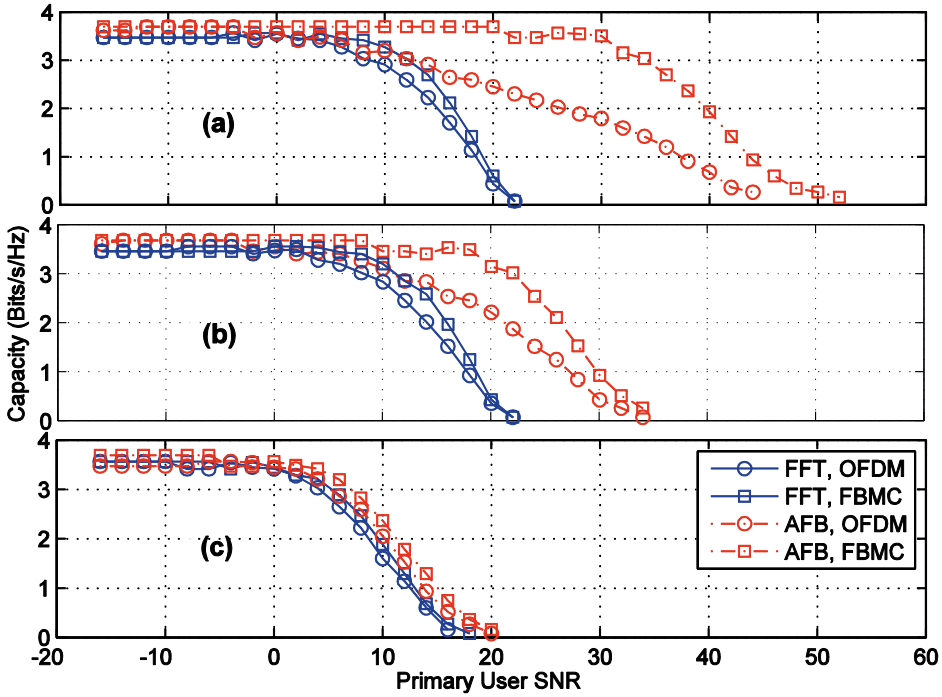

Figure 22. Capacity of a CR in a spectral gap between two PUs versus PU SNR when using PI algorithm for power allocation. (a) Ideal PA model, (b) Rapp PA with 15 dB backoff as the modest case, (c) Rapp PA with 5 dB backoff as the worst case. Both FFT and AFB based sensing are included.

5.6 Chapter Summary

The central topic of this chapter is the combined spectrum sensing and utilization method, while assuming a practical frequency selective channel model and practical nonlinear PA model. We found through simulations that the CR system performance in terms of theoretical transmission capacity while using water-filling based subcarrier power allocation. The AFB and FFT based sensing methods were evaluated for determining a spectral hole with OFDM and FBMC based PU signal models. Then, the PI resource allocation method was applied with the available number of unoccupied subbands, which was determined by the spectrum sensing part. In terms of the sensing performance, especially AFB based sensing performance depends greatly on the level of spectral regrowth due to the PA nonlinearity of adjacent PUs. AFB had clear benefits due to much better spectral containment of the subbands, even with modest nonlinearity of the primary users' PAs. The efficiency and computational complexity analysis of the considered sensing

methods are elaborately discussed in the references [49] - [53]. As a summary, while FFT in the receiver side of OFDM, or AFB in the receiver side of FBMC, can be used for the reception, it can also be used for the sensing purposes without extra hardware cost. In terms of the computational complexity of the proposed approaches, especially in the sensing stage, energy detector-based approaches using either FFT or AFB are the simplest and cost friendly sensing techniques compared to the advance eigenvalue-based approaches

In [P1], a sub-optimal resource allocation process is used. The interference leakage from the CRs to PUs was ignored, but the results are rather similar to the ones shown above. This indicates that the interference leakage from CR to PUs was not necessarily affecting, critically the achievable data rate of the CR. Also smplified resource allocation schemes might be sufficient without significant loss in CR's capacity. These aspects are worth to consider in further development of these methods. It is also worth to mention that [P1] also shows the effect of CRs' SNR on data rate usingthe SNR values of 10 dB and 3 dB.

One important benefit of FBMC as CR transmission technique was that it can utilize narrow spectral gaps in an effective and flexible way, even in the presence of strong primaries at the adjacent spectral slots. However, in case of adjacent PUs with poor spectrum localization or strong PA nonlinearity, there is an inevitable loss of capacity because the subcarriers close to the edges of PU spectra are determined to be occupied. According to the results of this study, the PI algorithm can be directly utilized with the developed highly enhanced and realistic CR system model, in comparison to earlier studies. Due to the above features, filter bank-based CR systems have a potential for higher capacity in comparison to the traditional OFDM based systems.

It is true that many primary systems use waveforms with poor spectrum localization and relaxed out-of-band emission requirements. This was especially the case in systems operating in the ISM bands. While FBMC has excellent spectrum localization, it has found very limited use in existing communication systems. However, there are various approaches for improving the spectrum localization of the CP-OFDM waveform, as briefly discussed in Section 5.1. We can expect similar results, as shown in this chapter for FBMC, to be achived with enhanced OFDM schmes with relatively low complexity, such as WOLA-OFDM, filrered OFDM, and other spectrum-agile multicarrier waveforms [22], [124]. Actually, in [48] we have tested a similar spectrum sensing and resource allocation scheme using an enhanced

OFDM scheme based on edge windowing and cancellation carriers for improving the spectrum localization.

While spectrum sensing has found limited use in existing wireless communication systems, it was found to be an interestig element in 5G furter development and beyond [22], [156]. In further studies of spectrum sensing and spectrum allocation, energy efficeincy is an important metric and artificial intelligence can be expected to have an important role.

6 CONCLUSIONS

Wireless communication research has been one of the very active areas of research mainly due to the ever-increasing need for higher capacity and higher data rates. As a result of intense research and due to substantial contribution from many researchers, the field has grown leaps and bounds. Main areas of focus have been to find more efficient methods for utilizing limited radio resources. For instance, OFDM methods have demonstrated increased spectral efficiency of data transmission especially in fading channels. Consequently, OFDMA is the leading modulation scheme used in current technologies. Spatial multiplexing and diversity combining through multiple antennas have also been widely used to exploit multipath channels.

In CRs, like in the latest wireless standards and technologies such as 5G-NR, apart from the modulation and coding improvements, interference handling plays a critical role. The idea of interference avoidance and interference management at higher layers was discussed and reviewed in the Chapter 2. Such methods aim at taking proactive action in shaping transmissions in such a way that any interference to the primary transmission is avoided or made negligible. One of the focus areas of this thesis is the interference rejection. Interference rejection techniques can be traced back to military communications in which a transmission needs to be protected from an intentional or unintentional jammer. With rapid increase in wireless communication, applications of interference rejection have increased in the commercial applications as well. Interference rejection combining gains a central role in the BS-CR approaches. Diversity combining methods amongst many other interference cancellation techniques have been considered in this thesis as they make the receiver robust and improve signal quality for the target CR user. The earlier works that have been completed on the area of cognitive interference cancellation, for instance [128], have been mostly transmitter centric approaches where the BS-CR is used as a repeater of the PU signal to guarantee that the CR does not cause interference to the nearby primaries.

Our work, explained in Chapter 3, primarily focuses on receiver centric methods like the IRC based BS-CR. For a concise summary of work done on the IRC based method, it is crucial to mention first that IRC-based BS-CR is a novel major contribution in the field. While IRC has been widely studied and adopted in practical systems, studying IRC with very strong interference and in the presence of practical RF imperfections are at the core of these studies. The effects of mobility, especially at high frequencies are of particular interest in this study. It can be seen from the performance analysis in Chapter 3 that there is a limited tolerance to mobility, especially with high carrier frequencies. Channel estimation and its utilization play central roles in the enhanced IRC based solution. They are aimed at minimizing the PU interference while maximizing the CR throughput. To further enhance the understanding of radio environment and to improve the BS-CR performance, the use of sample covariance estimates with silent gaps in CR transmission was explored. The pilot transmission and interpolation of covariance estimates between silent gaps was found to greatly enhance the IRC process. To answer the second research question of Section 1.2, we can state that he developed enhanced interference cancellation algorithms using multiple antennas enables BS-CR operation under strong interference from the PU. We considered scenarios where the PU signal power at the CR receiver is up to 30 dB higher that the target CR signal. Covariance interpolation between silent gaps improves greatly the robustness with time-varying channels. Good link performance can be reached with up to 20 km/h mobility at the 700 MHz carrier frequency considered for terrestrial TV spectrum reuse. This indicates that the proposed BS-CR scheme could be feasible at below 6 GHz frequencies with pedestrian mobilities, assuming typical channel delay spread and subcarrier spacing values for systems operating in those frequency bands.

Further studies on PU channel estimation-based BS-CR are worthwhile considering that the results shown in Chapter 3 are with perfect PU channel knowledge and are usually somewhat better than the performance with sample covariance estimation. We can expect it to have similar performance in practice. PU channel estimation could help in better handling of mobility issues. However, it needs more information about the PU signal structure (considering, e.g., different modes and variants of DVB, and their complicated pilot structures), which could make things complicated, e.g., requiring CR's to decode PUs control information.

On the other hand, the spatial covariance estimation-based scheme was found to be more robust against certain RF imperfections then the PU channel estimation-based approach. All these ideas need further study that is not in the scope of this thesis. In addition, to ensure that the nearby PU receivers are not affected by the interference from the BS-CR, further studies are needed, especially on cooperative spectrum sensing amongst the CRs. The CR devices should reliably estimate the PU power levels in their respective region of operation and cooperate to ensure that the interference on the PU is minimized.

The third research question was addressed in Chapter 4, where the impact of RF imperfections on the BS-CR performance were studied. One of the central issues is the CFO between the PU signal and CR receiver. This is essential for proper synchronization between the PU signals and the CR receivers. In the presence of CFO in both PU and CR signals at the CR receiver, the interference due to CFO is dominated by the high-power PU signal and this is the most critical issue concerning RF imperfections. The CFO requirements depend on the delay spread of the PU channel, and they are usually significantly (2-4 times) tighter than in traditional OFDM networks. However, due to the high-powered nature of the PU transmission, synchronization with the needed high accuracy is considered achievable. The analytical model developed for the PU CFO effect could also be a basis for analytical modeling of such BS-CR scenarios with mobility. The effects of PA nonlinearity in PU and CR transmitters were also examined and found to less critical, as expected.

The issue of nonlinearity of CR receiver electronics was also analyzed by simulations. As expected, the requirements for the receiver front-end linearity and ADC resolution were found to be harder than in traditional receivers. However, CRs are usually expected to utilize software defined radio (SDR) type receiver architectures with high flexibility and capability to support high dynamic range. This means ability to receive weak signals in the presence of strong adjacent channels, which are suppressed by digital signal processing after the ADC. Based on the results of Section 4, such SDR receivers can be expected to support the receiver nonlinearity requirements for IRC based BS-CR.

Finally, we moved to the transmitter related topic of spectrum utilization and resource allocation under power and interference constraints. The study focused on resource allocation aiming to effectively control the interference leakage to PUs operating in adjacent channels, while considering the spectrum localization and

limitations of spectrum sensing of different waveforms, CP-OFDM and FBMC. Regarding the first research question, it was demonstrated that the spectrally well-localized waveform, FBMC, together with optimized resource allocation strategies, provide clear benefits in effective spectrum utilization by CRs under interference leakage between adjacent PU and CR channels. However, the most efficient utilization of spectrum gaps is reached when both PUs and CRs use waveforms with good spectrum localization, which is not the case, e.g., in the frequency bands of legacy OFDM systems.

Various applications of the study done in this work could be used in the TVWS and TV black-space cases. The BS-CR scheme could also be applied in underlay device-to-device communication in the cellular networks [92]. Also fixed wireless access could also be an interesting area in which IRC based BS-CR could be trialed to check such systems' performance.

REFERENCES

[1] Spectrum Policy task force report, Federal Communications Commission, Tech. Rep. TR 02-155, Nov. 2002.

[2] Secondary Markets Initiative, online document 2006, Available: https://www.fcc.gov/secondary-markets-initiative-and-spectrum-leasing.

[3] ETSI TR 102 838 V1.1.1, "Reconfigurable Radio Systems (RRS)); Radio Base Station (RBS) Software Defined Radio (SDR) status implementations and costs aspects including future possibilities", 2009.

[4] ETSI TR 102 838 V1.1.1, "Reconfigurable Radio Systems (RRS)); Radio Base Station (RBS); Cognitive Radio System Concept", 2010.

[5] ETSI, "EN 300 744: Digital video broadcasting (DVB); Framing structure, channel coding and modulation for digital terrestrial television," January 2009.

[6] R4-163314, "Realistic Power Amplifier Model for the New Radio Evaluation," Nokia, 3GPP RAN79.

[7] I.F. Akyildiz, W.-Y. Lee, M.C. Vuran, S. Mohanty, "A Survey of Spectrum Management of Cognitive Radio Networks", IEEE Communications Magazine, April 2008, 40–48R.

[8] M. Alonso et al. Spectrum occupancy and hidden node margins for cognitive radio applications in the UHF band, in: eds Mobile Multimedia Communications. MobiMedia 2011, Lecture Notes of the Institute for Computer Sciences, Social Informatics and Telecommunications Engineering, vol 79. L. Atzori, J. Delgado, D. Giusto (Springer, Berlin, Heidelberg, 2012).

[9] J. Armstrong, "Analysis of New and Existing Methods of Reducing Intercarrier Interference Due to Carrier Frequency Offset in OFDM," IEEE Trans. Comm., vol. 47, no. 3, pp. 365-369, March 1999.

[10] A. Azarfar, C. Liu, J. Frigon, B. Sansò and D. Cabric, "Joint transmission and cooperative spectrum sensing scheduling optimization in multi-channel dynamic spectrum access networks," 2017 IEEE International Symposium on Dynamic Spectrum Access Networks (DySPAN), Baltimore, MD, USA, 2017, pp. 1-10

[11] Z. Bai et al., "On the Equivalence of MMSE and IRC Receiver in MU-MIMO Systems," IEEE Communications Letters, vol. 15, no. 12, pp. 1288-1290, December 2011.

[12] O. Bakr, M. Johnson, R. Mudumbai, K. Ramchandran, "Multi Antenna Interference Cancellation Techniques for Cognitive Radio Applications", in Proc. IEEE WCNC 2009.

[13] M.A. Beach et al, "Study into the Application of Interference Cancellation Techniques", Roke Manor Research Report 72/06/R/036/U, April 2006.

[14] N. C. Beaulieu and P. Tan, "On the Effects of Receiver Windowing on OFDM Performance in the Presence of Carrier Frequency Offset", IEEE Trans. on wireless comm., vol. 6, no. 1, January 2007.

[15] M. Bellanger, "FBMC physical layer: A primer," Physical layer for dynamic spectrum access and cognitive radio (PHYDYAS) project, Tech. Rep., Jun. 2010.

[16] V. Berg, J. Doré, and D. Noguet, "A flexible FS-FBMC receiver for dynamic access in the TVWS," in 2014 9th International Conference on Cognitive Radio Oriented Wireless Networks and Communications (CROWNCOM), Jun. 2014, pp. 285–290.

[17] Y. Beyene, K. Ruttik, R. Jantti, "Effect of secondary transmission on primary pilot carriers in overlay cognitive radios," in Proc. CROWNCOM2013, Washington, DC, 2013, pp. 111-116.

[18] E. Biglieri, J. Proakis and S. Shamai (Shitz), "Fading channels: Information-theoretic and communications aspects", IEEE Transactions on Information Theory, vol. 44, no. 6, Oct. 1998.

[19] E. Biglieri, A.Goldsmith, L.Greenstein, N.Mandayam,, & H. Poor,. "Principles of Cognitive Radio" 2012. Cambridge: Cambridge University Press T. X. Brown, "An analysis of unlicensed device operation in licensed broadcast service bands," in Proc. IEEE DySPAN'05, Baltimore, USA, Nov. 2005, pp. 11–29.

[20] T. E. Bogale, L. Vandendorpe and L. B. Le, "Wide-Band Sensing and Optimization for Cognitive Radio Networks With Noise Variance Uncertainty," in IEEE Transactions on Communications, vol. 63, no. 4, pp. 1091-1105, April 2015.

[21] T. E. Bogale and L. Vandendorpe, "Max-Min SNR Signal Energy Based Spectrum Sensing Algorithms for Cognitive Radio Networks with Noise

Variance Uncertainty," in IEEE Transactions on Wireless Communications, vol. 13, no. 1, pp. 280-290, January 2014.

[22] H. Bogucka; A. Kliks; P. Kryszkiewicz, "Multicarrier Technologies for Flexible Spectrum Usage," in Advanced Multicarrier Technologies for Future Radio Communication: 5G and Beyond, Wiley, 2016, pp.219-245.

[23] B. Farhang-Boroujeny and R. Kempter, "Multicarrier communication techniques for spectrum sensing and communication in cognitive radios," in IEEE Communications Magazine, vol. 46, no. 4, pp. 80-85, April 2008

[24] W. Brodersen, A. Wolisz, D. Cabric, S. M. Mishra, and D. Willkomm, "CORVUS: A cognitive radio approach for usage of virtual unlicensed spectrum," Berkley wireless research center, White paper, 2004.

[25] M.-L. Boucheret, I. Mortensen, and H. Favaro, "Fast convolution filter banks for satellite payloads with on-board processing," IEEE Journal on Selected Areas in Communications, vol. 17, no. 2, pp. 238–248, Feb. 1999.

[26] T. X. Brown, "An analysis of unlicensed device operation in licensed broadcast service bands," in Proc. IEEE DySPAN'05, Baltimore, USA, Nov. 2005, pp. 11–29.

[27] S.Buljore, H.Harada, S.Filin, P.Houze, K.Tsagkaris, O.Holland, T.Farnham, K.Nolte and V.Ivanov, "An Architecture and Enablers for Optimized Radio Resource usage: The IEEE P1900.4 Working Group", IEEE Communications Magazine, vol. 47, no. 1, pp. 122-129, Jan. 2009.

[28] D. Cabric, S. M. Mishra and R. W. Brodersen, "Implementation issues in spectrum sensing for cognitive radios," Conference Record of the Thirty-Eighth Asilomar Conference on Signals, Systems and Computers, 2004., 2004, pp. 772-776 Vol1.

[29] D. Cabric, "Cognitive Radios: System Design Perspective", Ph.D. Thesis, University of California, Berkeley, 2007.

[30] A.B. Carleial, "A Case where Interference Does Not Reduce Capacity," IEEE Trans. Information Theory, 01/1975

[31] A. B. Carleial, "Interference channels," IEEE Trans. Information. Theory, vol. IT-24, pp. 60–70, Jan. 1978

[32] J. M. Chapin and W. H. Lehr, "Cognitive Radios for dynamic spectrum access - The Path to Market Success for Dynamic Spectrum Access Technology," in IEEE Communications Magazine, vol. 45, no. 5, pp. 96-103, May 2007.

[33] Z.Chen , C.X .Wang, X Hong, JS Thompson, Vorobyov SA, Ge X, Xiao H, Zhao F. Aggregate interference modeling in cognitive radio networks with power and contention control. IEEE Transactions on Communications. 2012 Feb 9;60(2):456-68.

[34] Z. Chen, C.X. Wang, X. Hong, J. Thompson, S. A. Vorobyov and X. Ge, "Interference modeling for cognitive radio networks with power or contention control," in Proc. IEEE WCNC 2010, Sydney, Australia, Apr. 2010.

[35] C. C. Cheng, S. Sezginer, H. Sari and Y. T. Su, "Linear Interference Suppression with Covariance Mismatches in MIMO-OFDM Systems," in IEEE Trans. on Wireless Communications, vol. 13, pp. 7086-7097, Dec. 2014.

[36] K. Cichoń, A. Kliks and H. Bogucka, "Energy-Efficient Cooperative Spectrum Sensing: A Survey," in IEEE Communications Surveys & Tutorials, vol. 18, no. 3, 2016, pp. 1861-1886.

[37] K. Cichoń, H. Bogucka, G. Molis, J. Adamonis and T. Krilavičius, "Learning and detection mechanisms of spectral-activity information towards energy efficient 5G communication," *2018 Baltic URSI Symposium (URSI)*, Poznan, Poland, 2018, pp. 273-277.

[38] L. J. Cimini, "Analysis and simulation of a digital mobile channel using orthogonal frequency division multiplexing," IEEE Trans. Communication, vol. 33, no. 7, pp. 665–675, Jul. 1985.

[39] L. Cohen, "Time-frequency analysis: theory and applications," 1995, Prentice-Hall, Inc., USA.

[40] C. Cordeiro. "IEEE802.22: The First Worldwide Wireless Standard Based on Cognitive Radios". DySPAN, 2005(8-11):328-337.

[41] S. Cripps, RF Power Amplifiers for Wireless Communications, Second Edition, Artech, 2006.

[42] A. Davydov, V. Sergeev, B. Mondal, A. Papathanassiou and A. Sengupta, "Robust MMSE-IRC for Uplink Massive MIMO aided C-RAN Network," 2020 IEEE Globecom Workshops (GC Wkshps, 2020, pp. 1-5.

[43] N. Devroye, P. Mitran and V. Tarokh, "Achievable rates in cognitive radio channels," in IEEE Transactions on Information Theory, vol. 52, no. 5, pp. 1813-1827, May 2006.

[44] N. Devroye, P. Mitran and V. Tarokh, "Limits on communications in a cognitive radio channel," in IEEE Communications Magazine, vol. 44, no. 6, pp. 44-49, June 2006

[45] N. Devroye, P. Mitran, M. Sharif, S. Ghassemzadeh, and V. Tarokh, "Information theoretic analysis of cognitive radio systems, Cogn. Wireless Commun., 2007.

[46] N. Devroye and V. Tarokh, "Fundamental limits of cognitive radio networks, in Cognitive Wireless Networks: Concepts, Methodologies and Vision, F. Fitzek and M. Katz, Eds. New York: Springer, 2007.

[47] S. N. Diggavi, "Analysis of multicarrier transmission in time-varying channels," Proceedings of ICC'97 - International Conference on Communications, 1997, pp. 1191-1195 vol.3.

[48] S. Dikmese, A. Loulou, S. Srinivasan and M. Renfors, "Spectrum sensing and resource allocation models for enhanced OFDM based cognitive radio," 2014 9th International Conference on Cognitive Radio Oriented Wireless Networks and Communications (CROWNCOM), Oulu, Finland, 2014, pp. 360-365

[49] S. Dikmese, P. C. Sofotasios, T. Ihalainen, M. Renfors and M. Valkama, "Efficient Energy Detection Methods for Spectrum Sensing Under Non-Flat Spectral Characteristics," in IEEE Journal on Selected Areas in Communications, vol. 33, no. 5, pp. 755-770, May 2015

[50] S. Dikmese, P. C. Sofotasios, M. Renfors and M. Valkama, "Subband Energy Based Reduced Complexity Spectrum Sensing Under Noise Uncertainty and Frequency-Selective Spectral Characteristics," in IEEE Transactions on Signal Processing, vol. 64, no. 1, pp. 131-145, Jan.1, 2016

[51] S. Dikmese and M. Renfors, "Performance analysis of eigenvalue-based spectrum sensing under frequency selective channels," 2012 7th International ICST Conference on Cognitive Radio Oriented Wireless Networks and Communications (CROWNCOM), 2012, pp. 356-361,

[52] S. Dikmese, S. Srinivasan and M. Renfors, "FFT and Filter Bank-based Spectrum Sensing and Spectrum Utilization for Cognitive Radios," in Proc. 5th International Symposium on Communications, Control and Signal Processing, 2012, pp. 1-5.

[53] S.Dikmese, "Enhanced spectrum sensing techniques for Cognitive Radio systems", Ph.D thesis, Tampere University, 2015

[54] M. Escartin and P. A. Ranta, "Interference rejection with a small antenna array at the mobile scattering environment," First IEEE Signal Processing Workshop on Signal Processing Advances in Wireless Communications, 1997, pp. 165-168.

[55] R. H. Etkin, D. N. C. Tse and H. Wang, "Gaussian Interference Channel Capacity to Within One Bit," in IEEE Transactions on Information Theory, vol. 54, no. 12, pp. 5534-5562, Dec. 2008

[56] Amr, Fahim, "Radio Frequency Integrated Circuit Design for Cognitive Radio Systems" , Springer Nature, 2015

[57] M. Faulkner, "The effect of filtering on the performance of OFDM systems," in IEEE Transactions on Vehicular Technology, vol. 49, no. 5, pp. 1877-1884, Sept. 2000.

[58] A. B. Flores, R. E. Guerra, E. W. Knightly, P. Ecclesine and S. Pandey, "IEEE 802.11af: a standard for TV white space spectrum sharing," in IEEE Communications Magazine, vol. 51, no. 10, pp. 92-100, October 2013.

[59] K. G. Gard, H. M. Gutierrez and M. B. Steer, "Characterization of spectral regrowth in microwave amplifiers based on the nonlinear transformation of a complex Gaussian process," in IEEE Transactions on Microwave Theory and Techniques, vol. 47, no. 7, pp. 1059-1069, July 1999.

[60] M. Gastpar, "On capacity under received-signal constraints", in proc. 42nd Annual Allerton Conference Communication, Control Comput., Monticello, USA, Sep. 2004.

[61] R. Gerzaguet et al., "Comparison of promising candidate waveforms for 5G: WOLA-OFDM versus BF-OFDM," 2017 International Symposium on Wireless Communication Systems (ISWCS), 2017, pp. 355-359.

[62] A.Ghasemi and E.Sousa, "Fundamental limits of spectrum-sharing in fading environments", IEEE Transaction on Wireless Communication vol. 6, no.2, pp.649-658, Feb. 2007.

[63] A. Gokceoglu, S. Dikmese, M. Valkama and M. Renfors, "Energy Detection under IQ Imbalance with Single- and Multi-Channel Direct-Conversion Receiver: Analysis and Mitigation," in IEEE Journal on Selected Areas in Communications, vol. 32, no. 3, pp. 411-424, March 2014.

[64] A. Gokceoglu, S. Dikmese, M. Valkama and M. Renfors, "Enhanced energy detection for multi-band spectrum sensing under RF imperfections," 8th International Conference on Cognitive Radio Oriented Wireless Networks, 2013, pp. 55-60.

[65] A.J. Goldsmith and P. P. Varaiya, "Capacity of fading channels with channel side information", in IEEE Transaction Information on Theory, vol. 43, no.6, pp. 1986-1992, Nov. 1997.

[66] A.J. Goldsmith, "Wireless Communications," 2005, Cambridge University Press, USA

[67] A.J. Goldsmith, S. A. Jafar, I. Maric and S. Srinivasa, "Breaking Spectrum Gridlock with Cognitive Radios: An Information Theoretic Perspective," in Proceedings of the IEEE, vol. 97, no. 5, pp. 894-914, May 2009.

[68] S. Haykin, D. J. Thomson and J. H. Reed, "Spectrum Sensing for Cognitive Radio," in *Proceedings of the IEEE*, vol. 97, no. 5, pp. 849-877, May 2009.

[69] S. Haykin, "Cognitive Radio: Brain-Empowered Wireless Communications," IEEE JSAC, vol. 23, no. 2, Feb. 2005, pp. 201–20.

[70] S. Haykin, Adaptive Filter theory, Fourth Edition, Prentice-Hall, 2001.

[71] C. He, Z. Peng, Q. Zeng and Y. Zeng, "A Novel OFDM Interpolation Algorithm Based on Comb-Type Pilot," 2009 5th International Conference on Wireless Communications, Networking and Mobile Computing, 2009, pp. 1-4.

[72] S. J. Heinen and R. Wunderlich, "High Dynamic Range RF Frontends from Multiband Multi Standard to Cognitive Radio," in Proc. IEEE Semiconductor Conference., pp. 1-8, Sep. 2011.

[73] P. Hoeher, S. Kaiser and P. Robertson, "Two-dimensional Pilot-symbol-aided Channel Estimation by Wiener Filtering," in Proc. IEEE Int. Conf. on Acoustics, Speech, and Signal Processing, 1997, pp. 1845-1848 vol.3.

[74] X. Hong, C.X. Wang, and J. Thompson, "Interference Modeling of Cognitive Radio Networks," VTC Spring 2008 - IEEE Vehicular Technology Conference, 2008, pp. 1851-1855.

[75] X. Hong, C.X. Wang, H. -h. Chen and Y. Zhang, "Secondary spectrum access networks," in IEEE Vehicular Technology Magazine, vol. 4, no. 2, pp. 36-43, June 2009.

[76] X. Hong, Z. Chen, C.X. Wang, S. Vorobyov and J. Thompson, "Cognitive radio networks", IEEE Veh. Technol. Mag., vol. 4, pp. 76-84, Dec. 2009.

[77] E. Hossain, "Cognitive Wireless Communication Networks". 2009 Springer-Verlag, Berlin, Heidelberg.

[78] E. Hossain, L. Le, N. Devroye, and M. Vu, "Cognitive radio: From theory to practical network engineering," invited chapter in Advances in Wireless Communications, (Eds. V. Tarokh and I. Blake), Springer, 2009.

[79] G. Huang and J. K. Tugnait, "On cyclostationarity based spectrum sensing under uncertain Gaussian noise," IEEE Trans. Signal Process., vol. 61, no. 8, pp. 2042–2054, Apr. 2013.

[80] W. Hu *et al.*, "Cognitive Radios for dynamic spectrum access - Dynamic Frequency Hopping Communities for Efficient IEEE 802.22 Operation," in IEEE Communications Magazine, vol. 45, no. 5, pp. 80-87, May 2007.

[81] J. Huschke, J. Sachs, K. Balachandran and J. Karlsson, "Spectrum requirements for TV broadcast services using cellular transmitters," 2011 IEEE International Symposium on Dynamic Spectrum Access Networks (DySPAN), 2011, pp. 22-3.

[82] K. Hyunchul and J.S. Kenney, "Behavioral Modelling of Nonlinear RF Power Amplifiers Considering Memory Effects," IEEE Trans. Microw. Theory Tech., 2003, vol. 51, pp. 2495-2504, Dec 2003.

[83] S. A. Jafar and S. Srinivasa, "Capacity limits of cognitive radio with distributed and dynamic spectral activity," IEEE Journal on Selected Areas in Communications, vol. 25, no. 3, pp. 529 – 537, April 2007.

[84] A. Jafarian and S. Vishwanath, "On the capacity of multi-user cognitive radio networks," 2009 IEEE International Symposium on Information Theory, 2009, pp. 601-605.

[85] R. Jain, "Channel models: A tutorial", WIMAX forum, AATG, Feb. 2007.

[86] A. Jovicic and P. Viswanath, "Cognitive Radio: An Information-Theoretic Perspective," in IEEE Transactions on Information Theory, vol. 55, no. 9, pp. 3945-3958, Sept. 2009.

[87] X. Kang, Y. C. Liang, A. Nallanathan, H. K. Garg and R. Zhang, "Optimal power allocation for fading channels in cognitive radio networks: ergodic capacity and outage capacity", IEEE Transactions on Wireless Communications vol. 8 issue 2, pp. 940-950, Feb. 2009.

[88] Li, K. Kearney, E. Bala, and R. Yang, "A resource block based filtered OFDM scheme and performance comparison," in Proc. International Conference on Telecommunications (ICT), May 2013, pp. 1–5.

[89] J. S. Kenney and A. Leke, "Spectral Regrowth in Narrowband RF Power Amplifiers", Microwave Journals., vol. 38, no. 10, pp. 74-92, Oct. 1995

[90] G. Klang and B. Ottersten, "Space-time interference rejection cancellation in transmit diversity systems cancellation read combining," The 5th International Symposium on Wireless Personal Multimedia Communications, Honolulu, HI, USA, 2002, pp. 706-710 vol.2

[91] G. Klang, "On Interference Rejection in Wireless Multichannel Systems," PhD Thesis, KTH, Stockholm, Sweden, 2003

[92] K. Doppler, M. Rinne, C. Wijting, C. B. Ribeiro and K. Hugl, "Device-to-device communication as an underlay to LTE-advanced networks," in IEEE Communications Magazine, vol. 47, no. 12, pp. 42-49, Dec. 2009.

[93] G. Kramer, Outer bounds on the capacity of Gaussian interference channels, IEEE Transactions on. Information. Theory, vol. 50, pp. 581–586, Mar. 2004.

[94] G. Kramer, "Review of Rate Regions for Interference Channels," 2006 International Zurich Seminar on Communications, 2006, pp. 162-165.

[95] H.W. Kuhn, W.A. Tucker, "Nonlinear programming". Proceedings of the Second Berkeley Symposium on Mathematical Statistics and Probability, 1950, pp. 481–492. University of California Press, Berkeley and Los Angeles, Calif., 1951.

[96] S. Kusaladharma and C. Tellambura, "Aggregate Interference Analysis for Underlay Cognitive Radio Networks," in IEEE Wireless Communications Letters, vol. 1, no. 6, pp. 641-644, December 2012.

[97] J. Laster, and Reed, "Interference Rejection in digital Wireless Communication," IEEE Signal Processing Magazine, vol 14, Issue 3, May 1997.

[98] Y. Liang, Y. Zeng, E. C. Y. Peh and A. T. Hoang, "Sensing-Throughput Tradeoff for Cognitive Radio Networks," in IEEE Transactions on Wireless Communications, vol. 7, no. 4, pp. 1326-1337, April 2008.

[99] Y.C. Liang, A. T. Hoang Y. Zeng, and R. Zhang, "A Review on Spectrum Sensing for Cognitive Radio: Challenges and Solutions," EURASIP Journal on Advances in Signal Processing, pp. 1-15, January 2010

[100] A. Loulou, J. Yli-Kaakinen, T. Levanen, V. Lehtinen, F. Schaich, T. Wild, M. Renfors, and M. Valkama, "Multiplier less filtered-OFDM transmitter for narrowband IoT devices," IEEE Internet of Things Journal, May 2019.

[101] A. Loulou, J. Yli-Kaakinen, and M. Renfors, "Advanced low-complexity multicarrier schemes using fast-convolution processing and circular convolution decomposition," IEEE Transactions on Signal Processing, vol. 67, no. 9, pp. 2304–2319, May2019.

[102] F.-L. Luo, Ed., "Digital Front-End in Wireless Communications and Broadcasting: Circuits and Signal Processing", Cambridge: Cambridge University Press, 2011.

[103] D.G. Luenberger,. Optimization by vector space methods. John Wiley & Sons, 1997.

[104]M. Majidi, A. Mohammadi and A. Abdipour, "Analysis of the Power Amplifier Nonlinearity on the Power Allocation in Cognitive Radio Networks," in IEEE Transactions on Communications, vol. 62, no. 2, pp. 467-477, February 2014.

[105]Y. Medjahdi, R. Zayani, H. Shaïek, and D. Roviras, "WOLA processing: A useful tool for windowed waveforms in 5G with relaxed synchronicity," in Proc. International Conference on Communications Workshops (ICC Workshops), May 2017, pp. 393–398.

[106]A. R. Mishra, Fundamentals of cellular network planning and optimization: 2G/2.5G/3G... evolution to 4G. John Wiley & Sons, 2004.

[107]J. Mitola and J. G. Q. Maguire, "Cognitive radio: making software radios more personal," IEEE Personal Communication Magazine, vol. 6, no. 4, pp. 13–18, Aug. 1999.

[108]J. Mitola, "Cognitive Radio: An Integrated Agent Architecture for Software Defined Radio," Ph.D. dissertation Royal Institute of Technology (KTH), 2000.

[109]H. Minn and V. K. Bhargava, "An investigation into time-domain approach for OFDM channel estimation," in IEEE Transactions on Broadcasting, vol. 46, no. 4, pp. 240-248, Dec. 2000.

[110]M. Morelli and U. Mengali, "A comparison of pilot-aided channel estimation methods for OFDM systems," in IEEE Transactions on Signal Processing, vol. 49, no. 12, pp. 3065-3073, Dec. 2001

[111]M. Mueck *et al.*, "ETSI Reconfigurable Radio Systems — Software Defined Radio and Cognitive Radio standards," 2009 IEEE 20th International Symposium on Personal, Indoor and Mobile Radio Communications, 2009, pp. 1-5.

[112]L. Musavian and S. Aissa, "Ergodic and outage capacities of spectrum-sharing systems in fading channels", in proc. IEEE Global Telecommunications Conference (GLOBECOM'07), Washington. DC, USA, Nov. 2007

[113]B.Noble, "Methods based on the Wiener-Hopf technique for the solution of partial differential equations," Chelsea Pub Co,1988.

[114]J. Noh and S. Oh, "Beamforming in a Multi-User Cognitive Radio System with Partial Channel State Information," in IEEE Transactions on Wireless Communications, vol. 12, no. 2, pp. 616-625.

[115]Y. Ohwatari, N. Miki, Y. Sagae and Y. Okumura, "Investigation on Interference Rejection Combining Receiver for Space–Frequency Block Code

Transmit Diversity in LTE-Advanced Downlink," in IEEE Transactions on Vehicular Technology, vol. 63, no. 1, pp. 191-203, Jan. 2014.

[116]K. Okada, S. Kousai "Digitally-Assisted Analog and RF CMOS Circuit Design for Software-Defined Radio", Springer 2011.

[117]P. Popovski, H. Yomo, K. Nishimori, R. Di Taranto and R. Prasad, "Opportunistic Interference Cancellation in Cognitive Radio Systems," 2007 2nd IEEE International Symposium on New Frontiers in Dynamic Spectrum Access Networks, 2007, pp. 472-475

[118]M.-O. Pun, M. Morelli, and C.C. Kuo, Multi-Carrier Techniques for Broadband Wireless Communications, Imperial College Press, 2007.

[119]C.Rapp "Effects of the HPA nonlinearity on 4-DPSK OFDM signal for a digital sound broadcasting system", in proc. Conf. Rec. ECSC'91, Luettich, Germany, Oct. 1991.

[120]B. Razavi, "Cognitive Radio Design Challenges and Techniques," in IEEE Journal of Solid-State Circuits, vol. 45, no. 8, pp. 1542-1553, Aug. 2010.

[121]E. Rebeiz and D. Cabric, "How wideband receiver nonlinearities impact spectrum sensing," 2013 IEEE Global Conference on Signal and Information Processing, 2013, pp. 1178-1181.

[122]E. Rebeiz, A. Shahed Hagh Ghadam, M. Valkama and D. Cabric, "Spectrum Sensing Under RF Non-Linearities: Performance Analysis and DSP-Enhanced Receivers," in IEEE Transactions on Signal Processing, vol. 63, no. 8, pp. 1950-1964, April15, 2015.

[123]Ren, B., Wang, Y., Sun, S., Zhang, Y., Dai, X. and Niu, K. (2017), Low-complexity MMSE-IRC algorithm for uplink massive MIMO systems. Electron. Lett., 53: 972-974.

[124]M. Renfors, X. Mestre, E. Kofidis, F. Bader (eds.),Orthogonal Waveforms and Filter Banks for Future Communication Systems,Academic Press, 2017.

[125]J. Rinne and M. Renfors, "Pilot spacing in orthogonal frequency division multiplexing systems on practical channels," in IEEE Transactions on Consumer Electronics, vol. 42, no. 4, pp. 959-962, Nov. 1996.

[126]Z. Ru, E. A. M. Klumperink, G. J. M. Wienk and B. Nauta, "A software-defined radio receiver architecture robust to out-of-band interference," 2009 IEEE International Solid-State Circuits Conference - Digest of Technical Papers, 2009, pp. 230-231,231a.

[127]K. Ruttik, K. Koufos and R. Jäntti, "Computation of Aggregate Interference from Multiple Secondary Transmitters," in IEEE Communications Letters, vol. 15, no. 4, pp. 437-439, April 2011.

[128]K. Ruttik "Secondary spectrum usage in TV white space." Ph.D. Thesis, Aalto University publication series Doctoral Dissertation 128/2011, (2011).

[129]J. Sachs, I. Maric and A. Goldsmith, "Cognitive Cellular Systems within the TV Spectrum," 2010 IEEE Symposium on New Frontiers in Dynamic Spectrum (DySPAN), 2010, pp. 1-12

[130]H. Sato, "Two user communication channels," IEEE Trans. Information. Theory, vol. IT-23, pp. 295–304, May 1977.

[131]H. Sato, "On degraded Gaussian two-user channels," IEEE Trans. Information. Theory, vol. IT-24, pp. 637–640, Sep. 1978.

[132]T.Schenk, "RF imperfections in high-rate wireless systems: Impact and digital compensation" 2008.

[133]Y. Selén, R. Baldemair and J. Sachs, "A short feasibility study of a cognitive TV black space system," 2011 IEEE 22nd International Symposium on Personal, Indoor and Mobile Radio Communications, 2011, pp. 520-52.

[134]M. Shaat and F. Bader, "Computationally efficient power allocation algorithm in multicarrier-based cognitive radio networks: OFDM and FBMC systems", EURASIP Journal on Advances in Signal Processing vol. 2010, Article ID 528378, 13 pages.

[135]C. E. Shannon, "A mathematical theory of communication," in The Bell System Technical Journal, vol. 27, no. 3, pp. 379-423, July 1948.

[136]C. E. Shannon, "Communication in the presence of noise," Proceedings of the IEEE, vol. 86, pp. 447 – 457, February 1998.

[137]P. Siohan, C. Siclet and N. Lacaille, "Analysis and design of OFDM/OQAM systems based on filterbank theory," in IEEE Transactions on Signal Processing, vol. 50, no. 5, pp. 1170-1183, May 2002.

[138]S. Srinivasan, S. Dikmese, D. Menegazzo, and M. Renfors, "Multi-Antenna Interference Cancellation for Black Space Cognitive Radio Communications," in Proc. 2015 IEEE Globecom Workshops, San Diego, CA, 2015, pp. 1-6.

[139]S. Srinivasan, S. Dikmese, and M. Renfors, "Interpolation-Based Interference Rejection Combining for Black-Space Cognitive Radio in Time-Varying Channels". In Bader, F., Kryszkiewicz, P., Dimitriou, N., Kliks, A., Sybis, M., Triantafyllopoulou, D., Caicedo, C. E. & Sezgin, A. (eds.), Cognitive Radio-

Oriented Wireless Networks - 14th EAI International Conference, CROWNCOM 2019. Springer Verlag, p. 168-179 12 p. (Lecture Notes of the Institute for Computer Sciences, Social-Informatics and Telecommunications Engineering; vol. 291).

[140]G. Staple and K. Werbach, "The end of spectrum scarcity," IEEE Spectrum, March 2004, pp. 41–44.

[141]P.Stoica, and R. L. Moses, "Spectral analysis of signals" 2005, Prentice Hall, Upper Saddle River, New Jersey

[142]R. Tandra, and A. Sahai, "SNR walls for signal detection," IEEE J. Sel. Topics Signal Process., vol. 2, no. 1, pp. 4−17, Feb. 2008

[143]F. M. L. Tavares, G. Berardinelli, N. H. Mahmood, T. B. Sorensen and P. Mogensen, "On the Impact of Receiver Imperfections on the MMSE-IRC Receiver Performance in 5G Networks," in Proc. 2014 IEEE 79th Vehicular Technology Conference (VTC Spring), , pp. 1-6

[144]G. P. Villardi et al., "Enabling coexistence of multiple cognitive networks in TV white space," in IEEE Wireless Communications, vol. 18, no. 4, pp. 32-40, August 2011.

[145]M. Valkama, A. Shahed hagh ghadam, L. Anttila and M. Renfors, "Advanced digital signal processing techniques for compensation of nonlinear distortion in wideband multicarrier radio receivers," in IEEE Transactions on Microwave Theory and Techniques, vol. 54, no. 6, pp. 2356-2366, June 2006.

[146]S. Verdu, Multiuser Detection, Cambridge: Cambridge University Press, 1998.

[147]T. A.Weiss and F. K. Jondral, "Spectrum pooling: an innovative strategy for the enhancement of spectrum efficiency," in IEEE Communications Magazine, vol. 42, no. 3, pp. S8-14, March 2004

[148]T. A.Weiss, J. Hillenbrand, A. Krohn, and F. Jondral, "Mutual interference in OFDM-based spectrum pooling systems" in Proc. VTC 2004, May 2004

[149]S. Weinstein and P. Ebert, "Data Transmission by Frequency-Division Multiplexing Using the Discrete Fourier Transform," in IEEE Transactions on Communication Technology, vol. 19, no. 5, pp. 628-634, October.

[150]J.Winters, "Optimum Combining in Digital Mobile Radio with Cochannel Interference," IEEE Trans. on Vehicular Technology, vol 2, Issue 4, August 1984.

[151]A. M. Wyglinski et al, Cognitive Radio Communications and Networks: Principles and Practice, Academic Press, 2010.

[152]B. Yang, Z. Cao and K. B. Letaief, "Analysis of low-complexity windowed DFT-based MMSE channel estimator for OFDM systems," in IEEE Transactions on Communications, vol. 49, no. 11, pp. 1977-1987, Nov. 2001.

[153]T. Yucek and H. Arslan, "A Survey of Spectrum Sensing Algorithms for Cognitive Radio Applications," IEEE Comm. Surveys & Tutorials, vol. 11, no. 1, pp. 116-129, 2009.

[154]R. Zayani, Y. Medjahdi, H. Shaiek, and D. Roviras, "WOLA-OFDM: A potential candidate for asynchronous 5G," in Proc. Globecom Workshops (GC Wkshps), Dec.2016, pp. 1–5.

[155]Y. Zeng and Y. -. Liang, "Eigenvalue-based spectrum sensing algorithms for cognitive radio," in IEEE Transactions on Communications, vol. 57, no. 6, pp. 1784-1793, June 2009.

[156]L. Zhang, A. Ijaz, P. Xiao, M. M. Molu, and R. Tafazolli, "Filtered OFDM systems, algorithms, and performance analysis for 5G and beyond," IEEE Transactions on Communications, vol. 66, no. 3, pp. 1205–1218, Mar. 2018.

[157]G. Zhou and R. Raich, "Spectral Analysis of Polynomial Nonlinearity with Applications to RF Power Amplifiers," EURASIP J. on Applied Signal Proc., pp 1831-1840, Dec 2004.

[158]L. Zhou et al., "Creating secondary spectrum usage opportunity for D2D communication with interference cancellation," 2015 IEEE International Symposium on Dynamic Spectrum Access Networks (DySPAN), 2015, pp. 273-274.

[159]L. Zhou, K. Ruttik and O. Tirkkonen, "Interference Canceling Power Optimization for Device-to-Device Communication," 2015 IEEE 81st Vehicular Technology Conference (VTC Spring), 2015, pp. 1-5.

[160]F Zhu, et al. "Digital pre-distortion of power amplifier impairments in spectrally agile transmissions." 2012 35th IEEE Sarnoff Symposium. IEEE, 2012

[161]J. Zhu, R. H. Y. Louie, M. R. McKay and S. Govindasamy, "On the impact of unsynchronized interferers on multi-antenna OFDM systems," 2014 IEEE International Conference on Communications (ICC), Sydney, NSW, Australia, 2014, pp. 2203-2208.

PUBLICATIONS

PUBLICATION

1

Spectrum Sensing and Spectrum Utilization Model for OFDM and FBMC based Cognitive Radios

S. Srinivasan, S. Dikmese and M. Renfors

Proceedings of IEEE 13th International Workshop on Signal Processing Advances in Wireless Communications (SPAWC), 2012, pp. 139-143

SPECTRUM SENSING AND SPECTRUM UTILIZATION MODEL FOR OFDM AND FBMC BASED COGNITIVE RADIOS

Sudharsan Srinivasan, Sener Dikmese and Markku Renfors
Department of Communications Engineering
Tampere University of Technology
Tampere, Finland
sudharsan.srinivasan@tut.fi, sener.dikmese@tut.fi and markku.renfors@tut.fi

ABSTRACT

OFDM based 802.11g Wireless Local Area Networks (WLAN) operate in the 2.4 GHz ISM band. Various other wireless systems use the same band which causes interference and leads to significant performance degradation. Hence, Cognitive Radio's (CR) could better determine free spectrum and coordinate the spectrum usage in this band. Apart from this, to reduce the interference due to spectral leakage, Filter Bank Multicarrier (FBMC) type of system is considered as an alternative to FFT based systems. In this study, FFT and filter bank based spectrum sensing methods are compared by applying them for detecting spectral holes between WLAN and FBMC channels, considering also the spectral leakage effects appearing practical WLANs. Also the performance of alternative multicarrier techniques regarding the efficiency of spectrum utilization is studied.

Index Terms— CR, FFT, filter bank, spectrum sensing, spectrum utilization, loading algorithms

1. INTRODUCTION

Some of the challenges to reliable communication are increasing traffic rates, limited spectrum availability, and interferences between different systems/users [1]. For example, the 2.4 GHz ISM band is globally available and hence used by various wireless systems. To reduce interference and better utilize the spectrum, Cognitive Radio (CR) and advanced signal processing techniques have recently been studied extensively [2, 3, 4, 5].

CR relies on spectrum sensing to identify a spectrum hole. Once the spectrum information is obtained, a CR must establish and maintain a non-interfered reliable communication. Due to varying channel conditions, repeated monitoring and cooperation with other users is required for reliable spectrum sensing approaches [6].

Cyclic prefix based CP-OFDM techniques are simple and robust and many advances have been made in terms of signal processing functions on the receiver side. However, also alternative multicarrier techniques have been studied increasingly in the literature. Especially, FBMC techniques have been realized to have various potential benefits in the CR context. In case of FBMC, the analysis filter bank (AFB) on the receiver side can be applied also for spectrum analysis purposes [7], [8], [9], [10], [11].

In this study, wideband multichannel spectrum sensing techniques are considered. By averaging the output samples of a filter bank based spectrum analyzer simultaneously for multiple center frequencies and bandwidths, multiple spectral gaps can be tested and identified rapidly in an efficient and flexible way.

After the spectrum is sensed, efficient spectrum utilization is important in maximizing the cognitive radio's throughput. Spectrum utilization can be improved using proper loading algorithms [12, 13]. When the Channel State Information (CSI) is known, the transmit power or the data rate can be adapted according to the CSI. The adaptation algorithms, the so-called loading algorithms use commonly the water-filling principle. Water-filling solution can be thought of as the curve of inverted channel signal to noise ratio being filled with energy to a constant line. There are two different loading algorithms, rate adaptive and margin adaptive [14]. The loading algorithms commonly assume that the channel is quasi-static. Hence, the allocation of bits and energy can be done once at the beginning of the transmission and can be maintained until a new set of CSI is available.

In this paper, the rate adaptive algorithm is used for maximizing the data rate of a CR operating in a spectral hole. The power of the secondary transmission is determined so as not to interfere with the primary. Hence the rate adaptive algorithm is better suited for this study. To maximize the total data rate of the CR, there is a need to maximize the achievable rate for each subband, constraint on the total energy that is allowed for the CR transmission symbols [14].

In Section 2, OFDM based WLAN and FBMC signal models are given and FFT and AFB based spectrum sensing is reviewed, considering the spectrum analysis aspects related to the multicarrier techniques. Section 3 develops an efficient spectrum utilization model. Section 4 gives simulation results for the considered radio scene, and

finally, some concluding remarks are given about the performance of these methods.

2. SIGNAL MODELS AND AFB & FFT BASED SPECTRUM SENSING ALGORITHMS

2.1. OFDM and FBMC Signal Models

Even though CP-OFDM is the most well known multicarrier technology, OFDM/OQAM based FBMC signal model can be used to overcome the spectral leakage problems. The ideas are readily applicable to all FBMC models which are based on uniform highly selective filter banks [9]. The IFFT and FFT, or more generally, the synthesis filter bank (SFB) and analysis filter bank (AFB) are used as the core parts in multicarrier systems on the transmitter and receiver sides, respectively.

In our numerical studies, we consider a scenario with two active 802.11g based WLANs or two FBMC signals with similar parameters, as shown in figure 1. The two channels are assumed to have the same power level, normalized to 0 dB. In this case WLAN1 and WLAN2 signals and FBMC1 and FBMC2 use channels 3 and 8, respectively, out of the entire 11 different channels. The channels don't overlap and there is 8 MHz spectrum hole available in this scenario. Due to the transmitter power amplifier (PA) non-linearity, spectral regrowth gets introduced raising the spectral density in the nearby frequencies. Considering the worst case situation allowed by the 802.11g specifications, the power spectrum density in the gap between the two channels can be at about -20 dBr (20 dB below the passband level) [4]. The specific FBMC design, described in [7], has at least 50 dB stop band attenuation. However, depending on the linearity of the PA, some spectrum leakage would be present also in the FBMC case.

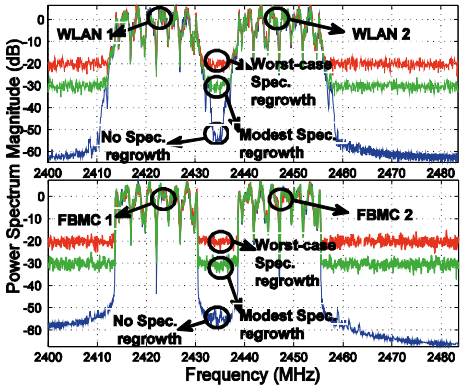

Figure 1. Two WLAN and FBMC signals using 3rd and 8th WLAN channels in 2.4 GHz ISM band.

2.2. FFT and AFB based Spectrum Sensing

Block diagram of alternative FFT and AFB based spectrum sensing algorithms are shown in Figure 2.

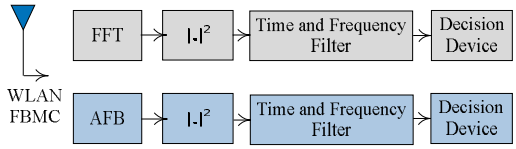

Figure 2. Block diagram of energy detector with AFB and FFT based spectrum analysis

In the following analysis, it is assumed that the subband sampling rate is equal to the ADC sampling rate divided by the number of FFT/AFB frequency bins. According to the subband-wise spectrum sensing idea, the subband signals can be formulated as [3]:

$$Y(m,k)=\begin{cases} W(m,k) & H_0 \\ S(m,k)H_k+W(m,k) & H_1 \end{cases} \quad (1)$$

where $S(m,k)$ is the transmitted primary user (PU) signal as seen in subband k of the m^{th} FFT or AFB output block, and $W(m,k)$ is the corresponding channel noise sample when the signal is absent. H_0 and H_1 express the absent hypothesis and present hypothesis of a PU, respectively. When there is only AWGN noise present, it is modeled as a zero-mean Gaussian random variable with variance σ_w^2, i.e., $W(m,k)=N(0,\sigma_w^2)$. The WLAN or FBMC signals can also be modeled as a zero-mean Gaussian variable $S(m,k)=N(0,\sigma_k^2)$ where, σ_k^2 is the variance (power) at subband k.

In energy detection based spectrum sensing, the absolute square of the FFT or AFB output $|Y(m,k)|^2$ is compared with a threshold value to decide between H_0 and H_1. The threshold is calculated according to the noise variance, which is here assumed to be known, e.g., based on previous measurements and target false alarm probability. Instead of using a single sample for the decision, time and frequency averaging method is applied in order to obtain more reliable decision statistic [3]. For this case, the decision statistics at different frequencies can be obtained as [7]

$$\tilde{Y}(m,k)=\frac{1}{L_t L_f}\sum_{l=k-\lfloor L_f/2\rfloor}^{k+\lceil L_f/2\rceil-1}\sum_{u=m-L_t+1}^{m}|Y(u,l)|^2 \quad (2)$$

and L_f and L_t are the filter lengths in frequency and time, respectively. The output of $\tilde{Y}(m,k)$ is received by threshold function to determine the possible occupancy of the corresponding frequency band at the corresponding time interval. To simplify notations, the sensing time index m is dropped in later expressions.

As $Y(m,k)$ has Gaussian distribution, the probability distribution functions (PDF) of the time filter outputs

$\tilde{Y}_K$ can be approximated as Gaussian distributions under H_0 and H_1 [3]. The threshold value λ can be obtained according to the target false alarm probability and noise variance. False alarm probability P_{FA} and detection probability P_D can be expressed as follows

$$P_D = \Pr(\tilde{Y}_K > \lambda \mid H_1) = Q\left(\frac{\lambda - (\sigma_n^2 + \sigma_k^2)}{\sqrt{(\sigma_n^2 + \sigma_k^2)^2 / L_t L_f}}\right) \quad (3)$$

$$P_{FA} = \Pr(\tilde{Y}_K > \lambda \mid H_0) = Q\left(\frac{\lambda - \sigma_n^2}{\sqrt{\sigma_n^4 / L_t L_f}}\right) \quad (4)$$

3. SPECTRUM UTILIZATION

The block diagram of spectrum utilization process is shown in figure 3. Loading algorithms maximize the spectrum utilization by a CR. Especially, rate adaptive loading algorithm are better suited as they offer better control of the interference from a CR to the PU receivers. Rate adaptive loading algorithm maximizes the number of bits per symbol subjected to a fixed energy constraint [14]. In the following, $1/T$ is the symbol rate, b_n is the number of bits in subcarrier n, and e_n is the nth subcarrier energy. Then the total number of bits in the available set of N parallel subcarrier symbols is $b = \sum_n b_n$. The overall data rate is $R = b/T$ and the total energy of the N parallel subcarrier symbols is constraint to $\sum_{n=1}^{N} e_n = N\bar{e}_n$ where $N\bar{e}_n$ is the total energy allowed in the system under consideration.

The largest data rate is achieved by maximizing the sum

$$b = \frac{1}{2}\sum_{n=1}^{N} \log_2\left(\frac{1 + e_n * g_n}{\Gamma}\right) \quad (5)$$

where $g_n = |H_n|^2 / (\sigma_n{}^2)$ is the subband SNR per unit energy from the transmitter, $|H_n|^2$ is the channel gain of the nth sub band and Γ is the gap formulation as given in [14]. $\sigma_n{}^2$ Is the noise and interference variance in subband n, i.e., it contains both the channel white noise and spectrum leakage from the WLAN channels.

The optimum loading can be formulated as:

$$\max_{e_n} b = \frac{1}{2}\sum_{n=1}^{N} \log_2\left(\frac{1 + e_n * g_n}{\Gamma}\right)$$
$$subject: N\bar{e}_x = \sum_{n=1}^{N} e_n \quad (6)$$

The solution to this optimization problem leads to the water filling constant K given below [14] .

Spectrum Utilization Algorithm

The rate maximization algorithm [14] used in this work is given below

1. Sort the sub-channels based on their gains $g_1 > g_2 > g_3 > \cdots > g_N$
2. Find the largest i for which $e_{N-i} = K - \Gamma / g_{N-i} \le 0$ with
$$K = \frac{1}{N-i}\left[Ne_n + \Gamma \cdot \sum_{n=1}^{N-i} \frac{1}{g_n}\right] \quad (7)$$
3. Eliminate the negative energies $e_n < 0$ and set $e_{n*} = 0$ and $b_n = 0$ for those subcarriers. Set $N^* = N - i$, where i is the number of subcarriers with negative energies, $e_i = K - \Gamma / g_i \le 0$. The water- filling constant is also recalculated for the new N^*.
4. Compute the water-filling energies $e_n = K - \Gamma / g_n$ where $n = 1, 2 \cdots, N^*$
5. Calculate the data rate for unsorted sub-channels as $b_n = \log_2(1 + e_n \cdot g_n)/2 \quad \forall n = 1, 2, \cdots, N^*$

To implement this algorithm, the channel estimate, in the form of subband gains H_n is needed, as well as estimates of the noise + interference powers $\sigma_n{}^2$ of the sub bands. The latter one is estimated using subcarrier wise FFT or AFB based energy metric, i.e., using (2) with $L_f = 1$.

One central issue in our discussion is the effect of the spectrum leakage in OFDM and FBMC systems on the throughput of the CR utilizing the spectral hole. Due to the good spectral containment of the sub bands in FBMC, we expect the spectrum leakage to be less critical in the FBMC case.

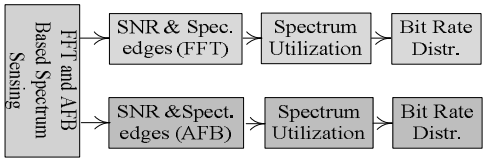

Figure 3. Block diagram of spectrum utilization with water filling after spectrum analysis

4. SIMULATION RESULTS

Here we consider using the gap between the two channels of figure 1 for secondary transmissions by a CR system. We can notice that the case where the two primary signals are at equal power levels is the worst-case situation for the CR. This is because otherwise the spectrum leakage effects would be less critical on the side of the weaker WLAN channel. The WLANs and WLAN-like FBMC systems use the main parameters of 802.11g. However, it is assumed that the spectrum sensing and CR transmissions use smaller

subchannel bandwidth of 81.5 kHz. For spectrum sensing, the time and frequency filtering lengths are chosen as 50 and 5, respectively, in order to be able to detect other narrowband systems, like Bluetooth [5]. Regarding the level of spectral regrowth, we consider three cases: no regrowth, modest regrowth at the level of -30 dBr, and worst-case regrowth at -20 dBr.

Figures 4 shows the number of subbands determined to be empty, both for OFDM and FBMC based primaries and with different levels of spectral regrowth. The target false alarm probability is chosen as P_{FA}=0.1. The ITU-R Vehicular A channel model is used. As we can see, with no or modest spactral regrowth, an FBMC primary would allow a clearly higher number of subchannels to be used by the CR system compared to OFDM-based WLAN. Also AFB finds higher number of empty subbands compared to FFT, in reliable way. With the worst-case regrowth allowed by 802.11g, the differences dissappear.

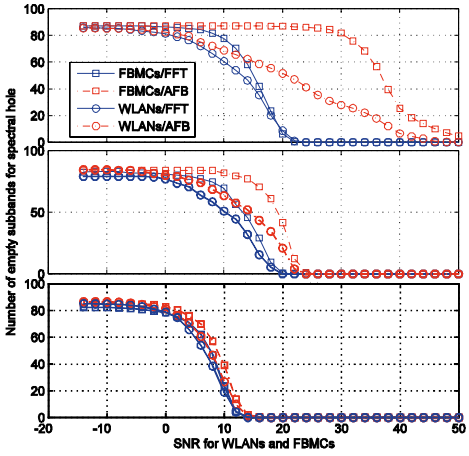

Figure 4. Number of empty subbands in the spectral hole between WLANs and FBMCs with target $P_{FA}=0.1$, time record length of 50 , sensing bandwidth of 5 subbands for (a) no spectrum regrowth, (b) modest-case spectrum regrowth, and (c) worst-case spectrum regrowth

The actual false alarm probabilities versus the active primary systems' SNR, as seen by the CR receiver, can be seen in figure 5. This is actually the probability that a group of 5 subchannels in the center of the gap would be detected to be occupied due to spectral leakage.

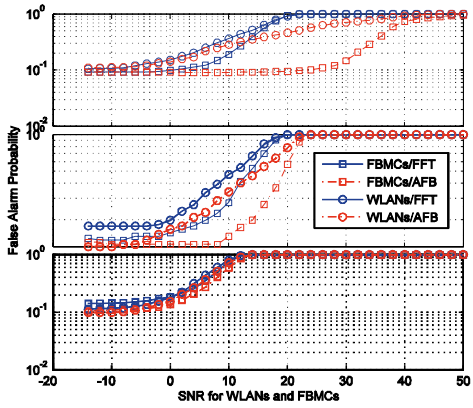

Figure 5. Actual false alarm probability with target $P_{FA}=0.1$ with (a)no spectrum regrowth, (b) modest-case spectrum regrowth, and (c)worst-case spectrum regrowth

Finally, the achievable data rate in the spectrum gap between two active primary channels, as determined by the rate adaptive algorithm, are shown in figures 6. Perfect channel estimation is assumed and the subband-wise SINR (signal to interference plus noise ratio) estimates are obtained using time filtering length of 50 samples. It can be seen that under the high SNR case, the number of subbands that can be used by the CR reduces in the OFDM case due to the spectral leakage. An FBMC primary with AFB based spectrum sensing at the CR would maximize the CR system performance, while AFB based sensing in the traditional WLAN case shows significant benefit with low or modest spectral regrowth. With the worst case spectral regrowth, the benefits of FBMC and AFB disappear. It can also be seen that with the used parameters, the spectrum sensing algorithm and the rate adaptive bit loading algorithm (which can be applied after the spectrum has first been detected to be available) end up in using about the same number of sub bands.

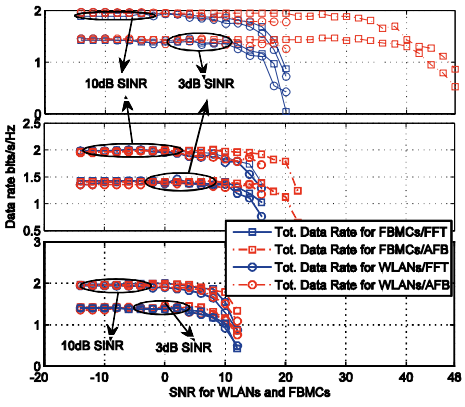

Figure 6. Available data rate as a function of signal to noise ratio with 10 dB and 3 dB CR with (a) no spectrum regrowth, (b) modest-case spectrum regrowth, and (c) worst-case spectrum regrowth.

5. CONCLUSION

We have analyzed the performance of energy detection based spectrum sensing techniques using either FFT or filter bank based spectrum analysis methods for both WLAN and FBMC signal models and utilizing spectral holes with water filling algorithms. As a spectrum sensing method, AFB has clear benefits due to much better spectral containment of the sub channels. One significant benefit of FBMC as a transmission technique in CR systems is that it can utilize narrow spectral gaps in an effective and flexible way. On the other hand, FBMC multicarrier eliminates the extra complexity due to AFB design because of its transmitter and receiver characteristics. As a conclusion, use of FBMC model, instead of OFDM based WLAN model provides better performance in terms of the spectral leakage problem.

In the future work, to complete the picture, we will consider the effects of the spectrum leakage from the CR transmissions to primary WLAN receivers. These effects should also be taken into consideration in the CR subcarrier allocation, based on known or assumed channel selectivity of the WLAN receiver.

6. ACKNOWLEDGMENT

This work was partially supported by Tekniikan Edistämissäätiö (TES), GETA Graduate School and Tekes (the Finnish Funding Agency for Technology and Innovation) under the project ENCOR in the Trial Program.

REFERENCES

[1] I. Mitola, J. and J. Maguire, G. Q., "Cognitive radio: making software radios more personal," IEEE Personal Commun. Mag., vol. 6, no. 4, pp. 13–18, Aug. 1999.

[2] Y. Zeng, Y.C. Liang, A. T. Hoang, and R. Zhang, "A Review on Spectrum Sensing for Cognitive Radio: Challenges and Solutions," EURASIP Journal. on Advances. in Sig. Proc, vol. 2010, pp. 1-15, Jan. 2010.

[3] T. Yucek and H. Arslan, "A survey of spectrum sensing algorithms for cognitive radio applications," IEEE Communications Surveys & Tutorials, vol. 11, no. 1, pp. 116–130, March 2009.

[4] S. Dikmese, M. Renfors and H. Dincer, "FFT and Filter Bank Based Spectrum Sensing for WLAN Signals," in Proc. ECCTD2011 conf., Linkoping, Sweden, August 2011.

[5] S. Dikmese and M. Renfors, "Optimized FFT and Filter Bank Based Spectrum Sensing for Bluetooth Signal" in Proc. Wireless Communications and Networking Conference (WCNC 2012), Paris, France.

[6] S. M. Mishra, A. Sahai, and R. W. Broderson, "Cooperative sensing among cognitive radios," in Proc.ICC, Istanbul, Turkey, Jun.11–15, 2006.

[7] M. Bellanger, T. Ihalainen, and M. Renfors, "Filter bank based cognitive radio physical layer," in Proc. of the ICTMobile Summit, Santander, Spain, June 2009.

[8] T. Ihalainen, A. Viholainen, T.H. Stitz, and M. Renfors, "Spectrum Monitoring Scheme for Filter Bank Based Cognitive Radios," in Proc. Future Network & MobileSummit, Florence, Italy, June 2010.

[9] B. F. Boroujeny and R. Kempter, "Multicarrier communication techniques for spectrum sensing and communication in cognitive radios," IEEE Commun. Mag. vol. 48, no. 4, Apr. 2008.

[10] T. Yucek and H. Arslan, "Spectrum characterization for opportunistic cognitive radio systems," in Proc. IEEE Military Commun. Conf., Washington, D.C., USA, Oct. 2006.

[11] V. Ringset, H. Rustad, F. Schaich, J. Vandermot, and M. N´ajar, "Performance of a filterbank multicarrier (FBMC) physical layer in the WiMAX context," in Proc. Future Network & Mobile Summit, Florence, Italy, June 2010.

[12] J. Cioffi," Digital Communication: Signal Processing" at Stanford University, Standford, California, USA, 2000.

[13] S. Dikmese and S. Srinivasan and M. Renfors, "FFT and Filter Bank Based Spectrum Sensing and Spectrum Utilization for Cognitive Radios" in Proc. (ISCCSP 2012), Rome, Italy, May 2012.

[14] K. Baamrani, A. Ouahmana, and S. Allakib, "Rate adaptive resource allocation for OFDM downlink transmission" AEU – Int. Jour. of Elec.and Comm.Vo. 61, Issue 1, 2 Jan. 2007.

PUBLICATION

2

Spectrum Sensing and Resource Allocation for Multicarrier Cognitive Radio Systems under Interference and Power Constraints

S. Dikmese, S. Srinivasan, M. Shaat, F. Bader and M. Renfors

EURASIP Journal on. Advanced. Signal Processing. 2014, 68 (2014)

Dikmese et al. EURASIP Journal on Advances in Signal Processing 2014, 2014:68
http://asp.eurasipjournals.com/content/2014/1/68

EURASIP Journal on Advances in Signal Processing
a SpringerOpen Journal

RESEARCH Open Access

Spectrum sensing and resource allocation for multicarrier cognitive radio systems under interference and power constraints

Sener Dikmese[1*], Sudharsan Srinivasan[1], Musbah Shaat[2], Faouzi Bader[3] and Markku Renfors[1]

Abstract

Multicarrier waveforms have been commonly recognized as strong candidates for cognitive radio. In this paper, we study the dynamics of spectrum sensing and spectrum allocation functions in cognitive radio context using very practical signal models for the primary users (PUs), including the effects of power amplifier nonlinearities. We start by sensing the spectrum with energy detection-based wideband multichannel spectrum sensing algorithm and continue by investigating optimal resource allocation methods. Along the way, we examine the effects of spectral regrowth due to the inevitable power amplifier nonlinearities of the PU transmitters. The signal model includes frequency selective block-fading channel models for both secondary and primary transmissions. Filter bank-based wideband spectrum sensing techniques are applied for detecting spectral holes and filter bank-based multicarrier (FBMC) modulation is selected for transmission as an alternative multicarrier waveform to avoid the disadvantage of limited spectral containment of orthogonal frequency-division multiplexing (OFDM)-based multicarrier systems. The optimization technique used for the resource allocation approach considered in this study utilizes the information obtained through spectrum sensing and knowledge of spectrum leakage effects of the underlying waveforms, including a practical power amplifier model for the PU transmitter. This study utilizes a computationally efficient algorithm to maximize the SU link capacity with power and interference constraints. It is seen that the SU transmission capacity depends critically on the spectral containment of the PU waveform, and these effects are quantified in a case study using an 802.11-g WLAN scenario.

Keywords: CR; OFDM; FBMC; Filter bank; Spectrum sensing; Energy detector; Spectrum utilization; Loading algorithms; Multicarrier

1 Introduction

One of the major challenges in cognitive radio (CR) operation is to utilize the available whitespace with minimal interference to the primary or prioritized secondary transmission systems [1]. Several spectrum sensing techniques have been proposed, e.g., in [2-5] to facilitate CR operation. Especially, energy detector-based spectrum sensing algorithms have been widely considered due to low computational complexity. On the other hand, the fading channel capacity has already been studied from an information theoretic perspective, e.g., in [6,7] in terms of resource allocation. Recently, the secondary user (SU) capacity has been widely studied. The SU channel capacity for additive white Gaussian noise (AWGN) channels under different power constraint is studied in [8]. The effect of various types of fading channels on the CR capacity has been studied in [9] under optimal power allocation strategy for the CR and subjected to an interference power constraint at the coexisting primary. Further, [10] discusses the effects of peak power and average interference power constraints on the outage capacity. In [11], the ergodic capacity, the delay-limited capacity, and the outage capacity of the CR in block-fading channels under spectrum sharing are discussed.

In this paper, we investigate two important features of the cognitive radio. We begin with the spectrum sensing function and later study the spectrum utilization

* Correspondence: sener.dikmese@tut.fi
[1]Department of Electronics and Communications Engineering, Tampere University of Technology, P.O. Box 692, Tampere 33101, Finland
Full list of author information is available at the end of the article

function implementing optimized resource allocation under power and interference constraints. Instead of elaborate spectrum sensing techniques, such as cyclostationary and eigenvalue-based methods [2,3], energy detector-based spectrum sensing is utilized. This is motivated by subband-based energy detector's capability to implement the needed spectrum analysis functions for identifying the available spectral slots and for estimating the signal-to-interference-plus-noise (SINR) ratios at subcarrier level for resource allocation purposes.

For a CR system, multicarrier modulation techniques are generally better suited as they are spectrally more efficient than single carrier systems and have the flexibility to allocate resources to the available spectral gaps and among different users to maximize system throughput. There are various ways of improving the spectral containment of multicarrier waveforms, including methods to suppress the strong side lobes of the orthogonal frequency-division multiplexing (OFDM) spectrum [12-14]. Filter bank multicarrier (FBMC) is another multicarrier modulation scheme which has significantly reduced spectrum leakage compared to the cyclic prefix-based OFDM systems [15]. Also, the analysis filter bank (AFB) module of an FBMC receiver can be easily used for spectrum analysis purposes [15-22].

This paper includes a brief summary of our earlier studies concerning simple energy detection-based wideband multichannel spectrum sensing techniques for identifying the spectrum holes, considering the 2.4-GHz ISM band as a case study. We apply an AFB-based energy detector, which averages the subband sample energies. By this way, multiple center frequencies, bandwidths, and multiple spectral gaps can be identified rapidly, efficiently, and flexibly for potential use by the CR. A similar fast Fourier transform (FFT)-based scheme is considered as a reference.

At the resource allocation stage, the transmit power of the subcarriers must be adjusted according to the channel state information (CSI) and the location of subcarriers with respect to the primary user's (PU) spectrum. In [23], an optimal and two sub-optimal power loading algorithms are developed. These algorithms use Lagrange formulation which maximizes the downlink capacity of the CR keeping the interference to the primary transmission below a threshold, without considering the total power constraint. In [23,24], the spectral hole and the signal-to-noise (SNR) are fixed to simplify the model. In [25], a low-complexity suboptimal algorithm is proposed. The algorithm gives maximum power to each subcarrier based on the results from conventional water filling and then modifies these values by applying power reduction algorithm in such a way that the interference constraint is satisfied. In [23,25], the used signal models are closer to the ideal signal model, e.g., assuming fixed spectral hole bandwidth, instead of a realistic system model. In reality, the spectral hole bandwidth varies with the SNR. A proper system model should include also a practical power amplifier model. Our study focuses on the missing aspects of these studies.

The optimal solution which maximizes the CR link capacity under both transmission power and interference constraints requires high computational complexity, and it is unsuitable for the practical applications. Low complexity algorithms are proposed in [25,26]. However, in these methods, the interfered subcarriers are deactivated without considering optimized power and bit loading based on each subcarrier's SINR. Such optimization can be carried out using the power interference (PI) algorithm [27,28]. The resource allocation method utilizes the results of spectrum sensing in an efficient way, so there is interdependence between the spectrum sensing and spectrum allocation functions, which has not been addressed in earlier work. We study this interdependence, focusing on its effects on efficient utilization of the sensed spectrum.

The main contributions of this study are listed as follows:

- We have generalized the study for realistic signal models which can be applied to any multicarrier CR system.
  Until now, simplistic CP-OFDM signal models have been used as the PU and CR signal models for spectrum allocation algorithms [23-26,29-32]. Except for [27,28], CP-OFDM has also been used for the CR. The primary knowledge we assume about the PU waveform is its transmitted power spectral density (PSD) and the receiver selectivity mask; otherwise, there are no limitations regarding the PU signal model. In our case study, we select the PU waveform either as CP-OFDM following the 802.11-g standard or an FBMC waveform with similar parameterization. Furthermore, a nonlinear transmitter power amplifier model (the so-called Rapp model [33]) is used for the PU system in order to obtain a realistic model for the PU spectrum. To the best of our knowledge, this aspect has not been considered in earlier work. In this way, we are able to quantify the effects of the PU spectral characteristics on the SU capacity. It is seen that the nonlinear power amplifier-induced spectral leakage (regrowth) effect, which is present in any radio communication system, has a significant impact on the SU capacity. As for the SU waveform, we have chosen the FBMC scheme for the case study because it has the sharpest spectrum, reaching the maximum spectral containment among the alternatives. However, generic multicarrier model is included in the overall system model, and the analysis and

optimization methods are readily applicable for any multicarrier waveform for the CR.
Furthermore, previous studies on CR resource allocation in [23-25,27-32] consider only flat fading channel models. However, the performance of spectrum sensing and resource allocation is affected significantly when frequency-selective fading channel is assumed. In our study, all the links within/between PU and SU systems associated with spectrum estimation and spectrum utilization are modeled as frequency selective block fading channels.

- Combined spectrum sensing and resource allocation algorithms for cognitive radios.
There has been no previous work addressing the combined spectrum sensing and resource allocation algorithm in the literature. Especially, different types of spectrum sensing algorithms have been applied without considering any particular spectrum utilization techniques to make efficient use of the available spectral holes [1-5]. Similarly, resource allocation algorithms have only been applied without any spectrum sensing information so far [27-32,34,35]. Constant number of available subbands has been considered in the spectral hole. However, the variation of the PUs' power level affects the actual number of available subbands, and this depends critically on the spectral characteristics of the PUs. Hence, spectrum sensing plays a crucial and enabling role for spectrum utilization process. The sensing function identifies the frequency band which is considered for allocation, but it is also needed for detecting possible other PU's starting to operate in the spectral gap during the SU operation. For this purpose, we assume that there are gaps in the CR transmission. In our study, efficient spectrum utilization methods are investigated and applied for maximizing the cognitive radio's throughput based on robust spectrum sensing results. It turns out that the PI algorithm is applicable in our scenario, with all the mentioned generalizations of the system model. The main contribution of this study is evaluating the SU performance with the combination of energy detection-based wideband sensing algorithm and the PI algorithm for spectrum utilization in a realistic cognitive radio scenario.

The rest of this paper is organized as follows. In Section 2, the signal models for the CR and the primary transmission system, along with the mutual interference model between the CR and primary are explained. The problem definition for this study is given in the same section. In Section 3, FFT- and AFB-based wideband spectrum sensing is reviewed considering the spectrum analysis aspects related to the multicarrier techniques. Section 4 develops the algorithms for spectrum allocation. Section 5 gives the numeric and graphic results obtained through simulations. Finally, some concluding remarks are given about the performance of these methods, along with discussion of possible further studies in this area.

2 Signal models and problem definition

As shown in Figure 1, the CR system works in the same band of frequencies with PU networks. Hence, there will be some interference between different PUs and CRs. The PU and CR systems are assumed to use the time-division multiplexing/duplexing (TDMA/TDD) principles, i.e., each system is using a fixed frequency slot for communications between all the stations. While the CR system has the capability to operate in other parts of the ISM band, we focus on the situation where the CR

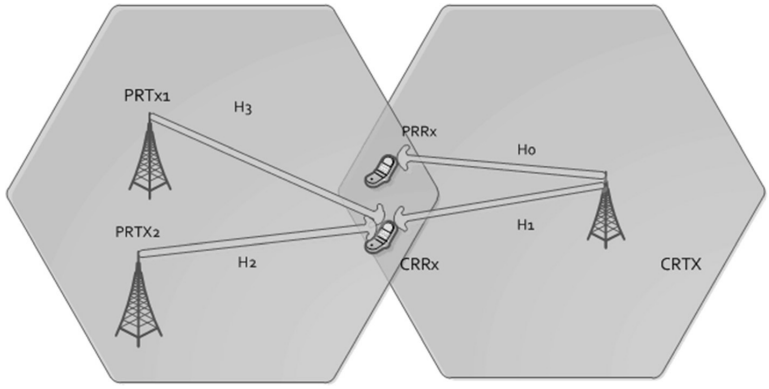

Figure 1 System model for spectrum sharing in CR.

system has identified a spectrum opportunity in the mentioned frequency slot and is initiating communications in it. The primary purpose of the spectrum sensing function is to detect possible other transmissions or reappearing PUs in the spectrum gap. It is also assumed that the stations of the CR systems have means to exchange control information with each other, e.g., using a cognitive control channel [36].

2.1 Signal model for PU

In this study, we focus on a specific spectrum use scenario with two active primary radio systems which are operating in the 2.4-GHz ISM band, using either as 802.11 g-based WLAN waveforms or 802.11 g-like FBMC signals. The WLAN and FBMC spectra considered here use third and eighth channels as illustrated in Figure 2. The signals do not overlap each other, and an 8-MHz spectral hole is available between the two PU spectra. Both active signals are assumed to have the same power level, normalized to 0 dB in our scenario. This means that the spectrum leakage effects on both edges of the white space are equally critical for the CR system performance.

The Rapp power amplifier (PA) nonlinearity model [33] is considered as seen in Figure 2. Using the complex I/Q baseband model, the amplitude function at the PA output is given as follows:

$$g_A = \frac{\kappa A}{\left(1 + [\kappa A / A_0]^{2p}\right)^{1/2p}} \quad (1)$$

where A is the input amplitude, κ is the small signal gain, A_0 is the saturated amplitude, and p is the amplitude smoothness factor of the transition from linear to saturated amplitude range. Three cases with respect to the PA nonlinearity are considered in this study. *No regrowth* is the ideal case, and the Rapp PA nonlinearity with two different back-off values of 15 dB (*modest case*) and 5 dB (*worst case*) is illustrated in Figure 2. Parameters of the Rapp model have been chosen according to the practical model for PU signals based on [37]. In our study, we use $\kappa = 1$, $p = 3$, and $A_0 = 1$ as Rapp model simulation parameters.

The 802.11-g-based WLAN signal specifications allow the spectral regrowth in this scenario to be at the level of about −20 dB, i.e., close to the worst case model. We investigate how the CR system performance is affected by improved spectral containment of the PU signal through enhanced multicarrier waveform and/or improved power amplifier linearity. These effects for both sensing and utilization functions will be addressed in the study.

2.2 Signal model for cognitive radio

In this work, the CR waveform is chosen as FBMC due to its high spectral containment. Offset quadrature amplitude modulation (OQAM) is used for FBMC-based CRs to achieve orthogonality of subcarriers, as discussed in [18,19,38]. In Figure 1, the channels h_0 and h_1 are the channels from a cognitive transmitter to a primary receiver and a cognitive receiver, respectively. Channels h_2 and h_3 are from two different primary transmitters to the cognitive radio receiver. The channel estimate for h_1 is made available by usual channel estimation procedure of the CR system. The knowledge about channel h_0 can be obtained through the channel reciprocity in TDD

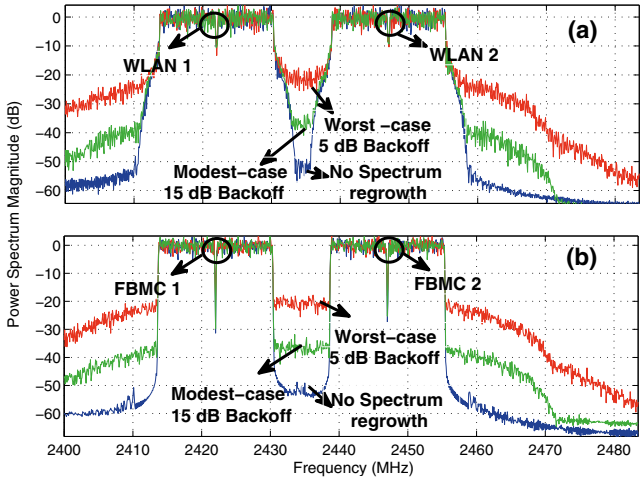

Figure 2 Effects of the Rapp power amplifier model on (a) OFDM- and (b) FBMC-based primary users' spectra.

operation. Here, the channel amplitude response is sufficient and the phase response is irrelevant. The amplitude responses of channels h_2 and h_3 are first obtained through the spectrum sensing function of the CR device and later on, during secondary transmission, through the SINR estimation function of the CR device. The effects of primary spectral dynamics at the edges of the white space play an important role both in spectrum sensing and in spectrum allocation. This dependency is captured by the analytical models and revealed by the simulations to be presented later.

For FBMC/OQAM, a signal model with real valued symbol sequence at twice the QAM symbol rate is applied, instead of complex symbols. The synthesis filter bank (SFB) for transmitter and AFB for receiver is designed with this idea in mind. The FBMC-based transmitted signal can be expressed mathematically as

$$s(n) = \sum_k \sum_{l \in Z} a_{k,l} g(n - l\tau_0) e^{j2\pi(k/N)n} e^{j\phi_{k,l}} \tag{2}$$

where $\{k\}$ is the set of active subbands, l is the symbol index belonging to the set of integers, g is the pulse shape (prototype filter impulse response), and $\phi_{k,l}$ is a phase term. The real symbol values, obtained alternatingly as real and imaginary parts of complex QAM symbols, are denoted as $a_{k,l}$ and τ_0, respectively, is the corresponding half-symbol duration. Both the real and imaginary parts of the QAM sequence have zero mean and equal variances $\sigma_r^2 = \sigma_I^2 = \sigma_s^2/2$. The PSD of the FBMC based CR waveform can be written as

$$\phi_{\mathrm{FBMC}}(f) = \frac{\sigma_r^2}{\tau_0} \sum_k \left| G\left(f - \frac{k}{N}\right) \right|^2 \tag{3}$$

where G is the frequency response of the prototype filter with impulse response $g(n)$ with $n = 0, 1 \ldots, L-1$. Here, $L = KN$ is the prototype filter length and K is the overlapping factor (length of each polyphase component) while N is the number of subbands. The prototype coefficients have even symmetry around the $(KN/2)$th coefficient, and the first coefficient is zero [13]. In our study, the prototype filter of the FBMC-based CR is designed according to the PHYDYAS model [38], with $K = 4$. Then its frequency response can then be expressed as

$$|G(f)| = g[L/2] + 2 \sum_{r=1}^{L/2-1} g[L/2 - r] \cos(2\pi f r) \tag{4}$$

Also, the nonlinear PA model can be straightforwardly included in the CR signal model and the interference models developed below. However, in the numerical studies of this paper, we consider an ideal FBMC waveform for the CR as the focus is on the SU capacity and its dependency on the PU waveform characteristics. Generally, good spectral containment is regarded as one of the key requirements for the CR transmitter. Detailed evaluation of the performance-complexity tradeoffs for the CR implementation, including the PA linearity requirements, is a rather complicated issue and is left as a topic for future studies.

2.3 Definition of the interference problem

According to the above scenario, the CR system coexists with the primary transmission system in the same geographical location. The CR transmitter causes some interference to the primary transmission system, and similarly, the secondary transmission between two active PU spectra is exposed to some interference due to the PUs. The secondary transmission system uses multicarrier transmission technique. There are N_{gap} subcarriers in the sensed spectrum hole and the subcarrier spacing is Δf. Since the transmitter and receiver are assumed to be static or slowly moving, the effect of inter-carrier interference (ICI) between subcarriers can be ignored. The primary and secondary transmission systems occupy contiguous frequency slots. The interference that the CR produces to each of the primaries is required to be is less than the maximum interference that can be tolerated by the primary, Ith. The spectral distance d_{PU} of a PU is defined as the frequency separation from the DC subcarrier of the CR to the center frequency of the PU (positive for a PU above the upper edge of the gap, negative for a PU below the gap). The interference to the primary transmission due to the kth CR subcarrier depends on the CR subcarrier powers P_k and d_{PU} [20]. Fixing the origin of the frequency axis at the DC subcarrier of the CR, the interference is given by the equation

$$I_k(P_k) = \int_{k\Delta f - B/2}^{k\Delta f + B/2} |H_0(f)|^2 P_k \Phi(f - k\Delta f) \Psi(f - d_{\mathrm{PU}}) df = P_k \Omega_k \tag{5}$$

Here, $H_0(f)$ is the channel frequency response between the CR transmitter and a primary receiver. $\Phi(f)$ represents the subcarrier power spectral density of the underlying multicarrier technique employed by the CR. $\Psi(f)$ denotes the PU sensitivity mask characterizing the effects of the PU receiver filtering. B denotes the CR subcarrier bandwidth which is considered significant for the interference estimation. Finally, Ω_k represents the combined interference factor for the kth CR subcarrier.

The signal-to-interference-plus-noise ratio due to interference introduced by primary signal to the kth subcarrier at the receiving CR is given by

$$\mathrm{SINR}_k = \frac{P_k|H_{1,k}|^2}{\sigma_w^2 + \int_{k\Delta f - B/2}^{k\Delta f + B/2} |H_2(f)|^2 \Phi(f - k\Delta f)\psi_{\mathrm{PA}}(f - d_{\mathrm{PU}})df} = \frac{P_k}{\sigma_w^2 + J_k} \tag{6}$$

where $H_2(f)$ is the channel frequency response between the primary transmitter and CR receiver. $H_{1,k}$ is the channel gain between the CR transmitter and the CR receiver at the frequency of kth subcarrier. This channel can be assumed to be flat-fading at the subcarrier level. $\Psi_{\mathrm{PA}}(f)$ is the power spectral density as seen at the output of the PU's transmitter antenna. This depends on the PU transmission power and its subcarrier spectrum, as well as on the spectral regrowth due to the PU power amplifier. $\Phi(f)$ is the CR receiver sensitivity mask characterizing the CR receiver subband filtering effects. σ_w^2 is the variance of the additive white Gaussian noise.

The power amplifier effects of the secondary transmission are not considered in our numerical study as they play no role in the spectrum sensing part and the effect of PA-related spectrum leakage on the interference to the PUs is expected to be relatively small. For this reason, the same $\Phi(f)$ function can be used in (5) for the CR subcarrier spectrum and in (6) for the CR receiver sensitivity mask. However, the developed generic signal model allows to include also the CR transmitter PA effects by using different CR-related spectral functions in (5) and (6).

The interference models of (5) and (6) assume certain knowledge about PU characteristics and the channels between PUs and CRs. Regarding the interference from an active PU transmitter to a CR receiver in (6), the joint effect of transmitter power spectrum and the transmission channel can be estimated by the receiving CR station by utilizing the spectrum sensing function. This information can be communicated through the control channel to the transmitting CR station for optimizing the spectrum utilization. Regarding the channel from the CR transmitter to PU receiver, the knowledge would be available in a TDMA/TDD-based PU system (like a WLAN) based on channel reciprocity, if the PU transmission power is known. Of course, for a PU station which is in idle mode over long periods, such information is not available.

3 Filter bank energy detector-based spectrum sensing algorithms

Energy detector, which is also known as radiometer, is the most common method of spectrum sensing due to its low computational and implementation complexity [2-5]. Furthermore, it is more generic compared to most of the other methods as it does not need any information about the PU waveform. Subband-based energy detection, using FFT or AFB for spectrum analysis, is in the focus of this study. Basically, the energy of the received signal is compared with a threshold value which is calculated according to noise variance and desired false alarm probability in detecting spectral holes.

A block diagram of alternative FFT- and AFB-based spectrum sensing algorithms is shown in Figure 3. The subband sampling rate is equal to the ADC sampling rate divided by the number of FFT/AFB frequency bins. With subband-wise spectrum sensing method, the subband signals can be expressed as [3]

$$Y(m,k) = \begin{cases} W(m,k) & \mathcal{H}_0 \\ S(m,k)H_k + W(m,k) & \mathcal{H}_1 \end{cases} \tag{7}$$

where $S(m, k)$ is the transmitted WLAN or FBMC based PU signals as seen in subband k during the mth symbol interval with zero mean and variance σ_{PU}^2. When there are no PU signals (hypothesis $\mathcal{H}_0$), the noise samples $W(m, k)$ are modeled as AWGN with zero-mean and variance σ_w^2. When a PU signal is present (hypothesis $\mathcal{H}_1$), the WLAN- and FBMC-based PU signals can also be modeled as zero-mean Gaussian distribution with variance $\sigma_{\mathrm{PU},k}^2 + \sigma_w^2$.

Time and frequency averaging techniques can be applied to obtain more reliable decision statistic [3]. The decision statistics at different frequencies can be obtained with this idea as follows in [39]:

$$\tilde{T}(m,k) = \frac{1}{L_t L_f} \sum_{l=k-\lfloor L_f/2 \rfloor}^{k+\lceil L_f/2 \rceil - 1} \sum_{u=m-L_t+1}^{m} |Y(u,l)|^2 \tag{8}$$

In this formula, L_f and L_t are the window lengths in frequency and time domain averaging, respectively. The output of $\tilde{T}(m,k)$ is passed to a decision device to determine the possible occupancy of the corresponding frequency band at the corresponding time interval. The window length in frequency direction is selected based on the expected minimum bandwidth of the PU signal or spectrum hole, and then the required time domain window length can be calculated from the target false

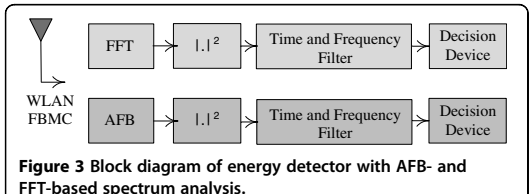

Figure 3 Block diagram of energy detector with AFB- and FFT-based spectrum analysis.

alarm and missed detection probabilities. The basic approach would be to calculate (8) for a nonoverlapping set of windows. However, using a sliding window in frequency and/or time direction can also be done with relatively small addition to complexity. Time-domain sliding window helps to detect rapidly re-appearing PU [4,5] whereas sliding window in the frequency direction helps to locate spectrum gaps with unknown center frequencies. Due to the Gaussian distribution of $Y(m, k)$, the probability distribution function (PDF) of $\tilde{T}(m,k)$ becomes approximately Gaussian under $\mathcal{H}_0$ and $\mathcal{H}_1$. [3].

Using Gaussian approximation, it is straightforward to model the effect of PU transmitter's spectral leakage on the actual false alarm probability $\tilde{P}_{\mathrm{FA}}$ as

$$\tilde{P}_{\mathrm{FA}}(k) = Q\left(\frac{\lambda - \left(\sigma_w^2 + I_{\mathrm{adj}}(k)\right)}{\sqrt{\frac{1}{L_t L_f}\left(\sigma_w^2 + I_{\mathrm{adj}}(k)\right)}}\right) \tag{9}$$

Here,

$$I_{\mathrm{adj}}(k) = \int_{f_1}^{f_2} |H_2(f)|^2 \psi_{\mathrm{PA}}(f) df \tag{10}$$

is the leakage power from the adjacent PU transmitter to the sensing frequency band between frequencies f_1 and f_2. $H_2(f)$ is the channel frequency response from a primary transmitter the CR receiver. In (9), λ is the decision threshold value which is calculated using a well-known analytical model from the noise variance estimate and target false alarm probability P_{FA}.

The detection probability P_D and threshold value λ can also be expressed as follows:

$$P_D(k) = Q\left(\frac{\lambda - \left(\left(\sigma_w^2 + I_{\mathrm{adj}}(k)\right) + \sigma_{\mathrm{PU},k}^2\right)}{\sqrt{\frac{1}{L_t L_f}\left(\left(\sigma_w^2 + I_{\mathrm{adj}}(k)\right) + \sigma_{\mathrm{PU},k}^2\right)}}\right) \tag{11}$$

$$\lambda = Q^{-1}(P_{\mathrm{FA}}(k))\sqrt{\frac{1}{L_t L_f}\left(\sigma_w^2 + I_{\mathrm{adj}}(k)\right)} + \left(\sigma_w^2 + I_{\mathrm{adj}}(k)\right) \tag{12}$$

In principle, if there is a reliable estimate of the PU transmission power and reliable knowledge about its spectrum shape, then the above analysis could be used for improving the spectrum sensing at the frequencies affected by the spectrum leakage. However, this would be very challenging in practice due to the unpredictability of the PA characteristics, and the above model is used only for the purpose of performance analysis.

For different PU SNR values, different number of empty subbands, N_{gap}, will be detected due to the PU spectral leakage effects and statistical nature of the spectrum sensing process. The expression (9) can be used for evaluating the false alarm probability for different sensing bandwidths in different parts of the spectrum gap.

The spectrum sensing function identifies groups of L_f subbands which are deemed to be available for secondary transmissions. In the following stage, the spectrum utilization function is employed to perform power and bit allocation to those subcarriers.

4 Spectrum utilization

After nonactive spectrum has been identified, spectrum utilization becomes an important consideration, when considering the overall efficiency of the CR system. The number of available nonactive subbands is the output of the sensing algorithm, along with information about the nonactive band edges.

In the multicarrier case, the rate at which transmission can take place is given by Shannon's capacity

$$R_{\mathrm{CR}} = \sum_{k=1}^{N_{\mathrm{gap}}} \Delta f \log_2\left(1 + \frac{P_k}{\sigma_k^2}\right) \tag{13}$$

$$\sigma_k^2 = \sigma_w^2 + \sum_{i=1}^{N_{\mathrm{PU}}} J_{k,i} \tag{14}$$

where $J_{k,i}$ is the effective interference power contributed by ith primary to the kth CR subcarrier as given by (6). N_{PU} is the number of PU's contributing to the interference at the receiving CR station. In our case study, $N_{\mathrm{PU}} = 2$, i.e., there is one PU adjacent to the lower and upper edges of the white space. The model could be simplified by assuming that these PUs affect only the lower and upper half of the subcarriers, respectively. P_k is the transmit power used by the CR for subcarrier k. It is assumed that the channel changes slowly so that the channel gains, and consequently $J_{k,i}$, will be approximately the same during each transmission frame. Further, there is no ICI in the CR reception due to low mobility. The main objective here is to maximize the capacity as given in (13).

The block diagram of spectrum utilization is shown in Figure 4. As seen in this block diagram, knowledge which comes from sensing part is passed to spectrum utilization part to obtain better capacity.

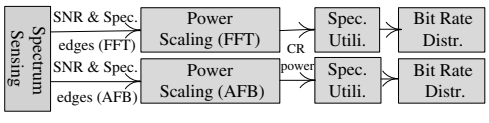

Figure 4 Block diagram of spectrum utilization with alternative AFB- and FFT-based spectrum analysis schemes.

The optimization problem can be formulated as follows [27]:

$$R_{\mathrm{CR}} = \max_{\{P_k\}} \sum_{k=1}^{N_{\mathrm{gap}}} \Delta f \log_2\left(1+\frac{P_k}{\sigma_k^2}\right) \tag{15}$$

Subject to

$$\sum_{k=1}^{N_{\mathrm{gap}}} P_k \le P_T \tag{16}$$

$$\sum_{k=1}^{N_{\mathrm{gap}}} P_k \Omega_k \le I_{th} \tag{17}$$

$$P_k \ge 0, \forall k \in \left\{1,2,\ldots,N_{\mathrm{gap}}\right\} \tag{18}$$

This is a convex optimization problem, and the Lagrangian can be written as

$$\begin{aligned} G_{\mathrm{snr}} &= \sum_{k=1}^{N_{\mathrm{gap}}} \Delta f \log_2\left(1+\frac{P_k}{\sigma_k^2}\right) \\ &-\lambda_0 \sum_{k=1}^{N_{\mathrm{gap}}} (P_k - P_T) - \lambda_1 (P_k \Omega_k - I_{\mathrm{th}}) + \lambda_2 \sum_{k=1}^{N_{\mathrm{gap}}} P_k \end{aligned} \tag{19}$$

The Karush-Kuhn-Tucker (KKT) conditions [27] can be written as

$$P_k \ge 0, \forall k \in \left\{1,2,\ldots,N_{\mathrm{gap}}\right\}, \tag{20}$$

$$\lambda_j \ge 0, \forall j \in \{0,1,2\} \tag{21}$$

$$\sum_{k=1}^{N_{\mathrm{gap}}} (P_k - P_T) \ge 0 \tag{22}$$

$$\lambda_1 (P_k \Omega_k - I_{\mathrm{th}}) \ge 0 \tag{23}$$

$$\lambda_2 \sum_{k=1}^{N_{\mathrm{gap}}} P_k \ge 0 \tag{24}$$

The optimal solution to the problem above as given in [27] is as follows:

$$P_k = \left[\frac{1}{\lambda_0 \Omega_k + \lambda_1} - \frac{\sigma_k^2}{|h_k|}\right]^+ \tag{25}$$

where $[y]^+ = \max(0, y)$. The optimal solution has high computationally complexity; hence, a lower complexity algorithm called the PI algorithm which divides the problem into stages has been developed [27]. First, the interference constraint is ignored, keeping only the total power constraint and this leads to the classical water filling solution

$$P_k{}' = \left[\gamma - \frac{\sigma_k^2}{|h_k|}\right]^+ \tag{26}$$

where γ is the water filling level. When the total power is ignored the solution [27] becomes

$$P_k{}' = \left[\frac{1}{\lambda'_0 \Omega_k} - \frac{\sigma_k^2}{|h_k|}\right]^+ \tag{27}$$

The value of λ'_0 can be obtained by substituting (27) into the constraint $\sum_{k=1}^{N_{\mathrm{gap}}} P_k{}' \Omega_k = I_{\mathrm{th}}$ to get

$$\lambda'_0 = \frac{|N_{\mathrm{gap},l}|}{I_{\mathrm{th}}^{N_{\mathrm{gap}}} + \left(\sum_i \Omega_k \sigma_k^2 / |h_k|^2\right)} \tag{28}$$

The above solution is optimal only when the total power is greater than or equal to the power under the interference constraint. Mostly, in practice, this condition is not true and this is the motivation for the PI algorithm. Detailed discussion and its comparison to various other algorithms for spectrum utilization are available in [27].

In this study, the PI algorithm is found to be directly applicable in case of the developed greatly enhanced system model for the secondary usage scenario. PI algorithm has four stages: maximum power determination, power constraint, power budget distribution, and power level re-adjustment [27].

5 Simulation results

In our test scenario, the CR's spectrum sensing function has identified a potential spectral gap between two relatively strong PUs, as illustrated in Figure 2. We should also consider the possibility that there is another, relatively weak PU signal, using one of the WLAN channels 4...7, and fully or partly occupying the gap between channels 3 and 8. Thus, one purpose of spectrum sensing is to secure that there are no other PUs active in the considered gap. We assume that there are no additional signals within the spectral gap, but the spectrum sensing makes anyway false alarms. Especially close to the edges of the gap, the spectrum leakage from the PUs raises the false alarm probability. This effect depends on the power level (SNR) of the PUs. In our case study, the spectrum sensing and CR transmissions use a smaller subband spacing of 81.5 kHz, instead of the 325-kHz subcarrier spacing of WLANs, in order to reduce the effects of frequency selective channels. Targeting at −5 dB SNR in spectrum sensing, false alarm probability of 0.1, and detection probability of 90%, the required sample complexity is around 250 complex samples. The time and frequency averaging lengths are chosen as 50 and 5, respectively. The spectral hole starts from the side lobes of WLAN 1 signal and ends at the side lobes of WLAN 2 spectrum. The available number of subbands/bandwidth

of the spectrum is obtained after subband-based energy detection, using FFT or AFB for spectrum analysis. Then, the initial SINR estimation and spectrum allocation is done based on the sensing results. Later on, the SINR estimates are updated during SU system operation to track the changing radio environment under frequency-selective fading channel conditions. It is assumed that the spectrum sensing is done in regular intervals during gaps in the CR transmission and this helps in detecting reappearing PU signals in the spectral gap.

It should be noticed that in the considered scenario, there is no way for the CR system to determine the useful received power level at the PU receiver. Therefore, we choose the interference threshold to be 6 dB below the thermal noise level, in order not to introduce significant performance loss in case the primary receiver is operating close to the sensitivity level (i.e., minimum received power level expected to be detectable). To determine the threshold value, we assume a simplified scenario, where the path losses of channels h_0 and h_1 are normalized to 1, i.e., the average power gains of channels h_0 and h_1, denoted as G_0 and G_1, are equal to one. Further, we assume that the average SNR of the CR receiver is 10 dB. Then, the interference threshold is −16 dB in reference to the total CR transmission power P_T, or $I_{\text{th}} = P_T/40$. More generally, relaxing the normalization of h_0 and h_1, this can be expressed as $I_{\text{th}} = G_1 P_T/(40G_0)$.

The bandwidth of the detected spectral hole is shown in Figure 5 as a function of the average PU SNR at the CR RX. The spectral leakage due to primary users' PA nonlinearity is affecting significantly on the width of the detected hole. In this respect, we consider three different cases, as explained in Subsection 2.1: ideal PA, modest PA nonlinearity with 15 dB back-off, and worst case nonlinearity with 5 dB back-off. All PU and CR channels h_0, h_1, h_2, and h_3 use frequency-selective channel models with 90 ns delay spread and 16 taps [40]. We consider the combinations of two PU waveforms, CP-OFDM- and FBMC-based WLANs, as well as two spectrum sensing techniques, based on FFT or AFB. The CR waveform is always FBMC.

From Figure 5, it can be easily seen that AFB-based spectrum sensing is able to detect the unoccupied spectrum close to strong primary users much better than FFT-based sensing. FBMC-based transmission results in much better spectral containment, which can be effectively utilized by AFB-based sensing. However, even with relatively modest power amplifier nonlinearity, this benefit of FBMC waveform is compromised.

In Figure 6, the actual false alarm probability within the spectral hole is shown as a function of the active PU's SNR for different levels of spectral regrowth. The results indicate the probability of the 5 subband groups to be detected to be occupied.

The efficiency of the utilization of the 8-MHz white space by SU in between two active PUs is shown in Figure 7 versus the PU SNR. In this figure, perfect CSI is considered for the CR channel, both for CR channel h_1

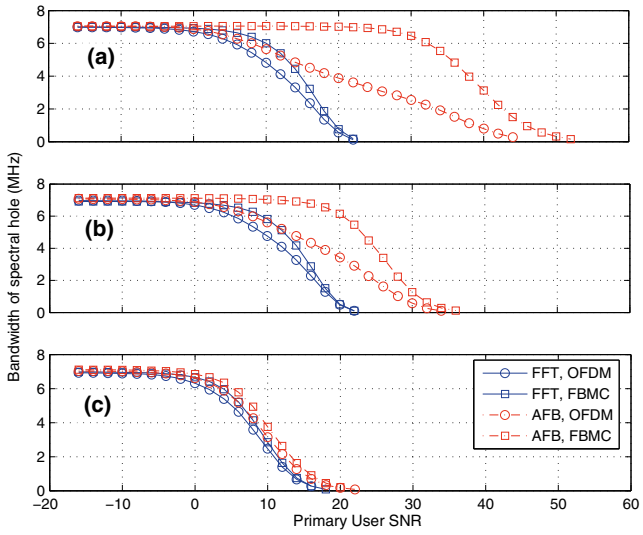

Figure 5 Average bandwidth of the detected spectral hole with target $P_{FA} = 0.1$. Using sample complexity of 250 samples under frequency-selective channel model for **(a)** ideal model, **(b)** Rapp PA with 15 dB back-off as the modest case, **(c)** Rapp PA with 5 dB back-off as the worst case. Different combinations of FFT/AFB-based sensing and OFDM/FBMC based PU waveforms.

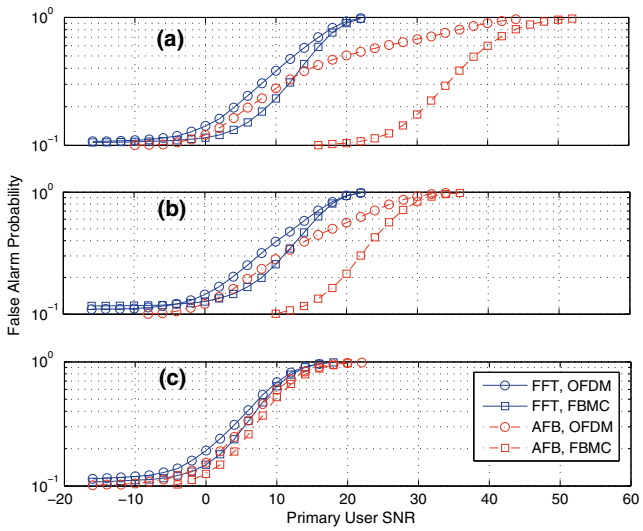

Figure 6 Actual false alarm probability for target $P_{FA} = 0.1$. Time record length of 50 and sensing bandwidth of 5 subbands under frequency selective channel model for **(a)** ideal model, **(b)** Rapp PA with 15 dB backoff as modest case, **(c)** Rapp PA with 5 dB backoff as worst case. Different combinations of FFT/AFB based sensing and OFDM/FBMC based PU waveforms.

equalization and in the PI algorithm for resource allocation. Perfect knowledge of the amplitude response of channel h_0 is also assumed, while channels h_2 and h_3 are known from spectrum sensing results. The subband-wise noise + interference estimates are obtained using time filtering length of 50. According to FFT- or AFB-based spectrum sensing results, a number of subbands are left empty in the spectrum utilization phase. The power of these occupied subchannels is reallocated to the other subbands that can be used by the CR. The

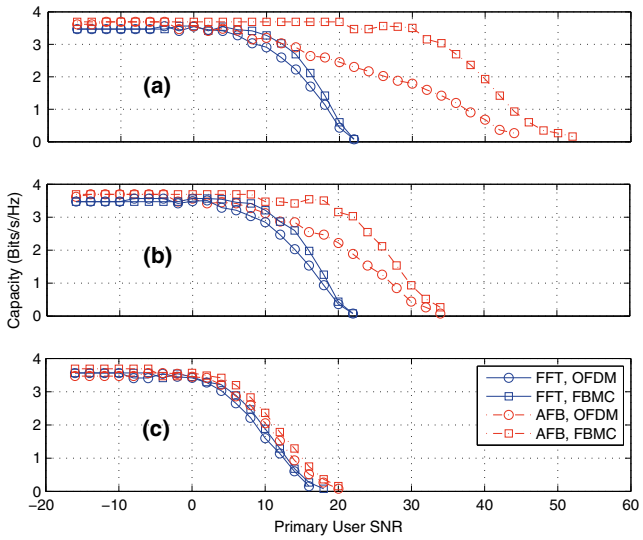

Figure 7 Capacity of a CR in a spectral gap between two PUs versus PU SNR. PI algorithm used for power allocation **(a)** Ideal model, **(b)** Rapp PA with 15 dB backoff as the modest case, **(c)** Rapp PA with 5 dB backoff as the worst case. Different combinations of FFT/AFB-based sensing and OFDM/FBMC-based PU waveforms.

power allocation is done utilizing the PI algorithm, and the resulting capacity, in terms of bits/s/Hz, is shown in Figure 7. The limitations of FFT-based spectrum sensing can again be clearly seen from the results, whereas AFB-based sensing is able to identify gaps between relatively strong PU signals. Regarding the transmission waveform, FBMC has clear benefit due to better spectral containment, if the effects of power amplifier nonlinearities can be kept at a modest level. As expected, the capacity is proportional to the available bandwidth in the gap, i.e., there is a clear connection between the results of Figures 5 and 6. The resource allocation algorithm (i) optimizes the performance with frequency selective channels in the presence of spectral leakage from the strong PUs and (ii) secures that the interference leakage from the CR transmission to the primaries is at an acceptable level.

6 Conclusions

We have studied the effects of combined spectrum sensing and spectrum utilization for FBMC-based cognitive radios with realistic signal model under frequency-selective fading channel conditions. Firstly, the performance of energy detection-based spectrum sensing technique was analyzed using both the FFT and filter bank-based spectrum analysis methods for both WLAN and FBMC signal models. Then, the utilization of dynamically identified spectral holes with spectrum allocation algorithms, subject to power and interference constraints, was investigated. Through this study, the effect of PU waveform's spectral containment on the CR transmission capacity was revealed. Here, we considered the choice between OFDM and FBMC primaries, together with the effect of spectral regrowth due to power amplifier nonlinearity.

In terms of the spectrum sensing performance, AFB has clear benefits due to much better spectral containment of the subbands. One important benefit of FBMC as a transmission technique in CR systems is that it can utilize narrow spectral gaps in an effective and flexible way, even in the presence of strong primaries at the adjacent spectral slots. This is due to the excellent spectral containment properties of the FBMC system. Additionally, an FBMC receiver can use the AFB for high-performance spectrum sensing with no additional complexity.

The utilization of the sensed spectrum can be optimized by using proper spectrum allocation algorithms. The PI algorithm has relatively low complexity, and it improves the capacity of the CR system as compared to the simple water filling-based spectrum allocation. One of the main observations of this work was that the PI algorithm can be directly utilized with the developed highly enhanced and realistic CR system model. The system model accommodates frequency-selective channel models for all the associated transmission links between PUs and SUs, as well as arbitrary transmitted power spectra and receiver frequency responses. Because of the above features, a FBMC-based CR system achieves higher capacity in comparison with traditional WLAN-based system. This increase in capacity can be attributed to the efficient use of the available spectrum and very small interference introduced to the primary transmissions at adjacent frequencies.

One of the important aims of this study was to understand the interdependence of the spectrum sensing and the spectrum utilization parts. It can be seen that increased false alarm probability has a direct effect on the available spectrum, and hence, it heavily influences the spectrum utilization. The PU power amplifier nonlinearity influences the sensed secondary spectrum introducing false alarms, hence lowering the CR system's spectrum utilization. It was demonstrated that, with heavy power amplifier nonlinearity, the FBMC-based primary is no better than the OFDM primary in what comes to the available capacity for secondary usage in the nearby frequencies.

In the numerical studies of this paper, we considered an ideal FBMC waveform for the CR, without considering the PA nonlinearity effects, since the focus is on the SU capacity and it dependency on the PU signal characteristics. Generally, good spectral containment is regarded as one of the key requirements for the CR transmitter. Also, the nonlinear PA model can be straightforwardly included in the developed interference models. Detailed evaluation of the performance-complexity tradeoffs for the CR implementation, including the PA linearity requirements, is a rather complicated issue and is left as a topic for future studies.

Competing interests

The authors declare that they have no competing interests.

Acknowledgements

This work was partially supported by Tekniikan Edistämissäätiö (TES), GETA Graduate School, the European Commission under Project EMPhAtiC (FP7-ICT-2012-09-318362), COST Action IC0902, Tekes (the Finnish Funding Agency for Technology and Innovation) under the project ENCOR in the Trial Program.

Author details

[1]Department of Electronics and Communications Engineering, Tampere University of Technology, P.O. Box 692, Tampere 33101, Finland. [2]Centre Tecnològic de Telecomunicacions de Catalunya (CTTC), Parc Mediterrani de la Tecnología (PMT), Avenida Carl Friedrich Gauss 7, 08860 Barcelona, Spain. [3]Signal, Communication & Embedded Electronics Research Group, Ecole Supérieur D'Électricité –SUPELEC University, F-35576 Cesson-Sévigné Cedex, Gif-sur-Yvette C.S. 47601, France.

Received: 10 December 2013 Accepted: 15 April 2014
Published: 12 May 2014

References

1. J Mitola, JGQ Maguire, Cognitive radio: making software radios more personal. IEEE Pers Commun Mag **6**(4), 13–18 (1999)

2. Y Zeng, YC Liang, AT Hoang, R Zhang, A review on spectrum sensing for cognitive radio: challenges and solutions. EURASIP J Adv Signal Process **2010**, 1–15 (2010)
3. T Yucek, H Arslan, A survey of spectrum sensing algorithms for cognitive radio applications. IEEE Commun Surv Tutorials **11**(1), 116–130 (2009)
4. S. Dikmese, M. Renfors, H. Dincer, *FFT and filter bank based spectrum sensing for WLAN signals, in Proc (European Conference on Circuit Theory and Design (ECCTD'11)* (Linkoping, Sweden, 2011)
5. S Dikmese, M Renfors, *Optimized FFT and filter bank based spectrum sensing for bluetooth signal, in Proc (Wireless Communications and Networking Conference (WCNC'12)* (France, Paris, 2012)
6. AJ Goldsmith, PP Varaiya, Capacity of fading channels with channel side information. IEEE Trans Inf Theory **43**(6), 1986–1992 (1997)
7. E Biglieri, J Proakis, S Shamai, Fading channels: information-theoretic and communications aspects. IEEE Trans Inf Theory **44**(6), (1998)
8. M Gastpar, *On capacity under received-signal constraints, in Proc (42nd Annual Allerton Conference Communication* (Control Comput, Monticello, USA, 2004)
9. A Ghasemi, E Sousa, Fundamental limits of spectrum-sharing in fading environments. IEEE Trans Wirel Commun **6**(2), 649–658 (2007)
10. L Musavian, S Aissa, *Ergodic and outage capacities of spectrum-sharing systems in fading channels, in Proc (IEEE Global Telecommunications Conference (GLOBECOM'07), Washington* (DC, USA, 2007)
11. X Kang, YC Liang, A Nallanathan, HK Garg, R Zhang, Optimal power allocation for fading channels in cognitive radio networks: ergodic capacity and outage capacity. IEEE Trans Wirel Commun **8**(2), 940–950 (2009)
12. A Sahin, H Arslan, Edge windowing for OFDM based systems. Commun Lett IEEE **15**(11), 1208–1211 (2011)
13. S Brandes, I Cosovic, M Schnell, *Sidelobe suppression in OFDM systems by insertion of cancellation carriers,' in Proc (Vehicular Technology Conference, (VTC'05-Fall)* (Dallas, USA, 2005)
14. A Loulou, M Renfors, *'Effective schemes for OFDM sidelobe control in fragmented spectrum use, in Proc (IEEE 24th International Symposium on Personal, Indoor and Mobile Radio Communications (PIMR'13)* (United Kingdom, London, 2013)
15. BF Boroujeny, R Kempter, Multicarrier communication techniques for spectrum sensing and communication in cognitive radios. IEEE Commun Mag (Spec Issue Cogn Radios Dynamic Spectr Access) **48**(4), 80–85 (2008)
16. A Amini, R Kempter, L Lin, B Farhang-Boroujeny, *Filter bank multitone: a candidate for physical layer of cognitive radio, in Proc (Software Defined Radio Technical Conference and Product Exhibition (SDR '05)* (Orange County, USA, 2005)
17. A Amini, R Kempter, B Farhang-Boroujeny, *A comparison of alternative filterbank multicarrier methods in cognitive radios, in Proc (Software Defined Radio Technical Conference and Product Exhibition (SDR '06)* (Orlando, USA, 2006)
18. M Bellanger, T Ihalainen, M Renfors, *Filter bank based cognitive radio physical layer, in Proc* (Future Network & Mobile Summit, Santander, Spain, 2009)
19. T Ihalainen, A Viholainen, *TH Stitz, M Renfors, Spectrum monitoring scheme for filter bank based cognitive radios, in Proc* (Future Network & Mobile Summit, Florence, Italy, 2010)
20. S Srinivasan, S Dikmese, M Renfors, *Spectrum sensing and spectrum utilization model for OFDM and FBMC based cognitive radios, in Proc (Signal Processing Advances in Wireless Communications (SPAWC'12)* (Cesme, Turkey, 2012)
21. V Ringset, H Rustad, F Schaich, J Vandermot, M Najar, *Performance of a filterbank multicarrier (FBMC) physical layer in the WiMAX context, in Proc* (Future Network & Mobile Summit, Florence, Italy, 2010)
22. S Dikmese, S Srinivasan, M Renfors, *FFT and filter bank based spectrum sensing and spectrum utilization for cognitive radios, in Proc (International Symposium on Communications, Control, and Signal Processing (ISCCSP'12)* (Rome, Italy, 2012)
23. G Bansal, MJ Hossain, VK Bhargava, *Adaptive power loading for OFDM-based cognitive radio systems, in Proc (IEEE International Conference on Communications (ICC '07)* (Glasgow, UK, 2007)
24. G Bansal, MJ Hossain, VK Bhargava, Optimal and suboptimal power allocation schemes for OFDM-based cognitive radio systems. IEEE Trans Wirel Commun **7**(11), 4710–4718 (2008)
25. T Qin, C Leung, *Fair adaptive resource allocation for multiuser OFDM cognitive radio systems, in Proc (2nd International Conference on Communications and Networking in China (ChinaCom '07)* (Shanghai, China, 2007)
26. Y Zhang, *Resource allocation for OFDM-based cognitive radio systems* (University of British Columbia, Vancouver, Canada, 2008). Dec, Ph.D. dissertation
27. M Shaat, F Bader, Computationally efficient power allocation algorithm in multicarrier-based cognitive radio networks: OFDM and FBMC systems. EURASIP J Adv Signal Process **13**, (2010). doi:Article ID 528378
28. M Shaat, F Bader, *Power allocation with interference constraint in multicarrier based cognitive radio systems, in Proc (7th International Workshop on Multi-Carrier Systems and Solutions (MCSS '09)* (Herrsching, Germany, 2009)
29. J Jang, KB Lee, Transmit power adaptation for multiuser OFDM systems. IEEE J Selected Areas Commun **21**(2), 171–178 (2003)
30. D Kivanc, G Li, H Liu, Computationally efficient bandwidth allocation and power control for OFDMA. IEEE Trans Wirel Commun **2**(6), 1150–1158 (2003)
31. Z Shen, JG Andrews, BL Evans, *Optimal power allocation in multiuser OFDM systems, in Proc (IEEE Global Telecommunications Conference (GLOBECOM '03)* (San Francisco, USA, 2003)
32. CY Wong, RS Cheng, KB Letaief, RD Murch, Multiuser OFDM with adaptive subcarrier, bit, and power allocation. IEEE J Selected Areas Commun **17**(10), 1747–1758 (1999)
33. C Rapp, Effects of the HPA-nonlinearity on 4-DPSK OFDM signal for a digital sound broadcasting system, in *Proc Conf. Rec. ECSC'91* (Luettich, Germany, 1991)
34. J Cioffi, *Digital Communication: Signal Processing* (Standford, California, USA, 2000)
35. Q Lu, T Peng, W Wang, Efficient multiuser water-filling algorithm under interference temperature constraints in OFDMA-based cognitive radio networks, in *Proc IEEE International Symposium Microwave, Antenna, Propagation, and EMC Technologies for Wireless Communications* (MAPE'07, Hangzhou, China, 2007)
36. V Stavroulaki, K Tsagkaris, P Demestichas, J Gebert, M Mueck, A Schmidt, R Ferrus, O Sallent, M Filo, C Mouton, L Rakotoharison, Cognitive control channels: from concept to identification of implementation options. IEEE Commun Mag **50**(7), 96–108 (2012)
37. AA Eltholth, AR Mekhail, A Elshirbini, MI Dessouki, AI Abdelfattah, Modeling the effect of clipping and power amplifier non-linearities on OFDM systems. Ubiquitous Comput Commun J **3**(1), 54–59 (2009)
38. PHYDYAS, Physical layer for dynamic spectrum access and cognitive radio. http://www.ict-phydyas.org/. Accessed 5 June 2013
39. T Yucek, H Arslan, *Spectrum characterization for opportunistic cognitive radio systems, in Proc* (IEEE Military Communication Conference, Washington, D.C., USA, 2006)
40. R Jain, Channel Models, A Tutorial (2007). http://www.cse.wustl.edu/~jain/cse574-08/ftp/channel_model_tutorial.pdf. Accessed 5 July 2013

doi:10.1186/1687-6180-2014-68
Cite this article as: Dikmese *et al.*: **Spectrum sensing and resource allocation for multicarrier cognitive radio systems under interference and power constraints.** *EURASIP Journal on Advances in Signal Processing* 2014 **2014**:68.

PUBLICATION

3

Interference Rejection Combining for Black-Space Cognitive Radio Communications

S. Srinivasan and M. Renfors

Cognitive Radio Oriented Wireless Networks. CROWNCOM 2018.

Interference Rejection Combining for Black-Space Cognitive Radio Communications

Sudharsan Srinivasan, Markku Renfors

Laboratory of Electronics and Communications Engineering
Tampere University of Technology, Tampere, Finland
{sudharsan.srinivasan, markku.renfors}@tut.fi

Abstract. *This paper focuses on multi-antenna interference rejection combing (IRC) based black-space cognitive radio (BS-CR) operation. The idea of BS-CR is to transmit secondary user (SU) signal in the same frequency band with the primary user (PU) such that SU's power spectral density is clearly below that of the PU, and no significant interference is inflicted on the PU receivers. We develop a novel blind IRC technique which allows such operation mode for effective reuse of the PU spectrum for relatively short-distance CR communication. We assume that both the PU system and the BS-CR use orthogonal frequency division multiplexing (OFDM) waveforms with common frame structure. In this case the PU interference on the BS-CR signal is strictly flat-fading at subcarrier level. Sample covariance matrix based IRC adaptation is applied during silent gaps in CR operation. During CR transmission, the target signal detection and channel estimation utilize multiple outputs from the IRC process obtained with linearly independent steering vectors. The performance of the proposed IRC scheme is tested considering terrestrial digital TV broadcasting (DVB-T) as the primary service. The resulting interference suppression capability is evaluated with different PU interference power levels, silent gap durations, and CR device mobilities.*

Keywords: *black-space cognitive radio, underlay cr, interference rejection combining, irc, receiver diversity, ofdm, dvb-t*

1 Introduction

Cognitive radios (CRs) are designed to operate in radio environments with a high level of interference and, at the same time, produce negligible interference to the primary users (PUs) [1]-[3]. CRs have been widely studied in recent years, with main focus on opportunistic white-space operation, i.e., dynamically identifying unused spectral resources for CR operation. Also underlay CR operation has received some attention. Here the idea is to transmit in wide frequency band with low power-spectral density, typically using spread-spectrum techniques [4]. Black space CR (BS-CR), where a CR deliberately transmits simultaneously along the primary signal in the same time-frequency resources without causing objectionable interference has received limited attention [5]-[8]. In general, BS-CR can operate without need for spectrum sensing and

requires only limited spectral resources. BS-CR can make very effective reuse of spectrum over short distances.

One of the major requirements for CR operation is to minimize the interference to the primary transmission system. In BS-CR this is reached by setting the CR transmission power at a small-enough level. The most important factor that enables such a radio system is that stronger interference is easier to deal with as compared to weaker interference [9], if proper interference cancellation techniques are utilized. Previous studies from information theory provide theoretically achievable bounds for such cognitive radios [10].

The use of multiple antennas allows for spatio-temporal signal processing, which improves the detection capability of the receiver under fading multipath channel and interference. Various methods of interference cancellation can be found in [11], [12]-[16] and the references therein. For a detector to be optimum under interference, it has to be a multi-user detector [11].

Interference rejection combining (IRC) receivers do not need detailed information about the interfering signals, such as modulation order and radio channel propagation characteristics. Therefore, IRC receivers are simple compared to optimum detectors, making them desirable for CR scenarios.

IRC techniques are widely applied for mitigating co-channel interference, e.g., cellular mobile radio systems like LTE-A [17]. The use of multiple antennas in CRs has been studied earlier, e.g., in [16]. Our initial study on this topic in highly simplified scenario with suboptimal algorithms was in [18], but to the best of our knowledge, IRC has not been applied to BS-CR (or underlay CR) elsewhere. The novel elements of the scheme proposed in this paper include the following:

- The spatial channel of the interfering PU signal does not need to be explicitly estimated, while an initial IRC solution is found by calculating the sample covariance matrix during a silent gap in CR transmission.
- The channel of the target CR transmission is estimated for the maximum number of linearly independent signals from which the PU interference has been suppressed.
- The IRC weights are obtained from the channel estimates and initial IRC solution through maximum ratio combining (MRC) of the linearly independent signal set.

In this paper we consider BS-CR operation in the terrestrial TV frequency band, utilizing a channel with an on-going relatively strong TV transmission. The PU is assumed to be active continuously. If the TV channel becomes inactive, this can be easily detected by each of the CR stations in the reception mode. Then the CR system may, for example, continue operation as a spectrum sensing based CR system. In our case study, we focus on the basic scenario of IRC based multi-antenna CR receiver with co-channel interference generated by a single PU transmitter. The performance of such a system under different interference levels, timing offsets, and modulation orders is studied. Also, the effect of silent period length and CR device mobility on the performance is evaluated. The rest of the paper is organized as follows: In Section 2, the BS-SC scenario and proposed IRC scheme are explained. The system model and IRC solution are formulated in Section 3. Section 4 presents the simulation setup and performance evaluation results. Finally, concluding remarks are presented Section 5.

2 IRC-Based Black-Space Cognitive Radio Scenario

In our basic scenario, illustrated in Fig. 1, we consider a CR receiver using multiple antennas to receive data from a single-antenna cognitive transmitter. The CR operates within the frequency band of the PU, and the PU power spectral density (PSD) is very high in comparison to that of the CR. The primary transmission is assumed to be always present when the CR system is operating. The primary transmitter generates a lot of interference to the CR transmission, which operates closer to the noise floor of the primary receiver, and due to this, the primary communication link is protected. We consider frequency reuse over relatively small distances, such as an indoor CR system. The multi-antenna configuration studied here is that of single-input multiple output (SIMO). Other configurations, involving also transmit diversity in the CR link are also possible, but they are left as a topic for future studies.

Here the PU is a cyclic prefix orthogonal frequency division multiplexing (CP-OFDM) based DVB-T system [19]. The CR system is also an OFDM based multicarrier system using the same subcarrier spacing and CP length as the primary system. Thus, it has the same overall symbol duration. The CR system is assumed to be synchronized to the primary system in frequency and in quasi-synchronous manner also in time. The CP length is assumed to be sufficient to absorb the channel delay spread together with the residual offsets between the two systems observed at the CR receiver. Consequently, the subcarrier-level flat-fading circular convolution model for spatio-temporal channel effects applies to the target CR signal and to the PU interference signal as well. Then the IRC process can be applied individually for each subcarrier. Since the CR receiver observes the PU signal at very high SINR level, synchronization task is not particularly difficult and low-complexity algorithms can be utilized. Considering short-range CR scenarios, the delay spread of the CR channel has a minor effect on the overall channel delay spread to be handled in the time alignment of the two systems. Basically, if all CR stations are synchronized to the PU, they are also synchronized with each other.

Both the primary and the CR systems use QAM subcarrier modulation, but usually with different modulation orders. The received CR signal consists of contributions from both the desired CR communication signal and the primary transmission signal, the latter one constituting a strong interference. Our proposed scheme includes two phases in the CR system operation:

1. During the first phase, the CR transmission is stopped (silent gap) and the IRC process is adapted blindly to minimize the energy of combined signal during the silent period. This is done individually for each subcarrier. Since the target channel is not available during this stage, IRC solutions are found for the maximum number of linearly independent (virtual) steering vectors. During the CR reception phase, the corresponding IRC output signals are used for channel estimation and data detection. They are referred to as partial IRC signals.
2. During the second phase, the CR system is operating. The CR channel coefficients are estimated for each partial IRC signal using training symbols (containing reference symbols in all subcarriers). For data symbols, the partial

IRC signals are combined using maximum ratio combining (MRC) based on the estimated channel coefficients.

This two-phase process is straightforward to implement and it is able to track the channel fading with relatively low mobility. In future work, it is worth to consider adaptation of the IRC process without silent gaps after the first one required for the initial solution. This would help to reduce the related overhead in throughput.

No explicit channel estimation of the PU channel is required in this approach. The CR channel is estimated from the partial IRC signals, from which the PU interference has been effectively suppressed.

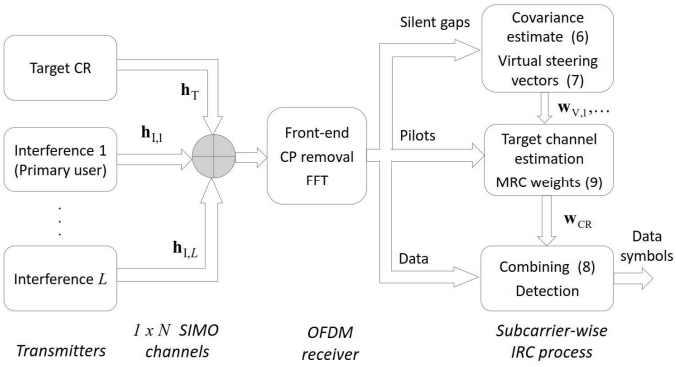

Fig. 1. Blackspace CR system model.

3 IRC for Black-Space Cognitive Radio

Following the quasi-synchronous OFDM system model explained in the previous section, the detection process at the CR receiver can be formulated at OFDM subcarrier symbol level as a flat-fading process. For the $1\times N$ SIMO antenna configuration of the CR transmission link and L interfering signals, the received signal can be expressed as

$$\mathbf{r} = \mathbf{h}_{\mathrm{T}} x_{\mathrm{T}} + \sum_{l=1}^{L} \mathbf{h}_{\mathrm{I},l}\, x_{\mathrm{I},l} + \boldsymbol{\eta}\,. \tag{1}$$

Here $\mathbf{h}_{\mathrm{T}} \in \mathbb{C}^{N\times 1}$ is the channel gain vector for the target CR transmission, $\mathbf{h}_{\mathrm{I},l} \in \mathbb{C}^{N\times 1}$ is the spatial channel from the lth interferer to the CR receiver, x_{T} and $x_{\mathrm{I},l}$ are the corresponding transmitted subcarrier symbols, and $\boldsymbol{\eta} \in \mathbb{C}^{N\times 1}$ is spatially white additive white Gaussian noise (AWGN). Naturally, during silent gaps of CR operation, the first term of (1) is missing. For detection, the signals from different antennas are weighted and combined using a linear combiner. This can be expressed as the inner product

$$y = \mathbf{w}^{\mathrm{H}}\mathbf{r}\,, \tag{2}$$

where $\mathbf{w} \in \mathbb{C}^{N\times 1}$ is the combiner weight vector, and H stands for Hermitian (complex-conjugate transpose). Finding the optimum weight vector is an optimization problem. Generally, the linear minimum mean-squared error (LMMSE) solution minimizes the mean-squared error in the target signal x_{T},

$$J = E\left[\left|x_{\mathrm{T}} - \mathbf{w}^{\mathrm{H}}\mathbf{r}\right|^2\right] . \tag{3}$$

In interference rejection combining (IRC) we assume knowledge of the covariance matrix of the interferences. If the channels from the interferers to the CR receiver antenna array are known, the noise plus interference covariance matrix can be expressed as

$$\mathbf{\Sigma}_{\mathrm{NI}} = \sum_{l=1}^{L} P_l \mathbf{h}_{\mathrm{I},l}\mathbf{h}_{\mathrm{I},l}^{\mathrm{H}} + P_{\mathrm{N}}\mathbf{I} . \tag{4}$$

Here $P_{\mathrm{I},l}$ is the power of interferer l, P_{N} is the noise power, and $\mathbf{I}$ is the identity matrix of size N. Then the well-known LMMSE solution [20] is

$$\mathbf{w} = \mathbf{\Sigma}_{\mathrm{NI}}^{-1}\mathbf{h}_{\mathrm{T}}\left(\mathbf{h}_{\mathrm{T}}^{\mathrm{H}}\mathbf{\Sigma}_{\mathrm{NI}}^{-1}\mathbf{h}_{\mathrm{T}} + 1/P_{\mathrm{T}}\right)^{-1} , \tag{5}$$

where P_{T} is the target CR signal power.

Estimating the interferer channel vector would increase the complexity of the CR receiver, even in the single interferer case of our basic scenario. In case of multiple interferers, e.g., from other BS-CR systems operating nearby, this would be quite challenging. Therefore, we use the sample covariance matrix of the received signal,

$$\bar{\mathbf{\Sigma}}_{\mathrm{NI}} = \sum_{m=1}^{M} \mathbf{r}(m)\mathbf{r}(m)^{\mathrm{H}} \tag{6}$$

during the silent gap of the CR transmission as the estimate of $\mathbf{\Sigma}_{\mathrm{NI}}$. Here m is the OFDM symbol index and M is the length of the estimation period (i.e., silent gap length) in OFDM symbols.

In the proposed scheme it is not possible to estimate the CR channel before the interference cancellation stage. Therefore, during CR operation phase 1, we carry out the IRC adaptation process for N orthogonal virtual steering vectors, resulting in N weight vectors $\mathbf{w}_{\mathrm{V},1}, \mathbf{w}_{\mathrm{V},2}, \ldots, \mathbf{w}_{\mathrm{V},N}$. We use the unit vectors $\mathbf{h}_{\mathrm{V},1} = [1,0,0,\ldots,0]^{\mathrm{T}}$, $\mathbf{h}_{\mathrm{V},2} = [0,1,0,\ldots,0]^{\mathrm{T}}, \ldots, \mathbf{h}_{\mathrm{V},N} = [0,0,0,\ldots,1]^{\mathrm{T}}$ as the virtual steering vectors for simplicity. Furthermore, instead of the scaling of (5), the weight vectors are scaled to have unit Euclidean norm,

$$\mathbf{w}_{\mathrm{V},n} = \bar{\mathbf{\Sigma}}_{\mathrm{NI}}^{-1}\mathbf{h}_{\mathrm{V},n} \Big/ \left\|\bar{\mathbf{\Sigma}}_{\mathrm{NI}}^{-1}\mathbf{h}_{\mathrm{V},n}\right\| . \tag{7}$$

This results in unit noise variance for the corresponding weighted output signals $y_n = \mathbf{w}_{\mathrm{V},n}^{\mathrm{H}}\mathbf{r}$, $n = 1,2,\ldots,N$, which is essential for the following maximum ratio combining (MRC) stage. The outputs y_n are different observations of the target signal, for

which the interference cancellation has been applied. When the number of receiver antennas is higher than the number of interference sources, there is diversity in these observations, and diversity combining can be used for enhancing the performance. Among the linear combination methods, MRC maximizes the signal to interference-plus-noise ratio of the combined signal.

During the second CR operation phase, data symbols are transmitted, along with training symbols at regular intervals. For each training symbol (containing reference symbols in all active subcarriers), the N channel coefficients $\hat{h}_{\mathrm{V},1}, \hat{h}_{\mathrm{V},2}, \ldots, \hat{h}_{\mathrm{V},N}$ are first estimated for each of the effective channels corresponding to the N observations as $\hat{h}_{\mathrm{V},n} = \mathbf{w}_{\mathrm{V},n}^{\mathrm{H}} \cdot \mathbf{r} / p$, where p is the transmitted pilot symbol value. Then the data symbol estimate is obtained by maximum ratio combining the N samples obtained by applying the virtual steering vectors,

$$\hat{d} = \mathbf{w}_{\mathrm{MRC}}^{\mathrm{H}} \cdot \left[\mathbf{w}_{\mathrm{V},1}\ \mathbf{w}_{\mathrm{V},2} \cdots \mathbf{w}_{\mathrm{V},N} \right]^{\mathrm{H}} \cdot \mathbf{r} \quad , \tag{8}$$

where the MRC weights are given by

$$\mathbf{w}_{\mathrm{MRC}} = [\hat{h}_{\mathrm{V},1} \hat{h}_{\mathrm{V},2} \ldots \hat{h}_{\mathrm{V},N}]^{\mathrm{T}} \Big/ \sqrt{\sum_{k=1}^{N} \left| \hat{h}_{\mathrm{V},k} \right|^2} \quad . \tag{9}$$

The effective weight vector becomes

$$\begin{aligned} \mathbf{w}_{\mathrm{CR}} &= \left[\mathbf{w}_{\mathrm{V},1}\ \mathbf{w}_{\mathrm{V},2} \cdots \mathbf{w}_{\mathrm{V},N} \right] \cdot \mathbf{w}_{\mathrm{MRC}} \\ &= \sum_{n=1}^{N} \hat{h}_{\mathrm{V},n} \mathbf{w}_{\mathrm{V},n} \Big/ \sqrt{\sum_{k=1}^{N} \left| \hat{h}_{\mathrm{V},k} \right|^2} \, . \end{aligned} \tag{10}$$

We can see that for data symbol detection with stationary channels, we just need to calculate and use this weight vector, instead of applying the MRC weights on the samples obtained by the weight vectors $\mathbf{w}_{\mathrm{V},n}$.

This model indicates various options for dealing with channel fading. Generally, the PU channel should not vary significantly between the silent periods. The most critical scenario in this respect is a moving CR receiver, which causes also the PU channel to be time varying. Due to the strong PU interference, the interference cancellation process is sensitive to the resulting errors in the channel covariance estimate. For slowly-fading CR channels, it is enough to calculate the effective weights for each training symbol and use the same weights until the next training symbol. With higher mobility, the effective weights can be interpolated between consecutive training symbols. The effect of mobility is investigated through simulations in the following section.

4 Performance Evaluation

The simulations are carried out for the system setup explained in Section 2. The carrier frequencies of CR and PU are the same and it is here set to 700 MHz, which is close to the upper edge of the terrestrial TV frequency band. The modulation order used by CR

varies between 4QAM, 16QAM, and 64QAM. The pilot symbols are binary and have the same power level as the data symbols. The primary transmitter signal follows the DVB-T model with 16QAM modulation, 8 MHz bandwidth, and CP length of 1/8 times the useful symbol duration, i.e., 28 μs. The IFFT/FFT length is 2048 for both systems. The DVB-T and CR systems use 1705 and 1200 active subcarriers, respectively. ITU-R Vehicular A channel model (about 2.5 μs delay spread) is used for the CR system and Hilly Terrain channel model (about 18 μs delay spread) for PU transmission. The CR receiver is assumed to have four antennas, and uncorrelated 1x4 SIMO configurations are used for both the primary signal and the CR signal.

The number of spatial channel realizations simulated in these experiments is 500. The ratio of CR and PU signal power levels at the CR receiver (referred to as the signal to interference ratio, SIR) is varied. The lengths of the OFDM symbol frame and silent gap for interference covariance matrix estimation are also varied (expressed in terms of CP-OFDM symbol durations). The training symbol spacing is 8 OFDM symbols, and the frame length is selected in such a way that training symbols appear as the first and last symbol of each frame, along with other positions. Channel estimation uses linear interpolation between the training symbols.

Fig. 2 shows a basic bit error-rate (BER) vs. SNR simulation result with 4QAM (QPSK) and 64QAM modulations and SIR values of -10, -20, and -30 dB. Also the interference-free baseline case (SIR=100 dB) is included. The CR block length is 41 OFDM symbols (6 training symbols and 35 data symbols), and the interference covariance estimation is based on a silent gap of 32 OFDM symbols. In this case, the interference covariance estimate is very good, and IRC performs very well. The effect of the interference power is relatively small: reducing the SIR from -10 dB to -30 dB, the performace loss at 1 % BER level is about 0.6 dB for QPSK and about 1.7 dB for 64QAM. When comparing the BS-CR performance with the interference-free case, the loss is about 3.5 dB for both QPSK and 64QAM at 1 % BER level and -30 dB SIR.

Next we consider the performance with slowly-fading channels. It was found also experimentally that the case where the CR transmitter is moving but CR receiver is stationary is much easier to handle, because the interference covariance matrix is stationary as long as the PU and CR receiver are stationary. Therefore, we focus on the case where the CR receiver is moving, while the CR transmitter is stationary, and both the target CR channel and the interference are fading with the same mobility, 3 km/h. Figs. 3 and 4 show both the effect of the silent gap length and the OFDM frame length on the performance. We can notice that by placing the silent gap in the middle of the frame and using the interference covariance estimate for detecting both the preceding and following OFDM symbols, the CR frame length could be doubled without performance loss. However, this is not assumed in Figs. 3 and 4, because it would require extensive data buffering on the receiver side. In this simulation set-up, the best length for the silent gap is about 32 OFDM symbols. Generally, while acceptable CR link performance can still be achieved, significant performance loss is observed with respect to the stationary case. Also the feasible CR frame length is rather limited, leading to relatively high overhead due to the silent gaps. The performace loss with 3 km/h mobility is about 4.7 dB and 10 dB with the the frame lengths of 17 and 41 OFDM symbols, respectively, compared to the stationary case.

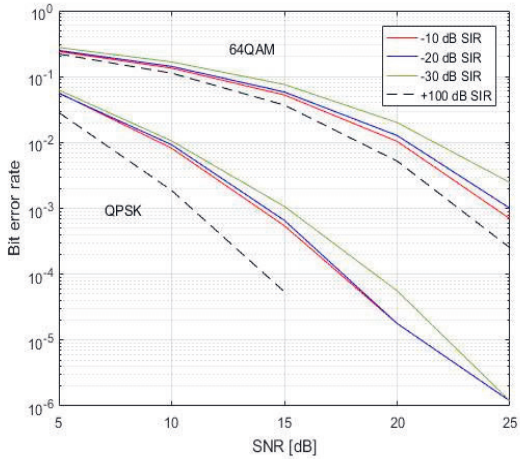

Fig. 2. Performance QPSK and 64QAM systems with stationary channel, silent gap duration of 32 symbols, and OFDM frame length of 41 symbols.

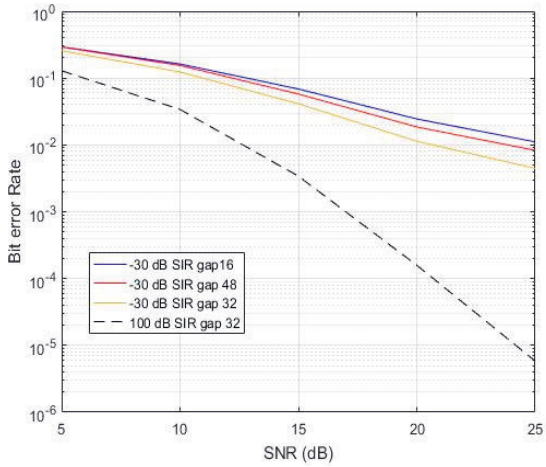

Fig. 3. Performance of a 16QAM system with 3 km/h mobility, 700 MHz carrier frequency, OFDM frame length of 17 symbols, with various gaps and SIR= -30 dB.

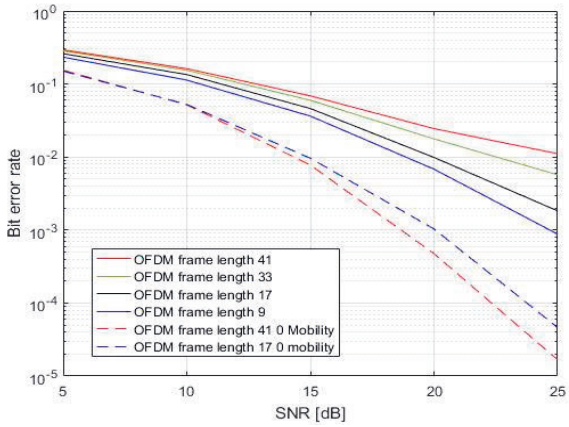

Fig. 4. Performance for a 16QAM system with 3 km/h mobility, 700 MHz carrier frequency, silent gap of 32 symbols, and SIR= -30 dB.

5 Conclusion

The performance of cognitive transmission links in the presence of strong interferences in the black-space CR scenario was investigated. The interference rejection capability of IRC using multiple receive antennas for various modulation orders was studied. It was found that the IRC performs very well in the basic SIMO-type BS-CR scenario when stationary channel model is applicable, e.g., in fixed wireless broadband scenarios. However, the scheme is rather sensitive to the fading of the PU channel. Due to the strong interference level, the interference cancellation process is affected by relatively small errors in the covariance matrix estimate. For covariance estimation, the silent gap length should be in the order of 32 OFDM symbols, and the CR OFDM frame length should be of the same order or less, even with 3 km/h mobility. This leads to high overhead due to the silent gaps.

In future work, it is worth to consider adaptation of the IRC process without silent gaps after the first one required for the initial solution. This would help to reduce the related overhead in throughput. One possible approach is to do this in a decision-directed manner: first estimating the covariance matrix in the presence of the target signal and then cancelling its effect based on detected symbols and estimated target channel.

In the basic TV black-space scenario, there is only one strong TV signal present in the channel, in agreement with our assumption about the primary interference sources. DVB-T system allows also single-frequency network (SFN) operation and the use of repeaters to improve local coverage. In both cases, the primary transmissions can be seen as a single transmission, with a spatial channel that depends on the specific transmission scenario, and the proposed scheme is still applicable.

The scheme can also be extended to scenarios where multiple CR systems are operating in the same region. If all CR systems are time-synchronized to the PU and they are at a relatively small distance from each other, they are also synchronized with each other, and could be handled by the IRC process as an additional interference source following the model of Eq. (1). In future studies, also the effect of antenna correlation will be taken into consideration. The complexity reduction of the IRC receiver with larger number of antennas is also an interesting topic for further studies.

References

1. T. Yucek and H. Arslan, "A Survey of Spectrum Sensing Algorithms for Cognitive Radio Applications," *IEEE Comm. Surveys & Tutorials,* vol. 11, no. 1, pp. 116-129, 2009.
2. Y.C. Liang, A. T. Hoang Y. Zeng, and R. Zhang, "A Review on Spectrum Sensing for Cognitive Radio: Challenges and Solutions," *EURASIP Journal on Advances in Signal Processing*, pp. 1-15, January 2010.
3. S. Dikmese, S. Srinivasan, M. Shaat, F. Bader and M. Renfors, "Spectrum Sensing and Resource Allocation for Multicarrier Cognitive Radio Systems under Interference and Power constraints", *EURASIP Journal on Advances in Signal Processing*, 2014:68.
4. A. M. Wyglinski et al, *Cognitive Radio Communications and Networks: Principles and Practice,* Academic Press, 2010.
5. Y. Selén, R. Baldemair and J. Sachs, "A short feasibility study of a cognitive TV black space system," *in Proc. IEEE PIMRC 2011*, Toronto, ON, 2011, pp. 520-524.
6. A. Rico-Alvariño and C. Mosquera, "Overlay spectrum reuse in a broadcast network: Covering the whole grayscale of spaces," in *Proc. IEEE* DySPAN 2012, WA, 2012, pp. 479-488.
7. Z. Wei, Z. Feng, Q. Zhang and W. Li, "Three Regions for Space–Time Spectrum Sensing and Access in Cognitive Radio Networks," *IEEE Transactions on Vehicular Technology*, vol. 64, no. 6, pp. 2448-2462, June 2015.
8. Y. Beyene, K. Ruttik, R. Jantti, "Effect of secondary transmission on primary pilot carriers in overlay cognitive radios," in *Proc. CROWNCOM2013*, Washington, DC, 2013, pp. 111-116.
9. A.B. Carleial, "A Case Where Interference Does Not Reduce Capacity," *IEEE Trans. Information Theory*, 01/1975.
10. N. Devroye, P. Mitran, and V. Tarokh "Achievable rates in Cognitive Radio Channels" *IEEE Transactions on Information Theory*, vol. 52, pp. 1813 – 1827, May 2006.
11. S. Verdu, *Multiuser Detection*, Cambridge: Cambridge University Press, 1998.
12. J. Winters, "Optimum Combining in Digital Mobile Radio with Cochannel Interference," IEEE transaction on Vehicular Technology, vol 2, Issue 4, August-1984.
13. J. Liaster, J. and Reed, "Interference Rejection in digital Wireless Communication," *IEEE signal Processing Magazine*, vol 14, Issue 3, May 1997
14. G. Klang, "On Interference Rejection in Wireless Multichannel Systems," PhD Thesis, KTH, Stockholm, Sweden, 2003.
15. M.A. Beach et al, "Study into the Application of Interference Cancellation Techniques", Roke Manor Research Report 72/06/R/036/U, April 2006.
16. O. Bakr, M. Johnson, R. Mudumbai, K. Ramchandran, Multi-Antenna Interference Cancellation Techniques for Cognitive Radio Applications, in Proc. IEEE WCNC, 2009.
17. C. C. Cheng, S. Sezginer, H. Sari and Y. T. Su, "Linear Interference Suppression With Covariance Mismatches in MIMO-OFDM Systems," in *IEEE Transactions on Wireless Communications*, vol. 13, pp. 7086-7097, Dec. 2014.
18. S. Srinivasan, S. Dikmese, D. Menegazzo, and M. Renfors, "Multi-Antenna Interference Cancellation for Black Space Cognitive Radio Communications," *2015 IEEE Globecom Workshops*, San Diego, CA, 2015, pp. 1-6.
19. U. Ladebusch and C. A. Liss, "Terrestrial DVB (DVB-T): A Broadcast Technology for Stationary Portable and Mobile Use," in *Proceedings of the IEEE*, vol. 94, no. 1, pp. 183-193, Jan. 2006.
20. S. Haykin, *Adaptive Filter theory*, Fourth Edition, Prentice-Hall, 2001.

PUBLICATION

4

Enhanced Interpolation-based Interference Rejection Combining for Black-space Cognitive Radio in Time-varying Channels

S. Srinivasan, S. Dikmese and M. Renfors

EURASIP Journal on. Wireless Communication Network 2020, 238 (2020).

Srinivasan *et al. J Wireless Com Network (2020) 2020:238*
https://doi.org/10.1186/s13638-020-01840-z

EURASIP Journal on Wireless Communications and Networking

RESEARCH **Open Access**

Enhanced interpolation-based interference rejection combining for black-space cognitive radio in time-varying channels

Sudharsan Srinivasan*, Sener Dikmese and Markku Renfors

*Correspondence:
sudharsan.srinivasan@tuni.fi
Electrical Engineering, Faculty of Information and Communication Sciences, Tampere University, Tampere, Finland

Abstract

In this paper, we investigate multi-antenna interference rejection combing (IRC)-based black-space cognitive radio (BS-CR) operation in time-varying channels. The idea of BS-CR is to transmit secondary user (SU) signal in the same frequency band with the primary user (PU) such that SU's power spectral density is clearly below that of the PU, and no significant interference is inflicted on the PU receivers. We explore the effects of interpolation and mobility on the novel blind IRC technique which allows such operation mode for effective reuse of the PU spectrum for relatively short-distance CR communication. We assume that both the PU system and the BS-CR use orthogonal frequency division multiplexing (OFDM) waveforms with common numerology. In this case, the PU interference on the BS-CR signal is strictly flat-fading at subcarrier level. Sample covariance matrix-based IRC adaptation is applied during silent gaps in CR operation. We evaluate the effect of the gap length on the link performance, using known PU channel-based interference covariance estimation as reference. We also propose an interpolation-based scheme for tracking the spatial covariance in time-varying channels, demonstrating significantly improved robustness compared to the earlier scheme. The performance of the proposed IRC scheme is tested considering terrestrial digital TV broadcasting (DVB-T) as the primary service. Also joint PU and co-channel CR interference cancellation is included in the study. The resulting interference suppression capability is evaluated with different PU interference power levels, silent gap durations, data block lengths, and CR device mobilities.

Keywords: Black-space cognitive radio, Underlay CR, IRC, Interference rejection combining, Multi-antenna system, Receiver diversity, Mobility, OFDM, DVB-T

1 Introduction

Cognitive radios (CRs) are intended to operate in radio environments with a high level of interference and, simultaneously, produce negligible interference to the primary users (PUs) [1–3]. CR studies in the past have been focusing on opportunistic white-space scenarios where the unused spectrum is dynamically identified and used. Also underlay CR operation has received some attention. Here the idea is to transmit in wide frequency band with low power-spectral density, typically using spread-spectrum techniques [4]. Black-space CR (BS-CR), where a CR deliberately transmits simultaneously along the

primary signal in the same time–frequency resources without causing objectionable interference, has received limited attention [5–8]. An underlay CR is ignorant about the existence of PUs in its frequency band. Commonly, it uses very low power spectral density and wide bandwidth, such that it does not cause interference to the PU transmission under any conditions [4]. BS-CR adapts its waveform and signal parameters depending on the ongoing PU transmissions and uses advanced signal processing techniques on the receiver side to facilitate low signal-to-interference ratio (SIR) at the receiver. BS-CR systems effectively reuse the spectrum for communication over short distances. It can operate with limited spectrum resources and can be used without any additional spectrum sensing.

As discussed in our previous papers [9, 10], one of the major requirements for CR operation is to minimize the interference to the primary transmission system. In BS-CR, this is reached by setting the CR transmission power at a small-enough level. The most important factor that enables such a radio system is that stronger interference is easier to deal with as compared to weaker interference [11], if proper interference cancellation techniques are utilized. Previous studies from information theory provide theoretically achievable bounds for such cognitive radios [12]. Multi-antenna systems allow for spatiotemporal signal processing, which do not only improve the detection capability of the receiver but also improve performance in fading multipath channels with interference. Various methods of interference cancellation can be found in [13, 14-18] and the references therein. All other detection algorithms except the multi-user detector perform sub-optimally [13].

The interference rejection combining (IRC) receivers have the significant advantage in comparison with the other receivers in multi-user scenarios that they do not need detailed information about the interfering signals, such as modulation order and radio channel propagation characteristics. For CR scenarios, IRC receivers in general are simple and desirable compared to optimum detectors. IRC techniques are widely applied for mitigating co-channel interference, e.g., in cellular mobile radio systems like LTE-A [19]. The use of multiple antennas in CRs has been studied earlier, e.g., in [18]. Our initial study on this topic in highly simplified scenario with suboptimal algorithms was in [20], but to the best of our knowledge, IRC has not been applied to BS-CR (or underlay CR) elsewhere. In this current study, we develop the ideas that we presented in [9] under more practical situations and study the performance of our algorithms in more details. Notably, the scheme studied in [9] was found to be very sensitive to mobility, because its performance is critically affected by errors in spatial covariance estimation. In this work, we extent our previous studies on the effects of mobility and propose a scheme to improve the quality of the covariance estimation with time-varying channels using interpolation between sample covariance-based estimates.

In this paper, we consider BS-CR operation in the terrestrial TV frequency band, utilizing a channel with an ongoing relatively strong TV transmission. The PU is assumed to be active continuously. If the TV channel becomes inactive, this can be easily detected by each of the CR stations in the reception mode. Then the CR system may, for example, continue operation as a spectrum sensing-based CR system. In our case study, we focus on a scenario with multi-antenna CR receiver having IRC capability to mitigate co-channel interference generated by a single PU transmitter and multiple independent

(uncoordinated) CR systems. Generally, interference covariance matrix estimation is a key element of IRC schemes. For this purpose, we propose to use sample covariance calculated from the received signal during silent periods (gaps) in the target CR transmission. More specifically, the contributions of this paper are listed below:

- This paper extends and refines our earlier studies in papers [9, 10] on IRC schemes operating under severe interference conditions, with applications in BS-CR.
- Under such conditions, the direct estimation of the target CR channel is not possible. After estimating the interference covariance matrix during silent gaps in the target CR transmission, our scheme extracts from the received signal a set of signals which span the interference-free subspace in spatial domain. The weight vector for the target CR signal is based on pilot-based target channel estimation in this subspace.
- In BS-CR scenarios, the target CR link performance is very sensitive to the quality of the interference covariance estimate. Therefore, we propose to use linear interpolation of the interference covariance matrix to track the channel variations between consecutive interference covariance estimates, i.e., consecutive silent gaps.
- Our case study focuses on a TV whitespace (TVWS) scenario. We consider a multi-antenna CR receiver having IRC capability to mitigate co-channel interference generated by a single PU transmitter and multiple independent (uncoordinated) CR systems. The performance of such a system under different interference levels, mobilities, silent gap lengths, frame structures, and modulation orders is studied, and the improved robustness obtained through covariance interpolation is highlighted

The rest of the paper is organized as follows: In Sect. 2, the BS-SC scenario and proposed IRC scheme are first explained. Then also the connections between the signal-to-interference ratios (SIRs) at the PU and CR receivers are analyzed based on the channel losses of the target and interference links. The system model and IRC process are formulated in Sect. 3. Section 4 presents the simulation setup and performance evaluation results. Finally, concluding remarks are presented in Sect. 5.

2 IRC-based black-space cognitive radio scenario—scenario and methods

In our basic scenario, illustrated in Fig. 1, we consider a CR receiver using multiple antennas to receive data from a single-antenna cognitive transmitter. The details of the receiver signal processing indicated in the figure are explained in Sect. 3. The CR operates within the frequency band of the PU, and the PU power spectral density (PSD) is very high in comparison with that of the CR. The primary transmission is assumed to be always present when the CR system is operating. The primary transmitter generates a lot of interference to the CR transmission, which operates closer to the noise floor of the primary receiver, and due to this, the primary communication link is protected. We consider frequency reuse over relatively small distances, such as an indoor CR system. The multi-antenna configuration studied here is that of single-input multiple output (SIMO). Other configurations, involving also transmit diversity in the CR link, are also possible, but they are left as a topic for future studies.

Here the PU is a cyclic prefix orthogonal frequency division multiplexing (CP-OFDM)-based DVB-T system [21]. The CR system is also an OFDM-based multi-carrier

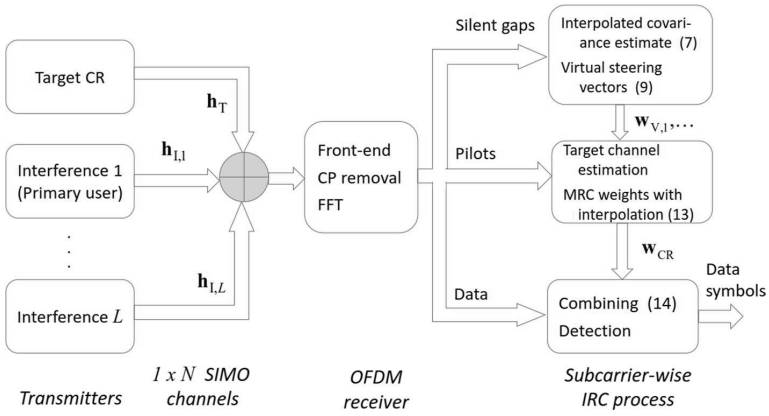

Fig. 1 Black-space CR system model with silent gap interpolation. The receiver signal processing-related equation numbers are indicated

system using the same subcarrier spacing and CP length as the primary system. Thus, it has the same overall symbol duration. The CR receiver is assumed to be synchronized to the primary system in frequency and in quasi-synchronous manner also in time. The CP length is assumed to be sufficient to absorb the channel delay spread together with the residual timing offsets between the two systems observed at the CR receiver. Consequently, the subcarrier-level flat-fading circular convolution model for spatiotemporal channel effects applies to the target CR signal and to the PU interference signal as well. Then the IRC process can be applied individually for each subcarrier. Since the CR receiver observes the PU signal at very high SINR level, synchronization task is not particularly difficult and low-complexity algorithms can be utilized. Considering short-range CR scenarios, the delay spread of the CR channel has a minor effect on the overall channel delay spread to be handled in the time alignment of the two systems. The same applies to the possible significant co-channel CR interferers, which are assumed to be at relatively short distance from the target CR system.

Basically, if all target and interfering CR stations are synchronized to their respective observed PU signals, they are also synchronized with each other in the quasi-synchronous manner, such that all multi-path components of all signals are within the CP length.

In addition to these, we assume that the secondary user experiences slow (e.g., pedestrian) mobility effects, due to either the mobility of devices or people moving around them. The effects of mobility on the CR system performance are evaluated in this study.

Both the primary and the CR systems use QAM subcarrier modulation, but usually with different modulation orders. The frame structures and pilot patterns of the PU and CR are independent. The received CR signal consists of contributions from the desired CR communication signal, co-channel CR interferers, and the primary transmission signal, the latter one constituting the dominating interference. Our proposed scheme includes two phases in the CR system operation as described in our previous work [9]. The spatial characteristics of the PU interference are modeled using multi-antenna sample covariance matrix, which is estimated during silent gaps in the target

CR transmission, independently for each active subcarrier. No explicit channel estimation of the PU channel is required. The CR channel is estimated from the partial IRC signals, from which the PU and other CR interferences have been effectively suppressed.

2.1 Methods

In this work, we study how channel fading with mobility affects the performance in the scenario described above. We consider adaptation of the IRC process using interpolation of the sample covariance matrices between the silent gaps. This is expected to improve the performance, allowing to increase the data block length between silent gaps, thus reducing the related overhead in throughput. The main elements of the scheme, covariance estimation and interpolation, IRC process, channel estimation [22], and MRC-based detection are formulated mathematically. Numerical performance results are obtained through Monte Carlo simulations based on a developed Matlab script, using a semi-analytical model based on PU channel knowledge as reference.

2.2 SIR analysis

Key parameters in BS-CR operation are the SIRs at the CR receiver and PU receiver. In the basic scenario with PU interference only, the SIRs can be expressed in dB units as follows:

$$SIR_{\mathrm{CR}} = (P_{\mathrm{CR}} - L_{\mathrm{CR-CR}}) - (P_{\mathrm{PU}} - L_{\mathrm{PU-CR}}) \tag{1}$$

$$SIR_{\mathrm{PU}} = (P_{\mathrm{PU}} - L_{\mathrm{PU-PU}}) - (P_{\mathrm{CR}} - L_{\mathrm{CR-PU}}), \tag{2}$$

where P_{CR} and P_{PU} are the transmission powers of CR and PU, respectively, in dBm units, while the other parameters are transmission losses in dB units of relevant transmission links. The first part of the subscript indicates the transmitter, and second part the receiver of the corresponding link. From these equations, it is easy to derive the maximum SIR of the CR receiver in terms of the minimum SIR of a PU receiver, $SIR_{\mathrm{PU,min}}$:

$$SIR_{\mathrm{CR,max}} = (L_{\mathrm{CR-PU}} - L_{\mathrm{CR-CR}}) + (L_{\mathrm{PU-CR}} - L_{\mathrm{PU-PU}}) - SIR_{\mathrm{PU,min}}. \tag{3}$$

The maximum SIR of the CR link depends on the differences of the channel losses from CR TX to both receivers and from PU TX to both receivers. For example, if the losses of the main links (CR-CR and PU–PU) are equal to the losses of the corresponding interfering links (CR-PU and PU-CR), then the CR RX would be able to operate with the SIR of $-SIR_{\mathrm{PU,min}}$. If the main link losses are lower than those of the interference links, the $SIR_{\mathrm{CR,max}}$ would be higher. The critical cases are:

1. If the losses of the main links (CR-CR and PU–PU) are much higher than the losses of the corresponding interfering links (CR-PU and PU-CR), then SIR of the CR receiver may be limited by the minimum acceptable PU SIR to a highly negative value. Then the SIR of the CR receiver may be limited to a highly negative value by the maximum transmit power of the CR device, which could be much lower than that of the PU transmitter.
2. If the PU transmitter is very close to the (short-range) CR system, then

$$SIR_{\mathrm{CR,max}} = P_{\mathrm{CR,max}} - L_{\mathrm{CR-CR}} - (P_{\mathrm{PU}} - L_{\mathrm{PU-CR}}). \quad (4)$$

Then the SIR of the CR receiver may be limited to a highly negative value by the maximum transmit power of the CR device, which could be much lower than that of the PU transmitter.

In both cases, the performance of the IRC scheme would be limited by the RF imperfections (e.g., receiver nonlinearity effects) in practice. The latter limitation appears especially in the TVWS application, but in rather limited geographical regions. Considering the first kind of limitation in the worst-case scenario, one should consider the hidden node margin (typically around 25–30 dB in the TVWS case [23] for the loss difference from PU ($L_{\mathrm{PU-PU}} - L_{\mathrm{PU-CR}}$), which would lead to very low SIR for the CR TX, unless the loss from the CR to the PU RX can be guaranteed to be much lower than that of the CR link. On the other hand, in short-range CR communication, especially if PU receivers use directive (possibly roof-top) antennas, the mentioned case where the SIR of CR RX is no less than $-SIR_{\mathrm{PU,min}}$ should be possible.

Generally, the CR TX should have knowledge of the link losses in order to maximize its transmission power while not causing excessive interference to the PU link. This paper focuses on the physical layer capabilities of IRC-based BS-CR, and detailed procedures for controlling the CR operation remain as a topic for future studies. One possible way to enhance BS-CR operation would be cooperative spectrum sensing of CR devices to reliably estimate the PU power level in the CR operation region.

3 IRC for black-space cognitive radio

Based on the OFDM model mentioned above, subcarrier-wise detection is considered with flat-fading channel coefficients to get rid of the challenge of frequency selectivity in the IRC process.

In the SIMO configuration, the CR is assumed to have N receiver antennas and L different interference sources are assumed. Based on this model, the signal received by the CR can be formulated for each active subcarrier as follows:

$$\mathbf{r} = \mathbf{h}_{\mathrm{T}} x_{\mathrm{T}} + \sum_{l=1}^{L} \mathbf{h}_{\mathrm{I},l} x_{\mathrm{I},l} + \boldsymbol{\eta}. \quad (4)$$

Here x_T is a transmitted subcarrier symbol and $\mathbf{h}_{\mathrm{T}} = [h_{\mathrm{T},1}, h_{\mathrm{T},2}, \ldots, h_{\mathrm{T},N}]^{\mathrm{T}}$ is the target channel vector with N receiver antennas in the CR, $x_{I,l}$ is the lth interfering signal, and $\mathbf{h}_{\mathrm{I,l}} = \left[h_{\mathrm{I,l},1}, h_{\mathrm{I,l},2}, \ldots, h_{\mathrm{I,l},N}\right]^{\mathrm{T}}$ is the channel vector for the lth interferer. The channel vectors consist of the complex channel gains from the corresponding transmit antenna to nth antenna of the CR receiver. Finally, $\boldsymbol{\eta}$ is the additive white Gaussian noise (AWGN) vector. In this generic system model, it is assumed that the PU is the dominant interferer, and the other interference sources are other CR systems introducing co-channel interference at relatively low power level.

3.1 Covariance matrix estimation

As it is illustrated in Fig. 1, the interference minimizing IRC weights are obtained during a silent period in the target CR transmission, while the co-channel interference sources are active. Due to that, Eq. (4) can be modified during silent gaps of CR operation as

$$\hat{\mathbf{r}} = \sum_{l=1}^{L} \mathbf{h}_{\mathrm{I},l} x_{I,l} + \boldsymbol{\eta}. \tag{5}$$

Here it is assumed that only interferences and noise are present during the silent period in the signal $\hat{\mathbf{r}}$ observed by the CR. Linear combiner is used for the signals from different antennas with a weight process in detection as follows:

$$y = \mathbf{w}^{\mathrm{H}}\mathbf{r}, \tag{6}$$

where y is the detected signal, $\mathbf{w}$ is the weight vector with N elements, and superscript H denotes the Hermitian (complex-conjugate transpose).

Determining the optimum weight values is an optimization problem which can be solved with the linear minimum mean-squared error (LMMSE) criterion [21, 22] that aims to minimize the mean-squared error with respect to the target signal x_T,

$$J = E\left[\left|x_{\mathrm{T}} - \mathbf{w}^{\mathrm{H}}\mathbf{r}\right|^2\right]. \tag{7}$$

When knowledge of the covariance matrix is available, IRC can be applied. Two cases are considered below: (i) calculating interference covariance from known channel coefficients and (ii) sample covariance-based approaches.

3.2 Perfect channel information case

The deterministic known channel case (with perfect channel information) is considered as the theoretical bound in this study. Assuming that the channel vectors form the interferers are perfectly known, the noise plus interference covariance matrix can be calculated for each subcarrier as

$$\boldsymbol{\Sigma}_{\mathrm{NI}} = \sum_{l=1}^{L} P_l \mathbf{h}_{\mathrm{I},l} \mathbf{h}_{\mathrm{I},l}^{\mathrm{H}} + P_{\mathrm{N}}\mathbf{I}, \tag{8}$$

where P_l is the variance of interferer l at the transmitter, P_{N} is the noise variance that can be obtained from the SNR, and $\mathbf{I}$ is the identity matrix of size *NxN*. Assuming that also the channel vector for the target signal is known and the target and interfering signals are Gaussian and statistically independent from each other, the conventional LMMSE solution for the weight vector is [15]

$$\mathbf{w} = \boldsymbol{\Sigma}_{\mathrm{NI}}^{-1}\mathbf{h}_{\mathrm{T}}\left(\mathbf{h}_{\mathrm{T}}^{\mathrm{H}}\boldsymbol{\Sigma}_{\mathrm{NI}}^{-1}\mathbf{h}_{\mathrm{T}} + \frac{1}{P_{\mathrm{T}}}\right)^{-1} \tag{9}$$

where P_{T} is the target CR transmitters signal power and unit noise variance is assumed.

In the BS-CR scenario with a single dominant interferer, the estimation of the PU channel is relatively straightforward if the CR knows PUs pilot structure. However, in the case of multiple interferers, the channel vectors of all interferers should be estimated, which becomes quite challenging. Furthermore, the target channel cannot be estimated before the interference cancellation. Therefore, the perfect channel information case serves mainly as an ideal reference in performance comparisons, as will be seen in Sect. 4.

3.3 Sample covariance-based case without PU channel information

The IRC process starts from interference covariance matrix estimation during silent gaps in the receiver. It is difficult to have the perfect channel state information on the CR receiver side. Alternatively, the joint interference and noise covariance matrix can be estimated for each subcarrier by the sample covariance matrix of the corresponding received subcarrier signal (after CP removal and FFT) in the absence of the target transmission, i.e., during the silent gaps as.

$$\overline{\Sigma}_{\mathrm{NI}} = \frac{1}{M} \sum_{m=1}^{M} \mathbf{r}(m)\mathbf{r}(m)^{H}. \tag{10}$$

Here m is the OFDM symbol index and M is the observation length in subcarrier samples, which is chosen equal to the length of the silent gap.

3.4 Linear interpolation for interference covariance tracking with mobility

Regarding the mobility aspects, there are significant differences in the effects of PU transmitter mobility, CR transmitter mobility, and CR receiver mobility. If the PU transmitter is stationery and CR receiver is stationary, the mobility of CR transmitter is easier to handle, because the dominating PU interference is stationary, and the variations in the noise and interference covariance matrix are only due to the co-channel CR interferes. However, even in this case, radio environment of the CR receiver may vary due to movement of people or vehicles nearby. Therefore, some tolerance to mobility is required also in such scenarios, at least with pedestrian mobilities. The mobility of PU transmitter or CR receiver makes the dominant interference time-varying, and in the BS-CR scenario, the CR link performance is very sensitive to quality of the PU interference covariance matrix estimate. Therefore, it is important to investigate these mobility effects and consider enhanced schemes for tracking the interference covariance with mobility.

While considering the sample covariance-based approach, increased observation (silent gap) length gives better PU interference covariance estimate in the stationary case or with low mobility. However, the channel variations during the silent gap affect critically the quality of the PU interference covariance matrix. Therefore, the optimum length of the silent gap (i.e., observation length) depends on the mobility, i.e., Doppler spread. Then we apply linear interpolation for the covariance matrix elements when calculating the weight vectors for the data symbols between two consecutive silent gaps.

There are two key parameters in this process, the silent gap length and the data block length between two consecutive gaps. Increasing the gap length improves the performance with low mobility but degrades the performance with higher mobility and

increases the overhead in throughput. Increasing the data block length increases the throughput but degrades the performance with mobility. These tradeoffs are investigated through simulations in Sect. 4 of this paper.

3.5 IRC process

As indicated in the model shown in Fig. 1, the CR channel cannot be estimated before the step of the interference cancellation, and the optimal steering vector for IRC cannot be directly calculated. Here we develop an IRC scheme which utilizes N orthogonal virtual steering vectors in the receiver's internal channel estimation process, which is based on pilot symbol structures typically used in OFDM systems. Actually, N-L vectors would be enough since IRC consumes L degrees of freedom. But this way the model is more straightforward and the IRC process is generic and robust since there is no need to estimate the number of interferers. Without loss of generality and for simplified computations, the following unit vectors are applied as the virtual steering vectors,

$$\begin{aligned} &\mathbf{h}_{\mathrm{V},1} = [1,0,0,0,\ldots,0]^T \\ &\mathbf{h}_{\mathrm{V},2} = [0,1,0,0,\ldots,0]^T \\ &\ldots \\ &\mathbf{h}_{\mathrm{V},N} = [0,0,0,0,\ldots,1]^T. \end{aligned} \tag{11}$$

Basically, the weight vectors obtained when applying the virtual steering vectors for $\mathbf{w}$ in Eq. (9) span the interference-free subspace in spatial domain. Assuming that the interference covariance is correctly estimated, using any linear combination $\mathbf{h}$ of these vectors instead of $\mathbf{h}_{\mathrm{T}}$ in (9) provides interference cancellation and maximizes signal power for the spatial CR channel h. The following process finds the combination of the virtual steering vectors for the actual target signal by first estimating the spatial channel vectors corresponding to the different virtual steering vectors. The obtained weight vectors are as follows:

$$\mathbf{w}_{\mathrm{V},n} = \overline{\Sigma}_{\mathrm{NI}}^{-1}\mathbf{h}_{\mathrm{V},n}. \tag{12}$$

It should be noted that the denominator of Eq. (9) is a complex scaling coefficient, which will be included in the MRC weights.

3.6 Target channel estimation with linear interpolation and MRC combining

In the second stage, data symbols of the CR link are transmitted together with the training/pilot symbols. While receiving pilot symbols, the weighted output signals corresponding to each virtual steering vector are calculated as

$$y_n = \mathbf{w}_{\mathrm{V},n}^{\mathrm{H}}\mathbf{r}, \quad n = 1,2,\ldots,N. \tag{13}$$

The IRC process cancels the interference from all of the weighted output signals, y_n corresponding to different virtual steering vectors. For each subcarrier, the N channel coefficients for each of the weighted output signals can be estimated using the pilot symbols as follows:

$$\hat{g}_{\mathrm{V},n} = \frac{y_n}{p} = \frac{\mathbf{w}_{\mathrm{V},n}^{\mathrm{H}} \cdot \mathbf{r}}{p},\ n = 1, 2, \ldots, N, \tag{15}$$

where p is the transmitted pilot symbol value.

3.7 Linear interpolation for channel estimation

In the traditional pilot-based channel estimation process, it is required to use efficient interpolation techniques, such as Wiener interpolation, based on the channel information at pilot sub-carrier symbols. For simplicity and to avoid excessive received signal buffering over high number of OFDM symbols, we apply linear interpolation. The performance of linear interpolation technique is better than the piecewise-constant interpolation methods [24, 25]. In the simulation studies of Sect. 4, a basic training symbol scheme is assumed where training symbols contain pilots in all active subcarriers, and the interpolation is done in time domain only, between two consecutive pilots in each subcarrier.

The MRC weights for a data symbol are then calculated as

$$\mathbf{w}_{\mathrm{MRC}} = \frac{[\overline{g}_{\mathrm{V},1}, \overline{g}_{\mathrm{V},2,} \cdots, \overline{g}_{\mathrm{V},N}]^{\mathrm{T}}}{\sqrt{\sum_{n=1}^{N} \left|\overline{g}_{\mathrm{V},n}\right|^2}}, \tag{16}$$

where $\overline{g}_{\mathrm{V},n}$, $n = 1, \ldots, N$, denote the corresponding interpolated channel estimates. Generally, the interpolated channel estimates are different for each subcarrier in each OFDM symbol. For simplicity, the subcarrier and OFDM symbol indexes are not included in the notation above. Then the interpolated channel estimates are given as

$$\overline{g}_{\mathrm{V},n}^{(k,m)} = \left(m - S_{\mathrm{p}}\right) \cdot \hat{g}_{\mathrm{V},n}^{(k,S_{\mathrm{p}})} + (S_{\mathrm{f}} - m) \cdot \hat{g}_{\mathrm{V},n}^{(k,S_{\mathrm{f}})} \tag{17}$$

where m is the OFDM symbol index, k is the subcarrier index, S is the pilot spacing, $S_{\mathrm{p}} = \frac{m}{S} \cdot S$ S is the preceding training symbol index,$S_{\mathrm{f}} = \frac{m}{S} \cdot S$ is the following training symbol index, and $\mathsf{L}.\,\mathsf{J}$ and $\lceil . \rceil$ stand for the floor and ceiling operations, respectively.

3.8 Combining for detection

In the final stage, while receiving data symbols, the equalized data symbols are calculated by maximum ratio combining the N samples obtained by applying the virtual steering vectors. The effective weight vectors for CR can be obtained as,

$$\begin{aligned}
\mathbf{w}_{\mathrm{CR}} &= [\mathbf{w}_{\mathrm{V},1}, \mathbf{w}_{\mathrm{V},2}, \ldots, \mathbf{w}_{\mathrm{V},N}]\mathbf{w}_{\mathrm{MCR}} \\
&= \sum_{n=1}^{N} \left(\mathbf{w}_{\mathrm{V},n}\overline{g}_{\mathrm{V},n}\right) / \sqrt{\sum_{n=1}^{N} \left|\overline{g}_{\mathrm{V},n}\right|^2} \\
&= \sum_{n=1}^{N} \left(\overline{\Sigma}_{\mathrm{NI}}^{-1}\mathbf{h}_{\mathrm{V},n}\overline{g}_{\mathrm{V},n}\right) / \sqrt{\sum_{n=1}^{N} \left|\overline{g}_{\mathrm{V},n}\right|^2} \\
&= \mathbf{\Sigma}_{\mathrm{NI}}^{-1}\overline{\mathbf{g}} / \overline{\mathbf{g}},
\end{aligned} \tag{18}$$

where $\overline{\mathbf{g}} = \left[\overline{g}_{\mathrm{V},1}, \overline{g}_{\mathrm{V},2}, \ldots, \overline{g}_{\mathrm{V},N,}\right]^{\mathrm{T}}$. It is enough to calculate and use this weight vector $\mathbf{w}_{\mathrm{CR}}$, instead of separately applying the MRC weights on the samples obtained by the weight vectors $[\mathbf{w}_{\mathrm{V},n}]$. The equalized data symbols are then calculated as follows:

$$\hat{d} = \mathbf{w}_{\mathrm{CR}}^{\mathrm{H}}\mathbf{r}. \tag{19}$$

In Eq. (19), $\overline{\mathbf{g}}$ appears as the spatial channel estimate for the target CR transmitter. Overall, this is the zero-forcing IRC solution which maximizes the received signal power over normalized steering vectors.

4 Results and discussion

The simulations are carried out for the system setup explained in Sect. 2. The carrier frequencies of CR and PU are the same, and it is here set to 700 MHz, which is close to the upper edge of the terrestrial TV frequency band. The modulation order used by CR varies between 4QAM, 16QAM, and 64QAM. The pilot symbols are binary and have the same power level as the data symbols. The primary transmitter signal follows the DVB-T model with 16QAM modulation, 8 MHz bandwidth, and CP length of 1/8 times the useful symbol duration, i.e., 28 μs. The IFFT/FFT length is 2048 for both systems. The DVB-T and CR systems use 1705 and 1200 active subcarriers, respectively. PUs frame structure and pilots follow the DVB-T standard. Data in all signals are generated randomly. ITU-R Vehicular A channel model (about 2.5 μs delay spread) is used for the CR system. For short-range/indoor CR communication, Ricean-fading channel model would be more relevant, but the Rayleigh-fading Vehicular A model is used as worst-case model. We have also tested basic scenarios with the Ricean-fading SUI-1 model (0.9 μs delay spread) for the CR, showing slight improvements in performance. Hilly Terrain channel model (about 18 μs delay spread) is used for PU transmission. The CR receiver is assumed to have four antennas, and uncorrelated 1×4 SIMO configurations are used for both the primary signal and the CR signals.

The number of spatial channel realizations simulated in these experiments is 300–1000. The ratio of CR and PU signal power levels at the CR receiver (referred to as the signal-to-interference ratio, SIR) is varied. In the case of co-channel CR interference, the average power levels of interfering and target CRs are the same at the target receiver and the channels are independent instances of the Vehicular A model with random timing offsets, while all multi-path delays remain with the CP. The lengths of the OFDM symbol frame and silent gap for interference covariance matrix estimation are also varied (expressed in terms of CP-OFDM symbol durations). A very basic training symbol scheme is assumed for the CR: training symbols contain pilots in all active subcarriers and the spacing of training symbols is 8 OFDM symbols. Frame length is selected in such a way that training symbols appear as the first and last symbol of each frame, along with other positions. Channel estimation uses linear interpolation between the training symbols. We have tested the BS-CR link performance with SIR values of $\{-10, -20, -30\}$ dB using silent gap durations of {8, 16, 32} OFDM symbols (known channel case also with 128 symbols), and data block lengths of {17, 25, 33, 41} OFDM symbols.

4.1 The effect of silent gap length

This subsection analyzes the BER performance of the proposed sample covariance-based IRC process using Eqs. (10), (12), (18), and (19), considering the known channel-based process as an ideal reference. As it was explained in Sect. 3, the known channel case assumes perfect knowledge of the interference channel and it provides a theoretical

performance bound for practical IRC schemes. It uses the LMMSE solution (8) with known channel-based covariance estimate (9). Otherwise, the receiver process is the same as in the sample covariance-based scheme, thus providing a theoretically achievable bound for the practical sample covariance-based approach. Below, the known channel model is applied with PU interference only, assuming no cochannel CR interferers.

Figure 2 shows the BER performance considering both the known channel and sample covariance-based approaches in stationary case (no mobility). Here, the silent gap durations are 8, 16, 32, and 128 OFDM symbols and the data block length is 17. With zero-mobility, link performance is independent of the data block length and short block is used here mainly to reduce simulation time. It can be observed that the sample covariance-based simulation results converge to the corresponding known channel results with increasing gap length, since the covariance estimate is improved with increasing sequence length. This demonstrates that the known channel-based bound is theoretically achievable.

In Fig. 3, the BER performance of known channel and sample covariance approaches is shown considering SIR values of $\{-10, -20, -30\}$ dB. Similar to Fig. 2, the data block length is 17 and the gap duration is selected as 16 OFDM symbols. Zero-mobility case is considered also here. As seen in Fig. 3, the CR link performance of both known channel and sample covariance schemes is rather independent of the SIR.

A detailed comparison between the required SNR values of the known channel and sample covariance-based approaches for BER = 0.01 is provided in Table 1. As seen in the table, the required SNR values of known channel and sample covariance-based algorithms match adequately under the gap length of 128 OFDM symbols. Additionally, the numerical results clearly show that the differences in required SNR values are almost independent of the SIR while considering the SIR values of $\{-10, -20, -30\}$ dB. The SNR loss due to limited gap length is about 0.3 dB, 1 dB, 1.9 dB, and 4.4 dB for gap lengths of 128, 32, 16, and 8, respectively.

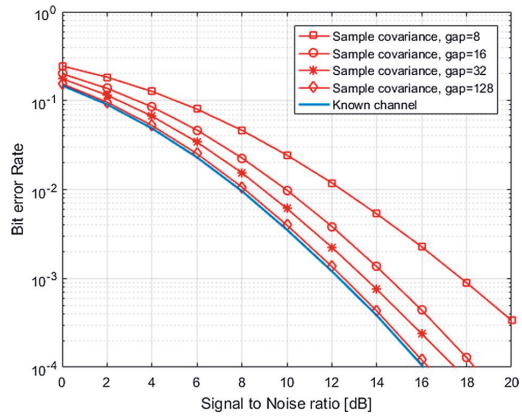

Fig. 2 Performance of QPSK BS-CR systems with known channel-based and sample covariance-based approaches for SIR = −30 dB considering block fading channel (no-mobility) with silent gap lengths of 8, 16, 32 and 128 symbols, and OFDM frame length of 17 symbols

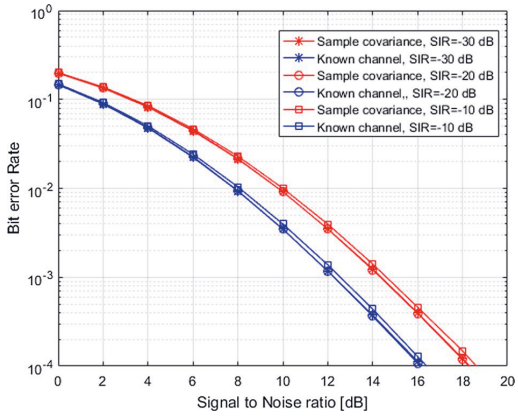

Fig. 3 Performance of QPSK BS-CR systems with known channel and sample covariance-based approaches for SIR values of {− 10, − 20, − 30} dB considering block fading channel (no-mobility) with silent gap length of 16 OFDM symbols and OFDM frame length of 17 symbols

Table 1 Required SNR values of known channel and sample covariance-based approaches for the BER = 0.01 in QPSK BS-CR systems for SIR values of {− 0, − 20, − 30} dB considering block fading channel (no-mobility) with silent gap lengths of 8, 16, 32 and 128 symbols, and OFDM frame length of 17 symbols.

Req. SNR for BER = 0.01	SIR = − 30 dB		SIR= − 20 dB		SIR = − 10 dB	
	Known Chn. (dB)	Sample Cov. (dB)	Known Chn. (dB)	Sample Cov. (dB)	Known Chn. (dB)	Sample Cov. (dB)
Gap = 8	7.9	12.3	7.9	12.3	7.9	12.2
Gap = 16	7.9	9.8	7.9	9.8	7.9	9.7
Gap = 32	7.9	8.9	7. 9	8.9	7.9	8.8
Gap = 128	8.0	8.3	8.0	8.3	8.0	8.2

4.2 Performance analysis of proposed scheme with mobility

This subsection reports the performance analysis of the proposed algorithms considering also the effects of mobility and different system parameters. It is noted that only sample covariance-based approach is considered in the following results. The results presented above still serve as ideal reference when evaluating the effects of mobility in different configurations. First we evaluate the performance with slow mobilities with and without pilot interpolation, still assuming that the interference is due to the PU only.

Figure 4 shows the impact of covariance matrix interpolation on the BS-CR link performance. Here the data block length and gap duration are fixed to 17 and 16 OFDM symbols, respectively. This choice provides performance that is no more than 1 dB from the configuration reaching 1% or 10% BER with lowest SNR, among the tested configurations with even higher overhead. We can see that covariance interpolation provides significant improvement of robustness in time-varying channels. Focusing on the 1 – 10% BER region, the performance with interpolation at 10 km/h mobility clearly exceeds the performance at 3 km/h without interpolation. However, for the 64QM case with -30 dB SIR, this is true only for BER of 10% or higher, due to the high error floor at very low

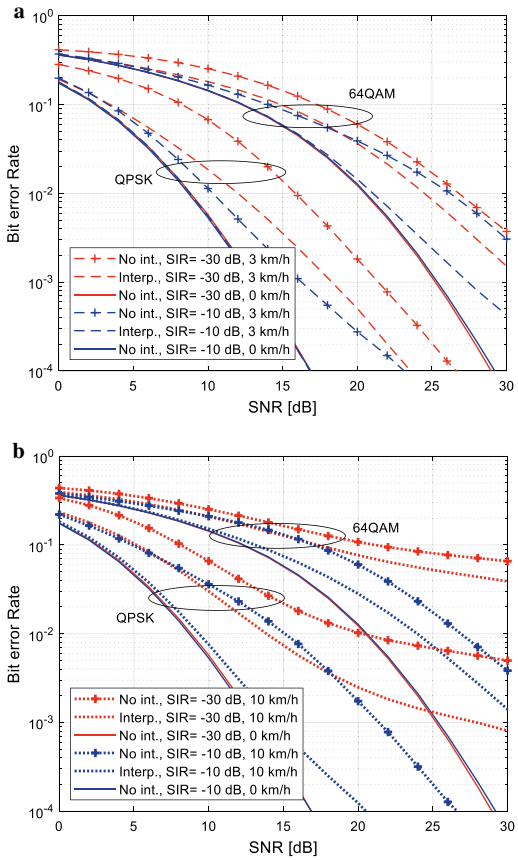

Fig. 4 Performance of QPSK and 64QAM BS-CR systems for SIR {− 10, − 30} dB with or without covariance matrix interpolation. **a** 0 and 3 km/h CR receiver mobilities. **b** 0 and 10 km/h CR receiver mobilities. Silent gap length of 16 symbols, and OFDM frame length of 17 symbols

SIR and high mobility. We can also see that with stationary channel, the performance is practically independent of the SIR. (Compared with [9], the performance is slightly improved by fine-tuning the used algorithms.)

In Fig. 5, the effect of silent gap duration is tested with 16 QAM modulation, SIR of − 20 dB, and data block length of 17. The overhead in data rate is about 58% and 44% for gap lengths of 16 and 8, respectively. The shorter gap length results in about 1.5 dB performance loss in the 1–10% range in stationary case and about 1.8–3.5 dB loss with 10 km/h mobility, compared to the gap length of 16. With 20 km/h mobility, the corresponding loss is about 2.2 dB at 10% BER, but longer gap leads to higher error floor, and the performance with shorter gap becomes better for BER below 3%.

Finally, we evaluate the link performance in the presence of co-channel CR interference, in addition to PU interference. While still assuming four antennas in the target CR receiver and − 20 dB SIR for the PU signal, also two interfering CR signals are included

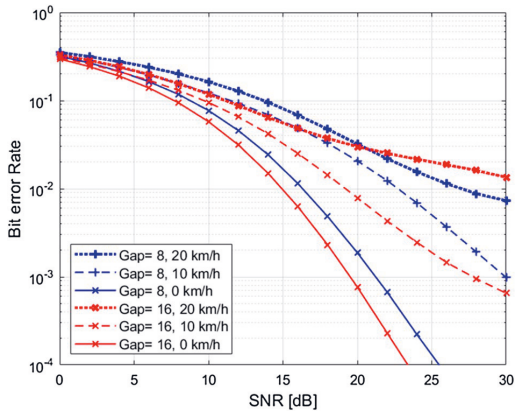

Fig. 5 Performance of QPSK and 16QAM BS-CR systems for SIR = − 20 dB with covariance matrix interpolation for CR receiver mobilities of 0, 10 km/h, and 20 km/h. Silent gap length of 8 or 16 symbols and OFDM frame length of 17 symbols

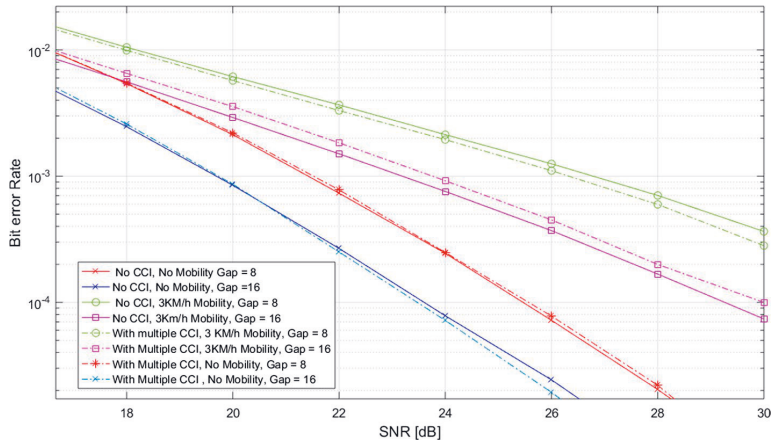

Fig. 6 Link performance in the presence of PU and two CR co-channel interferers using gap lengths of 8 and 16, mobilities of 0 and 3 km/h, 16QAM modulation in target CR link, SIR of − 20 dB for PU, and equal power levels of all CR signals

in the model. All CR signals are at the same average power level and their channels are independent instances of the Vehicular A channel model. The results are shown in Fig. 6, indicating that the impact of co-channel CRs on the target link performance is very minor.

5 Conclusion

The performance of black-space CR transmission links in the presence of strong interferences and mobility was investigated using spatial covariance interpolation between silent gaps. The interference rejection capability of IRC using multiple receive antennas

for various modulation orders under varying mobility and channel setups was studied. It was found that the IRC performs very well in the basic SIMO-type BS-CR scenario when stationary channel model is applicable, e.g., in fixed wireless broadband scenarios. However, the scheme is rather sensitive to the fading of the PU channel, e.g., due to people moving close to the CR receiver. Due to the strong interference level, the interference cancellation process is affected by relatively small errors in the covariance matrix estimate. For covariance estimation, the silent gap length in the order of 16—32 OFDM symbols provides the best performance with stationary channels, but even with 3 km/h mobility, the performance degrades greatly when considering SIR levels below -10 dB. The data block length should be of the same order or less, which leads to high overhead due to the silent gaps. Covariance interpolation was shown to greatly improve the robustness with time-varying channels, such that good link performance can be obtained with up to 20 km/h mobility at 700 MHz carrier frequency. This indicates that the proposed BS-CR scheme could be feasible at below 6 GHz frequencies with pedestrian mobilities. However, there is a significant tradeoff between link performance and overhead in data rate due to the silent gaps.

In the basic TV black-space scenario, there is only one strong TV signal present in the channel, in agreement with our assumption about the primary interference sources. DVB-T system allows also single-frequency network (SFN) operation and the use of repeaters to improve local coverage. In both cases, the primary transmissions can be seen as a single transmission, with a spatial channel that depends on the specific transmission scenario, and the proposed scheme is still applicable.

One important issue in the proposed scheme is its sensitivity to the nonlinearities of the CR receiver's analog front-end. Wide linear range is required in order to prevent nonlinear distortion from the high-power PU signal from degrading the CR link performance. This is a common issue with opportunistic CR operating in white spaces close to high-power PU channels and also with digital signal processing (DSP) intensive receiver architectures. An interesting technology in this context is advanced DSP algorithms for compensating the nonlinear effects of the receiver's analog front end [26]. On the other hand, sample covariance-based IRC may exhibit some capability to reject also the nonlinear distortion due to the strong PU signal. This remains as an important topic for future studies.

The scheme was also extended to scenarios where multiple CR systems are operating in the same region. If all CR systems are time-synchronized to the PU and they are at a relatively small distance from each other, they are also synchronized with each other, and can be handled by the IRC process as additional interference sources following the model of Eq. (3).

In future work, it is important to optimize the silent gap and data block lengths along with the modulation order to maximize throughput with given PU interference level and mobility. Lower-order modulations are more robust to errors in covariance estimation, allowing significantly lower gap and training overhead than higher order modulation. Complexity reduction of the covariance interpolation and IRC process is also an important topic for further studies. It is also worth to consider adaptation of the IRC process without silent gaps after the first one required for the initial solution. This would help to reduce the related overhead in throughput. One possible approach is to do this in a

decision-directed manner: first estimating the covariance matrix in the presence of the target signal and then cancelling its effect based on detected symbols and estimated target channel. In future studies, also the effect of antenna correlation will be taken into consideration.

Abbreviations

BER: Bit error rate; BS-CR: Black-space cognitive radio; CP-OFDM: Cyclic prefix orthogonal frequency division multiplexing; CR: Cognitive radio; dB: Decibels; DVB-T: Digital video broadcasting, terrestrial; FFT: Fast Fourier transform; IFFT: Inverse fast Fourier transform; IRC: Interference rejection canceller; LMMSE: Linear minimum mean-squared error; OFDM: Orthogonal frequency division multiplexing; QAM: Quadrature amplitude modulation; QPSK: Quadrature phase shift keying; MRC: Maximum ratio combining; MIMO: Multiple input multiple output; PU: Primary user; SFN: Single frequency network; SIR: Signal-to-interference ratio; SINR: Signal to interference and noise Ratio; SIMO: Single input multiple output; SU: Secondary user; TVWS: TV white space.

Acknowledgements

This work was supported in part by the Finnish Cultural Foundation.

Authors' contributions

The idea, analysis, simulations and writing were done by SS, with the help of SD and MR. All authors read and approved the final manuscript.

Funding

This work was supported in part by the Finnish Cultural Foundation.

Availability of data and materials

Not applicable.

Competing interests

The authors declare that they have no competing interests.

Received: 15 January 2020 Accepted: 20 October 2020
Published online: 23 November 2020

References

1. T. Yucek, H. Arslan, A survey of spectrum sensing algorithms for cognitive radio applications. IEEE Comm. Surv. Tutor. **11**(1), 116–129 (2009)
2. Y.C. Liang, A. T. Hoang Y. Zeng, R. Zhang, A review on spectrum sensing for cognitive radio: challenges and solutions, in *EURASIP Journal on Advances in Signal Processing*, pp. 1–15, January 2010.
3. S. Dikmese, S. Srinivasan, M. Shaat, F. Bader, M. Renfors, Spectrum sensing and resource allocation for multicarrier cognitive radio systems under interference and power constraints, in *EURASIP Journal on Advances in Signal Processing*, 2014:68.
4. A.M. Wyglinski et al., *Cognitive Radio Communications and Networks: Principles and Practice* (Academic Press, Cambridge, 2010)
5. Y. Selén, R. Baldemair, J. Sachs, A short feasibility study of a cognitive TV black space system, in *Proc. IEEE PIMRC 2011*, Toronto, ON, 2011, pp. 520–524.
6. A. Rico-Alvariño, C. Mosquera, Overlay spectrum reuse in a broadcast network: covering the whole grayscale of spaces, in *Proc. IEEE* DySPAN 2012, WA, 2012, pp. 479–488.
7. Z. Wei, Z. Feng, Q. Zhang, W. Li, Three regions for space-time spectrum sensing and access in cognitive radio networks. IEEE Trans. Veh. Technol. **64**(6), 2448–2462 (2015)
8. Y. Beyene, K. Ruttik, R. Jantti, Effect of secondary transmission on primary pilot carriers in overlay cognitive radios, in *Proc. CROWNCOM2013*, Washington, DC, 2013, pp. 111–116.
9. S. Srinivasan, M. Renfors Interference rejection combining for blackspace cognitive radio communications, in *Proc. Crowncom 2018*, Ghent, Belgium, pp. 200–210, Sept. 2018.
10. Srinivasan S., Renfors M. (2019) Interference rejection combining for black-space cognitive radio communications, in: eds *Cognitive Radio Oriented Wireless Networks*, I. Moerman, J. Marquez-Barja, A. Shahid, W. Liu, S. Giannoulis, X. Jiao, CROWNCOM 2018.
11. A.B. Carleial, A case where interference does not reduce capacity, in *IEEE Trans. Information Theory*, 01/1975.
12. N. Devroye, P. Mitran, V. Tarokh, Achievable rates in cognitive radio channels. IEEE Trans. Inf. Theory **52**, 1813–1827 (2006)
13. S. Verdu, *Multiuser Detection* (Cambridge University Press, Cambridge, 1998)
14. J. Winters, Optimum combining in digital mobile radio with cochannel interference, in *IEEE Trans. on Vehicular Technology*, vol 2, Issue 4, August 1984.
15. J. Liaster, J. and Reed, Interference rejection in digital wireless communication, in *IEEE Signal Processing Magazine*, vol 14, Issue 3, May 1997
16. G. Klang, On interference rejection in wireless multichannel systems, PhD Thesis, KTH, Stockholm, Sweden, 2003.

17. M.A. Beach et al, Study into the Application of Interference Cancellation Techniques, Roke Manor Research Report 72/06/R/036/U, April 2006.
18. O. Bakr, M. Johnson, R. Mudumbai, K. Ramchandran, Multi antenna interference cancellation techniques for cognitive radio applications, in *Proc. IEEE WCNC 2009*.
19. C.C. Cheng, S. Sezginer, H. Sari, Y.T. Su, Linear interference suppression with covariance mismatches in MIMO-OFDM systems. IEEE Trans. Wirel. Commun. **13**, 7086–7097 (2014).
20. S. Srinivasan, S. Dikmese, D. Menegazzo, and M. Renfors, Multi-antenna interference cancellation for black space cognitive radio communications, in *Proc.* 2015 *IEEE Globecom Workshops*, San Diego, CA, 2015, pp. 1–6
21. U. Ladebusch, C.A. Liss, Terrestrial DVB (DVB-T): a broadcast technology for stationary portable and mobile use. Proc. IEEE **94**, 183–193 (2006).
22. S. Haykin, *Adaptive Filter Theory*, 4th edn. (Prentice-Hall, New York, 2001)
23. M. Alonso et al. Spectrum occupancy and hidden node margins for cognitive radio applications in the UHF band, in: eds *Mobile Multimedia Communications. MobiMedia 2011*, Lecture Notes of the Institute for Computer Sciences, Social Informatics and Telecommunications Engineering, vol 79. L. Atzori, J. Delgado, D. Giusto (Springer, Berlin, Heidelberg, 2012)
24. C. He, Z. Peng, Q. Zeng, Y. Zeng, A novel OFDM interpolation algorithm based on comb-type pilot, in *Wireless Communications Networking and Mobile Computing 2009*. WiCom '09. 5th International Conference on, pp. 1–4, 2009.
25. L.J. Cimini, Analysis and simulation of a digital mobile channel using orthogonal frequency division multiplexing. IEEE Trans. Commun. **33**(7), 665–675 (1985)
26. M. Valkama, A. Shahed hagh ghadam, L. Anttila, M. Renfors, Advanced digital signal processing techniques for compensation of nonlinear distortion in wideband multicarrier radio receivers. IEEE Trans. Microw. Theory Tech. **54**(6), 2356–2366 (2006)

Publisher's Note

PUBLICATION

5

Effects of RF Imperfections on Interference Rejection Combining Based Black-Space Cognitive Radio

S. Srinivasan, S. Dikmese and M. Renfors

In Proceedings of IEEE 93rd Vehicular Technology Conference (VTC2021-Spring), 2021, pp. 1-6

Effects of RF Imperfections on Interference Rejection Combining Based Black-Space Cognitive Radio

Sudharsan Srinivasan, Sener Dikmese and Markku Renfors
Electrical Engineering, Faculty of Information Technology and Communication Sciences
Tampere University, Tampere, Finland
{sudharsan.srinivasan, sener.dikmese, markku.renfors}@tuni.fi

Abstract - In this paper, we investigate the effects of RF transceiver's imperfections on the multi-antenna interference rejection combing (IRC) based black-space cognitive radio (BS-CR) operation. In particular, we explore the effects of power amplifier (PA) nonlinearities and carrier frequency offset (CFO) on the blind IRC technique. The BS-CR operation mode supports effective reuse of the primary user (PU) spectrum, especially for relatively short-distance CR communication. We assume that both the PU system and the BS-CR use orthogonal frequency division multiplexing (OFDM) waveforms with common numerology. In this case the PU interference on the BS-CR signal is strictly flat-fading at subcarrier level, and it can be suppressed using subcarrier-wise IRC processing. Spatial sample covariance matrix-based IRC adaptation is applied during silent gaps in CR operation. We propose an analytical framework for modeling CFO effects, together with experimental study of CFO and PA nonlinearity effects. The performance of the IRC scheme is tested considering terrestrial digital TV broadcasting (DVB-T) as the primary service. The validity of the offered expressions for CFO effects are justified through comparisons with respective results from computer simulations. The effect of CFO between the primary and secondary systems is found to be critical for BS-CR operation, while the effect of CR transmitter's nonlinearity is no worse than in basic OFDM schemes, and the PU transmitter's nonlinearity has minor effect on BS-CR operation.

Keywords *Black-space cognitive radio, underlay CR, IRC, interference rejection combining, MRC, multi-antenna system, receiver diversity, PA nonlinearity, CFO, OFDM, DVB-T.*

I. INTRODUCTION

Spectrum reuse has become an essential part of today's wireless communication systems. Cognitive radios (CRs) are becoming a prominent means by which the spectrum reuse is implemented [1]-[3]. To operate in radio environments with a high level of interference and, simultaneously, produce negligible interference to the primary users (PUs), CR transmitters (TXs) have to have good power amplifiers (PA) that have good power efficiency and high linearity [4]. Indeed, the power efficiency and linearity requirements are conflicting. There is also the need to use the spectrum as efficiently as possible and, therefore, spectrally efficient modulation techniques such as orthogonal frequency division multiplexing (OFDM) are commonly used. OFDM systems are very sensitive to the nonlinear distortions introduced by the analogue parts. To avoid significant degradation of the signal quality, the requirements of the analogue radio frequency (RF) components, such as PA are becoming stricter [4, 5].

In this paper we study interference rejection combing (IRC) based multi-antenna receiver diversity schemes with co-channel interference rejection capability. Our focus is on the black-space cognitive radio (BS-CR) application, where the power level of the CR signal is much below the PU power level at the CR receiver, and IRC is used for co-channel interference suppression.

Linear minimum mean square error (MMSE) based multi-antenna interference cancellation of co-channel interferes was studied in [6]. The equivalence of such MMSE schemes and interference rejection combing (IRC) was described in [7]. The use of multiple adaptive antennas in the context of interference cancelation for systems based on OFDM was discussed in [8]. The effects of MMSE based IRC receiver imperfections in cellular radio systems were studied in [9].

It is important to study the effects of different kinds of RF imperfections also in the design of transceivers for CRs [4],[5],[10] and [11]. This is particularly important for black-space cognitive radio (BS-CR) operation as some of the RF imperfections may become critical due to the wide signal dynamic range in the receiver [12]-[15]. In BS-CR, the RF nonidealities may affect in two different ways: (i) Directly degrading the CR link performance and/or (ii) harming the IRC process leading to reduced PU interference suppression capability, e.g., by distorting the spatial covariance estimate. In this paper, we investigate the effects of transmitter nonlinearities and carrier frequency offset (CFO) in IRC based BS-CR systems.

In the following, we introduce first the IRC-based BS-CR system model in Section II. In Section III, the used nonlinear PA model is first introduced and then simulation results for the effects PU TX nonlinearity and target CR TX nonlinearity are presented. In Section IV, we analyze the CFO effect and develop a novel analytical model for the post-combining signal-to-interference ratio (SIR) at the CR receiver and validate the model through comparisons with simulation results. Here the post-combining SIR is the ratio of the target CR signal power at CR receiver to the residual PU interference power due to the CFO, and it is a function of the CFO in relation to the subcarrier spacing, maximum delay spread of the PU channel, and the ratio of the PU and target CR powers at the CR receiver. Finally, concluding remarks are presented in Section V.

II. IRC-BASED BLACKSPACE COGNITIVE RADIO

The scenario considered in this study is illustrated in Fig. 1. In this scenario, we consider a CR receiver using multiple antennas to receive data from a single-antenna cognitive transmitter. The CR operates within the frequency band of the PU, and the PU power spectral density (PSD) is very high in comparison to that of the CR. The PU transmitter generates a lot of interference to the CR transmission, which operates closer to the noise floor of the primary receiver, and due to this, the PU communication link is protected. We consider frequency reuse over relatively small distances, such as an indoor CR system. The multi-antenna configuration studied here is that of single-input multiple output (SIMO). Other configurations, involving also transmit diversity in the CR link are also possible, but they are left as a topic for future studies.

In the case presented in the study, the PU is a DVB-T system that uses CP-OFDM [13]-[15]. The CR system is also an OFDM based multicarrier system using the same subcarrier spacing and CP length as the primary system. Thus, it has the same overall symbol duration. The CR system is assumed to be synchronized to the primary system in frequency and in quasi-synchronous manner also in time. The CP length is assumed to be sufficient to absorb the channel delay spread

together with the residual offsets between the two systems observed at the CR receiver. Consequently, the subcarrier-level flat-fading circular convolution model for spatio-temporal channel effects applies for the target CR signal, and for the PU interference signal as well. Then the IRC process can be applied individually for each subcarrier. Since the CR receiver observes the PU signal at a very high SINR level, the synchronization task is not particularly difficult and low-complexity algorithms can be utilized. Considering short-range CR scenarios, the delay spread of the CR channel has a minor effect on the overall channel delay spread to be handled in the time alignment of the two systems. Basically, if all CR stations are synchronized to the PU, they are also synchronized with each other in quasi synchronous manner. In our earlier paper, we have investigated the effects of mobility on the BS-CR system performance [15]. Here we assume stationary operation for simplicity.

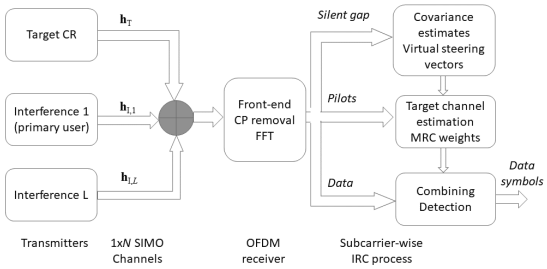

Fig. 1: BS-CR system model with silent gap for interference covariance estimation.

Both the primary and the CR systems use QAM subcarrier modulation, but usually with different modulation orders. The received CR signal consists of contributions from both the desired CR communication signal and the primary transmission signal, the latter one constituting a strong interference. Our BS-CR scheme includes two phases in the CR system operation, silent gaps and actual data transmission, as described in our previous work [15]. The spatial characteristics of the PU interference are modeled using multiantenna sample covariance matrix, which is estimated during silent gaps in the CR transmission, independently for each active subcarrier [13]. No explicit channel estimation of the PU channel is required. The CR channel is estimated from the partial IRC signals, from which the PU interference has been effectively suppressed. Based on the OFDM model mentioned above, subcarrier-wise detection is considered with flat-fading channel coefficients to get rid of the challenge of frequency selectivity in the IRC process.

In the SIMO configuration, the CR is assumed to have N receiver antennas and $L < N$ different interference sources are assumed. Based on this model, the signal received by the CR can be formulated for each active subcarrier (for simplicity of notation, the subcarrier index is not shown) as follows:

$$\mathbf{r} = \mathbf{h}_{\mathrm{T}} x_{\mathrm{T}} + \sum_{l=1}^{L} \mathbf{h}_{\mathrm{I},l} x_{\mathrm{I},l} + \boldsymbol{\eta}. \quad (1)$$

Here x_T is a transmitted subcarrier symbol and $\mathbf{h}_{\mathrm{T}} = \left[h_{\mathrm{T},1}, h_{\mathrm{T},2}, \ldots, h_{\mathrm{T},N}\right]^{\mathrm{T}}$ is the target channel vector with N receiver antennas in the CR, $x_{I,l}$ is the lth interfering signal, and $\mathbf{h}_{\mathrm{I},l} = \left[h_{\mathrm{I},l,1}, h_{\mathrm{I},l,2}, \ldots, h_{\mathrm{I},l,N}\right]^{\mathrm{T}}$ is the channel vector for the lth interferer. The channel vectors consist of the complex channel gains from the corresponding transmit antenna to nth antenna of the CR receiver. Finally, $\boldsymbol{\eta}$ is the additive white Gaussian noise (AWGN) vector. In this generic system model, it is assumed that the PU is the dominant interferer, and the other interference sources are other CR systems introducing co-channel interference at relatively low power level. The interference minimizing IRC weights are obtained during the silent period. Due to that, Eq. (1) is modified during silent gaps of CR operation as

$$\hat{\mathbf{r}} = \sum_{l=1}^{L} \mathbf{h}_{\mathrm{I},l} x_{I,l} + \boldsymbol{\eta}. \quad (2)$$

Linear combiner is used for the signals from different CR receiver antennas with a weight process in detection as follows:

$$y = \boldsymbol{w}^{\mathrm{H}} \boldsymbol{r}\,, \quad (3)$$

where y is the detected signal, $\boldsymbol{w}$ is the weight vector with N elements, and superscript H denotes the Hermitian (complex-conjugate transpose).

In this paper, we assume, for simplicity, that the PU is the only interference source. Then, if the PU channel vector is perfectly known, the noise plus interference covariance matrix can be calculated for each subcarrier as

$$\boldsymbol{\Sigma}_{\mathrm{NI}} = P\mathbf{h}_{\mathrm{I}}\mathbf{h}_{\mathrm{I}}^{\mathrm{H}} + P_N\mathbf{I}, \quad (4)$$

where P is the transmitted signal power in the subcarrier, P_N is the subcarrier noise power, and $\mathbf{I}$ is NxN identity matrix. The sample covariance based estimate is

$$\bar{\boldsymbol{\Sigma}}_{\mathrm{NI}} = \frac{1}{M} \sum_{m=1}^{M} \hat{\mathbf{r}}(m)\hat{\mathbf{r}}(m)^{H}. \quad (5)$$

Here m is the OFDM symbol index and M is the observation length in subcarrier samples, which is chosen equal to the length of the silent gap. In the following, our focus is on the sample covariance approach, but also results with known channel approach are included as a reference corresponding to ideal interference covariance estimation.

Using IRC, interference-free signals can be obtained for a transmissiom with target channel vector (known as steering vector) $\mathbf{h}_{\mathrm{S}}$ by using a linear weight vector $\mathbf{w}$ as follows:

$$\mathbf{w} = \bar{\boldsymbol{\Sigma}}_{\mathrm{NI}}^{-1}\mathbf{h}_{\mathrm{S}}. \quad (6)$$

Our approach is to calculate first such weight vectors for N orthogonal steering vectors during silent gaps and then use these weight vectors to obtain N variants of the following received CR signal block from which the PU interference is removed. Then the target CR channel is estimated for each of these signals, which are finally combined using maximum ratio combining (MRC). Details and results of these approaches can be found in our previous work [15].

III. Nonlinear PA Effects In BS-CR

A. Transmitter power amplifier models

The non-linearity of transmitter PAs causes significant effects on the performance with respect to spectrum characteristics, multiuser interference on the desired signal, and transmit power, depending on the used modulation scheme [16, 17]. Especially, the non-linearity brings about spectral regrowth causing adjacent channel interference and in-band performance degradation. The latter one is in the main focus of our study. Generally, the error vector magnitude (EVM) metric quantifies the in-band distortion causing performance loss in bit error rate (BER).

Various PA modeling approaches are available in the literature [16, 17]. While advanced PA models involving memory effects are able to model nonlinear PAs in a more reliable way, especially in wideband transmission, basic memoryless models are still widely used, e.g., in the 3GPP standardization related studies. For 5G New Radio studies at below 6 GHz frequency bands, a Rapp-type model is proposed for the base-station TX (downlink) and a polynomial model for the PAs of user devices (uplink) in [18]. Both of these gives AM/AM and AM/PM conversion characteristics, modeling how the PA output amplitude and phase, respectively, depend on the input amplitude.

Here we use the uplink model, which is an empirical polynomial model based on measurement of a real PA [18]. The PA output $y(t)$ is computed from input amplitude $x(t)$, given in dBm units, using the formula

$$y(t) = p_0 + p_1 x(t) + p_2 x(t)^2 + \cdots + p_9 \cdot x(t)^9. \quad (7)$$

The coefficients for AM/AM and AM/PM conversion, organized as $[p_9\ p_8\ p_7\ \ldots\ p_0]$ are as follows:

$$p_{\text{am}} = [\ 7.9726\text{e-}12\ \ 1.2771\text{e-}9\ \ 8.2526\text{e-}8\ \ 2.6615\text{e-}6\ \ 3.9727\text{e-}5\ \ 2.7715\text{e-}5\ \ -7.1100\text{e-}3\ \ -7.9183\text{e-}2\ \ 8.2921\text{e-}1\ \ 27.3535] \quad (8)$$

$$p_{\text{pm}} = [\ 9.8591\text{e-}11\ \ 1.3544\text{e-}8\ \ 7.2970\text{e-}7\ \ 1.8757\text{e-}5\ \ 1.9730\text{e-}4\ \ -7.5352\text{e-}4\ \ -3.6477\text{e-}2\ \ -2.7752\text{e-}1\ \ -1.6672\text{e-}2\ \ 79.1553]\ . \quad (9)$$

The AM/PM model gives the input amplitude dependent phase rotation in degrees.

B. PA nonlinearity effects

We test the effects of PU and CR transmitter nonlinearities through simulations. For simplicity, it is assumed that there are no other interference sources. First the spectral regrowth due to nonlinearities is demonstrated in Figs. 2 and 3 for PU TX and CR TX, respectively, for linear PA and the mentioned 5G uplink PA model. For the nonlinear model, we use two different back-off values of 9 dB (modest case) and 5 dB (worst case).

Here and in all later simulations, we assume the OFDM IFFT/FFT size of 2048 and the subcarrier spacing of 4.4643 kHz, corresponding to the 2k mode of DVB-T. The CP length is 1/8 times the main OFDM symbol duration, and the PU signal has all the elements of DVB-T transmission. For the CR signal we use the same main parameters and 1200 active subcarriers in the center of the DVB-T spectrum consisting of 1705 active subcarriers. We use the silent gap length of 24 OFDM symbols, and data block length of 65 OFDM symbols between silent gaps. We consider both sample covariance and known channel based IRC schemes. In the sample covariance based case, the covariance matrix is estimated from the received signal during silent gaps of length 24 in the target CR transmission. The reference case is based on perfect knowledge of the PU-CR channel. The CR channel is estimated using training symbols. All simulations use 1x4 SIMO antenna configuration.

Next, we consider the BER performance of the CR link with PA nonlinearity. The CR TX nonlinearity should not affect the interference covariance estimation, so we expect that it affects the BS-CR link performance in the same way as in basic OFDM transmission with the same numerology.

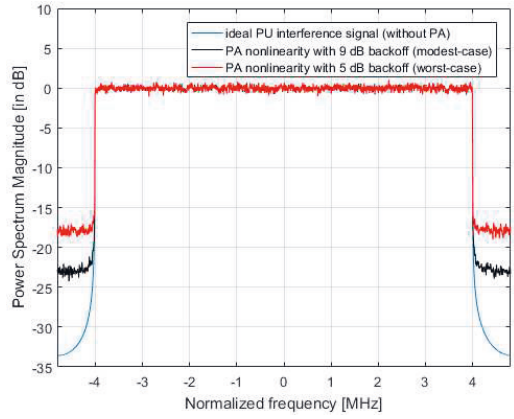

Fig. 2. Effects of PA model on PU interference signal considering ideal, modest and worst cases.

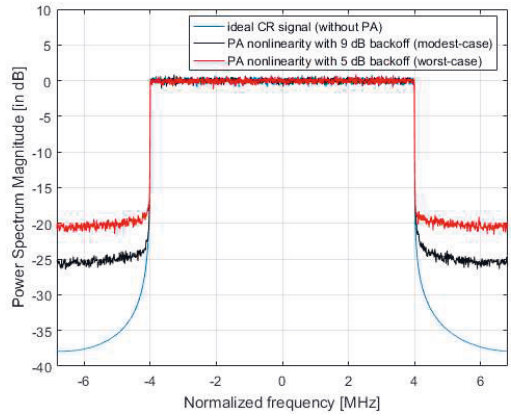

Fig. 3. Effects of PA model on CR signal considering ideal, modest and worst cases.

Regarding the PU TX nonlinearity, we notice that basic PA nonlinearity models do not harm the cyclic convolution model of CP-OFDM, i.e., the end part of the main OFDM symbol is affected in the same way as its copy, the cyclic prefix. Then the interference covariance should not be affected by PU TX nonlinearity, and we don't expect significant effects in the link performance. However, if the PA exhibits strong memory effects, the cyclic convolution model might be distorted, and this effect is worth investigating in future studies.

Monte Carlo simulation results are provided for the CR link performance with PA nonlinearity, assuming the CR/PU power ratio of $SIR_{\text{PU}} = -30$ dB and 64QAM subcarrier modulation. We use a modest input back-off value of 9 dB for the CR TX, and a low back-off value of 5 dB for the PU TX. The latter choice, as well the use of 5G-UL PA model for the PU TX is for demonstrating the robustness of BS-CR operation towards the PU TX nonlinearity. For these results, we use the Hilly terrain (HT) channel model having about 18 µs maximum delay spread for the PU signal and the ITU-R Vehicular A (VehA) model with about 2.5 µs maximum delay spread for the CR signal.

Fig. 4 shows the sample covariance based BS-CR link's BER performance with linear and nonlinear PA models in comparison to a basic interference-free link using MRC based receiver diversity. We can see that the used modest nonlinearity affects in a similar way in BS-CR and basic OFDM systems with the same numerology and same antenna configuration. With used parameters, sample covariance based BS-CR has about 3.5 dB SNR loss due to PU interference at 1 % BER level.

Fig. 5 shows the BER performance with linear/nonlinear PA in PU or CR TX, considering both sample covariance and known channel based schemes. We can see that even the very hard nonlinearity tested for PU TX has very minor effect on the CR link performance. It is also interesting to notice that, at 1 % BER level, the proposed sample covariance based method has about 1.2 dB SNR loss in comparison to the known channel based reference method.

IV. Analysis of CFO Effects in BS-CR

In the following analysis, we assume that the CR receiver is synchronized to the target CR signal while there is a frequency offset between the PU and CR carrier frequencies. We ignore the possible inconsequential initial carrier phase offset in the receiver. For convenience of notation, without loss of generality, we also assume that the active subcarriers are indexed from 0 to N_{A}-1. Then the PU interference part of the received digital baseband multi-antenna signal can be expressed in the presence of CFO as:

$$\boldsymbol{r}_{\mathrm{PU}}(n) = \widetilde{\boldsymbol{h}}_{\mathrm{PU}}(n) * x_{\mathrm{PU}}(n) e^{\frac{j2\pi\delta_{\mathrm{CFO}} n}{N}} \tag{10}$$

where n is the time index, δ_{CFO} is the CFO normalized to the subcarrier spacing, $\widetilde{\boldsymbol{h}}_{\mathrm{PU}}(n)$ is the vector of channel impulse responses from PU to the CR receiver antennas, $x_{\mathrm{PU}}(n)$ is the PU signal, and $*$ denotes cyclic convolution. Then, after the receiver's FFT process, the corresponding PU interference contributions to the kth subcarrier samples of different antenna branches can be expressed as [19]

$$\begin{aligned}\mathbf{Y}_{\mathrm{PU},k} &= \sum_{n=0}^{N-1}\left(\sum_{l=0}^{N_{\mathrm{A}}-1}\mathbf{h}_{\mathrm{PU},l} d_{\mathrm{PU},l} e^{j2\pi ln/N} e^{j2\pi\delta_{\mathrm{CFO}} n/N}\right) e^{-j2\pi kn/N} \\ &= \sum_{l=0}^{N_{\mathrm{A}}-1}\mathbf{h}_{\mathrm{PU},l} d_{\mathrm{PU},l} \sum_{n=0}^{N-1} e^{j2\pi(l-k+\delta_{\mathrm{CFO}})n/N} \\ &= \sum_{l=0}^{N_{\mathrm{A}}-1}\phi(l-k+\delta_{\mathrm{CFO}})\beta(l-k+\delta_{\mathrm{CFO}})\mathbf{h}_{\mathrm{PU},l} d_{\mathrm{PU},l}\end{aligned} \tag{11}$$

where $\boldsymbol{h}_{\mathrm{PU},l}$ is the PU channel vector for subcarrier l, $d_{\mathrm{PU},l}$ is the PU data symbol in subcarrier l, and

$$\begin{aligned}\phi(z) &= e^{j\pi z(N-1)/N} \\ \beta(z) &= \frac{\sin(\pi z)}{N\sin(\pi z/N)},\end{aligned} \tag{12}$$

with $z = l-k+\delta_{\mathrm{CFO}}$. The orthogonality of subcarriers is maintained only if the CFO is zero or integer, i.e., if the frequency offset is an integer multiple of subcarrier spacing. Otherwise, the sample observed at the kth subcarrier contains intercarrier interference (ICI) from all other active subcarriers.

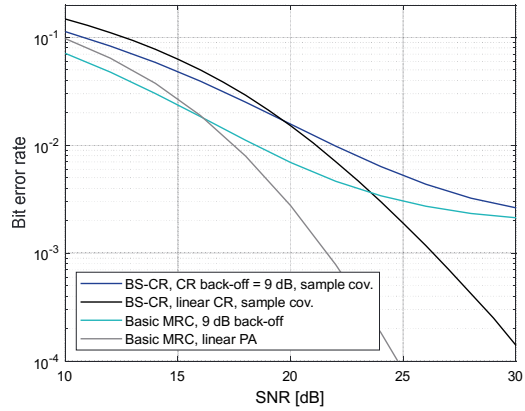

Fig. 4. BER performance of sample covariance based BS-CR with 64QAM modulation and $SIR_{\mathrm{PU}} = -30$ dB vs. basic transmission link with MRC based receiver diversity. 5G-UL PA model is used for the target link, linear PA in PU TX.

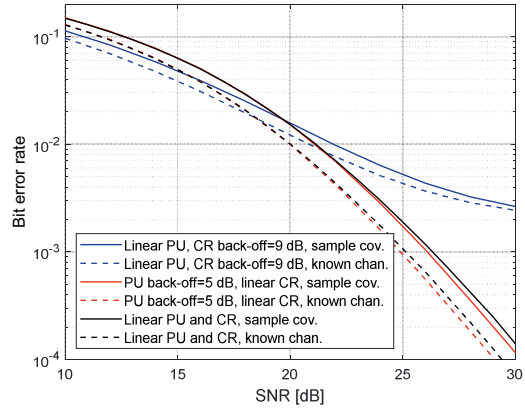

Fig. 5: BER performance of BS-CR with 64QAM subcarrier modulation, $SIR_{\mathrm{PU}} = -30$ dB, and linear or nonlinear 5G-UL PA model for PU or CR transmitter.

Now the known PU channel based spatial covariance matrix for subcarrier k can be evaluated as

$$\begin{aligned}\tilde{\boldsymbol{\Sigma}}_{\mathrm{PU},k} &= \left(\sum_{l=0}^{N_{\mathrm{A}}-1}\phi(z)\beta(z)\mathbf{h}_{\mathrm{PU},l}\right)\left(\sum_{l=0}^{N_{\mathrm{A}}-1}\phi(z)\beta(z)\mathbf{h}_{\mathrm{PU},l}\right)^{\mathrm{H}} \\ &= \sum_{l=0}^{N_{\mathrm{A}}-1}\phi(z)\beta(z)\mathbf{h}_{\mathrm{PU},l}\left(\phi(z)\beta(z)\mathbf{h}_{\mathrm{PU},l}\right)^{\mathrm{H}} \\ &= \sum_{l=0}^{N_{\mathrm{A}}-1}\beta^2(l-k+\delta_{\mathrm{CFO}})\boldsymbol{\Sigma}_{\mathrm{PU},l},\end{aligned} \tag{13}$$

where $\boldsymbol{\Sigma}_{\mathrm{PU},l}$ is the spatial covariance matrix of subcarrier l in the absence of CFO. The cross-terms between different subcarriers are not included here, based on the common assumption that the subcarrier symbol sequences are uncorrelated.

In the following, we aim to model the effect of CFO on the interference covariance matrix in the IRC context using basic parameters of the channel model. For this purpose, we first introduce a model for the correlation of the spatial channels of different subcarriers. We use the model commonly applied in Wiener filtering based channel estimation [20] for the correlation between the channel coefficients of different subcarriers. It is based on assuming uniform power delay profile with maximum delay spread of τ_{max}. We also assume that the spatial channel of each subcarrier is uncorrelated. Then the correlation between subcarriers k and l can be expressed as [20]

$$R(k,l) = \mathrm{sinc}\left((k-l)\tau_{\max} f_S / N\right) e^{-j(k-l)\tau_{\max} f_s / N}. \quad (14)$$

It should be noted that in case of flat-fading channel, different subcarriers have equal channel matrices and, consequently, equal spatial covariance matrices. In this case, CFO affects the channel covariance matrices on by an inconsequential real scaling factor. On the contrary, with highly frequency selective channels, the spatial covariance matrix of each subcarrier is distorted by the uncorrelated parts of the channel vectors of other subcarriers. Noting that $R(k,k)=1$, we can express the spatial covariance matrix of subcarrier k as

$$\tilde{\mathbf{\Sigma}}_{\mathrm{PU},k} = \beta^2(\delta_{\mathrm{CFO}})\mathbf{\Sigma}_{\mathrm{PU},k} + \sum_{\substack{l=0 \\ l\neq k}}^{N_A-1} \left(1-R(k,l)\right)^2 \beta^2(l-k+\delta_{\mathrm{CFO}})\mathbf{\Sigma}_{\mathrm{PU},l}. \quad (15)$$

The actual spatial covariance matrix of each subcarrier is scaled by $\beta^2(\delta_{\mathrm{CFO}})$, while the distorting uncorrelated part of the covariance of subcarrier k is given by the latter term. We assume that the IRC process suppresses completely the PU interference power corresponding to the first term, but the uncorrelated part remains as interference to the target CR signal. Let $SIR_{\mathrm{PU}} = P_{\mathrm{T}} / P_{\mathrm{PU}}$ denote the ratio of the target CR power at the CR receiver, P_{T}, to the PU interference power before interference cancellation, P_{PU}. Assuming that the subcarriers have equal power levels, the target signal's post-combining SIR due to the CFO of the PU signal can be evaluated as:

$$SIR_{\mathrm{CFO}}(\delta_{\mathrm{CFO}}) = \frac{SIR_{\mathrm{PU}}}{\sum_{\substack{l=0 \\ l\neq k}}^{N_A-1} \left(1-R(k,l)\right)^2 \beta^2(l-k+\delta_{\mathrm{CFO}})}. \quad (16)$$

In the numerical results, we show the average of this expression over active subcarriers. This calculation can be simplified by noting that subcarriers $k+\kappa$ and $k-\kappa$ contribute equally to the interference and that, considering all active subcarriers, there are $2(N_A-\kappa)$ subcarriers at the distance of $|l-k|=\kappa$.

Fig. 6 compares the theoretical SIR values based on Eq. (16) with simulated SIR values considering both sample covariance based and known channel -based IRC schemes with different values of CFO. Here the known channel reference case is based on perfect knowledge of the PU channel in the absence of CFO. The subcarrier modulation is 16QAM, and the other parameters are as mentioned in Section III-B.

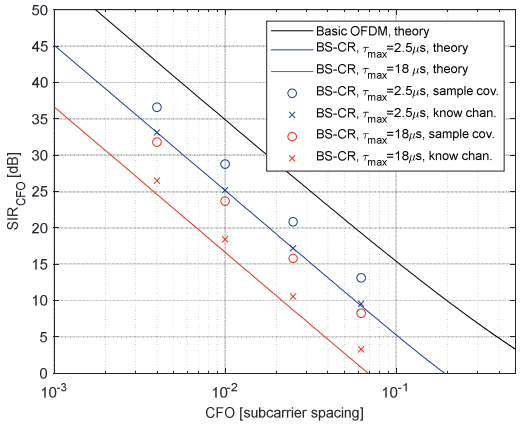

Fig. 6. Theoretical and experimental CFO-based SIR in BS-CR with Vehicular-A and Hilly terrain channel models and SIR_{PU} = -30 dB.

Here both HT and VehA channels are considered for the PU signal. No channel noise is included in these simulations, so the interference is due to imperfect spatial covariance matrix estimation due to CFO and due to limitations of sample covariance based estimation in the corresponding case. The CFO-based SIR is shown also for the basic OFDM scheme [19].

We can see that the CFO requirements are 3-10 times tighter than in basic OFDM schemes, depending on the channel delay spread and covariance estimation scheme. We can see that with the VehA-type PU channel, there is a very good match between the theoretical model and the known channel based simulation results. With HT-type PU channel, the theoretical model is somewhat pessimistic. We can also see that the sample covariance based estimation gives clearly better SIR than the theoretical model or the case of CFO-free channel knowledge based covariance estimation. This is because the sample covariance based estimation is able to take into account the CFO-induced contribution to the covariance estimates of different subcarriers.

Fig. 7 shows the BER performance with 64QAM modulation, VehA channel for the CR link, and CFO values of $\delta_{\mathrm{CFO}} \in \{0,\ 0.01,\ 0.005\}$, while the other parameters are the same as in the other numerical results. We can see that with CFO=0, the PU channel's delay spread has a very minor effect on the performance. When relating these results with SIR performance of Fig. 6, it should be noted for Fig. 6, the interference covariance is estimated in the absence of channel noise, and in low SNR region of Fig. 7, the covariance estimate is degraded due to noise. However, we can see that in the high SNR region, the performance of sample covariance -based scheme may exceed the performance of the known channel -based covariance estimate. Generally, the hard requirements for CFO can be seen also in these results.

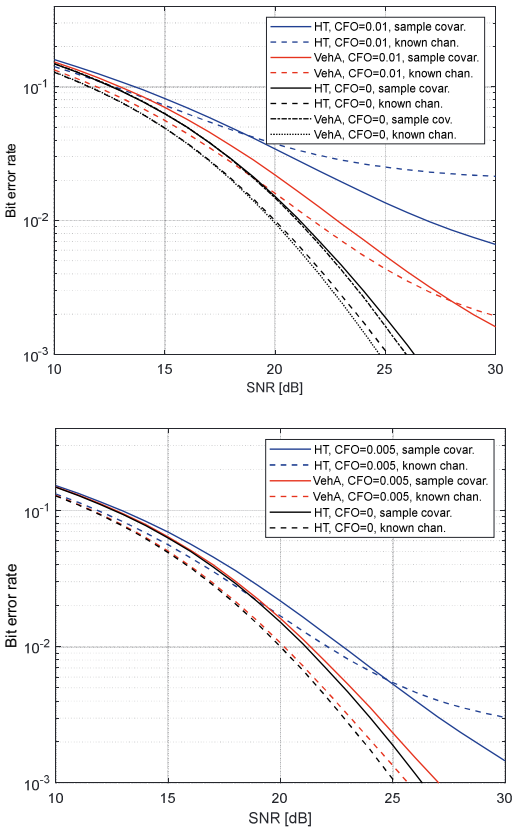

Fig. 7. BER performance with different CFO values {0, 0.005, 0.01}, 64QAM subcarrier modulation, SIR_{PU} = -30 dB, VehA channel for CR link, and VehA or HT channel for PU.

V. Concluding Remarks

Clearly, the most critical one among the considered RF imperfections is the CFO between the PU signal and CR receiver. However, since the PU signal is received at a high power level, synchronizing the CR stations to the PU signal with the needed high accuracy should be achievable. Considering other cases, e.g., when both the PU signal and target CR signal have CFOs, the effect of the high-powered PU signal dominates and still remains the most critical issue. The effects of PA nonlinearity in PU and CR transmitters were also tested, and found to less critical, as expected. The developed analytical model for the PU CFO effect could be a basis for analytical modeling BS-CR scenarios with mobility, which was tested experimentally in our earlier work in [15]. This is an important topic for future studies. Also, the nonlinearity of the CR receiver electronics may be critical due to the wide signal power range to be dealt with. This remains as another important topic for future work.

References

[1] T. Yucek and H. Arslan, "A Survey of Spectrum Sensing Algorithms for Cognitive Radio Applications," *IEEE Comm. Surveys & Tutorials*, vol. 11, no. 1, pp. 116-129, 2009.

[2] H. Viswanathan and P.E. Mogensen, "Communications in the 6G Era," *IEEE Access*, vol. 8, pp. 57063-57074, March 2020.

[3] A. M. Wyglinski et al, *Cognitive Radio Communications and Networks: Principles and Practice*, Academic Press, 2010.

[4] S. Dikmese, S. Srinivasan, M. Shaat, F. Bader and M. Renfors, "Spectrum Sensing and Resource Allocation for Multicarrier Cognitive Radio Systems under Interference and Power constraints," *EURASIP J. on Adv. in Signal Proc.,* 2014:68.

[5] M. Majidi, A. Mohammadi and A. Abdipour, "Analysis of the Power Amplifier Nonlinearity on the Power Allocation in Cognitive Radio Networks," *IEEE Trans. Comm.*, vol. 62, no. 2, pp. 467-477, Feb. 2014

[6] J. H. Winters, "Optimum Combining in Digital Mobile Radio with Co-channel Interference," *IEEE J. Select Areas Commun.*, vol. SAC-2, pp.528-539, July 1984

[7] Z. Bai et al., "On the Equivalence of MMSE and IRC Receiver in MU-MIMO Systems," *IEEE Communications Letters*, vol. 15, no. 12, pp. 1288-1290, December 2011

[8] Ye Li and N. R. Sollenberger, "Adaptive Antenna Arrays for OFDM Systems with Cochannel Interference," *IEEE Trans. Comm.*, vol. 47, no. 2, pp. 217-229, Feb. 1999.

[9] F. M. L. Tavares, G. Berardinelli, N. H. Mahmood, T. B. Sorensen and P. Mogensen, "On the Impact of Receiver Imperfections on the MMSE-IRC Receiver Performance in 5G Networks," *in Proc. 2014 IEEE 79th Vehicular Technology Conference (VTC Spring)*, , pp. 1-6

[10] S. J. Heinen and R. Wunderlich, "High Dynamic Range RF Frontends from Multiband Multi Standard to Cognitive Radio," in *Proc. IEEE Semiconductor Con.* , pp. 1-8, Sep. 2011.

[11] D. Cabric, S. M. Mishra, and R. W. Brodersen, "Implementation Issues in Spectrum Sensing for Cognitive Radios," in *Signals, Systems and Computers Conference Record of the Thirty Eighth Asilomar*, vol.1, pp. 772-776, Nov. 2004.

[12] H. Zamat and B. Natarajan, "Use of Dedicated Broadband Sensing Receiver in Cognitive Radio,"in *Proc. IEEE Communications Workshop*, pp. 508-512, May 2008.

[13] Y. Selén, R. Baldemair and J. Sachs, "A Short Feasibility Study of a Cognitive TV Black Space System," in *Proc. IEEE PIMRC 2011*, pp. 520-524.

[14] S. Srinivasan and M. Renfors "Interference Rejection Combining for Black-space Cognitive Radio Communications", in *Proc. Crowncom 2018*, pp. 200-210, Sept. 2018.

[15] S. Srinivasan, S. Dikmese and M. Renfors "Enhanced Interpolation-based Interference Rejection Combining for Black-space Cognitive Radio in Time-varying Channels," *J. Wireless Com. Network* 2020, 238 (2020).

[16] K. Hyunchul and J.S. Kenney, "Behavioral Modelling of Nonlinear RF Power Amplifiers Considering Memory Effects," *IEEE Trans. Microw. Theory Tech.,* 2003, vol. 51, pp. 2495-2504, Dec 2003.

[17] G. Zhou and R. Raich, "Spectral Analysis of Polynomial Nonlinearity with Applications to RF Power Amplifiers," *EURASIP J. on Applied Signal Proc.*, pp 1831-1840, Dec 2004.

[18] R4-163314, "Realistic Power Amplifier Model for the New Radio Evaluation," Nokia, 3GPP RAN79.

[19] J. Armstrong, "Analysis of New and Existing Methods of Reducing Intercarrier Interference Due to Carrier Frequency Offset in OFDM," *IEEE Trans. Comm.*, vol. 47, no. 3, pp. 365-369, March 1999.

[20] P. Hoeher, S. Kaiser and P. Robertson, "Two-dimensional Pilot-symbol-aided Channel Estimation by Wiener Filtering," in *Proc. IEEE Int. Conf. on Acoustics, Speech, and Signal Processing*, 1997, pp. 1845-1848 vol.3.